Exploring the Relationship between Morphological Parameters and Hemodynamic Characteristics in Ascending Thoracic Aortic Aneurysms Using Fluid-Structure Interaction with Patient-specific Models

by

Meng Xiao

A thesis submitted in partial fulfillment of the requirements for the degree of

Master of Science

in

Biomedical Engineering

Department of Electrical and Computer Engineering
University of Alberta

ABSTRACT

Ascending thoracic aortic aneurysm (ATAA) is an abnormal bulge in the ascending part of the aorta. It is associated with the risk of dissection and rupture and has been known as the "silent killer". When dissection or rupture, the outcome is usually severe and associated with high mortality. To prevent those adverse events from happening, surgical repair or replacement of the ascending aorta is necessary. The elective surgical criterion must be selected carefully to balance the risk of surgery and the risk of the adverse aortic events associated with ATAA. Current clinical guidelines were purely diameter based and established based on the natural history study of ATAA. However, recent findings have shown that diameter alone is a not good predictor and hence incorporating other parameters such as ascending aortic length (AAL) into the current clinical standard is desired.

With the development of computer technology, computational fluid dynamics and finite elements analysis have emerged as useful tools in cardiovascular studies. By employing those computational methods, researchers could study the interaction of the blood flow with the aortic wall and gain insights into the pathology of ATAA. A pathological flow can trigger vascular remodelling and subsequent wall degeneration, resulting in ATAA formation. In this thesis, we hypothesized that the change in morphology of the aorta results in the worsening of hemodynamic conditions, which subsequently initiates aortic wall degeneration. we perform a comprehensive fluid-structure interaction analysis to simulate the blood-aortic wall interaction.

By assessing the hemodynamic characteristics of ATAA with different morphologies, we confirmed that aortic elongation was associated with the worsening in hemodynamics in ATAA, providing more evidence of using AAL as a surgical indicator. The correlations between AAL

and various hemodynamic parameters were comparable to the correlations between diameter and those parameters, meaning that aortic elongation can negatively impact the flow conditions as aortic dilation does. A strong association was also found between the increase in AAV and compromised hemodynamic conditions. Thus, we propose to incorporate AAV, a 3D parameter, into the current clinical elective surgery criterion to account for the variation in the entire aortic geometry instead of just the largest part. Compared with diameter and AAL, AAV showed higher statistical significance and stronger associations with hemodynamic and biomechanical parameters. Hence, by using AAV as an independent or in combination with AAL and diameter, a better prediction might be achieved.

PREFACE

This thesis is an original work by Meng Xiao. The patient data used in this study was obtained from Guangdong Provincial People's Hospital (Guangzhou, China) and approved by the Institutional Review Board of Guangdong Provincial People's Hospital (ID number: KY-Z-2022-218-01).

Some of the material presented in Chapter 2, 3, 4, and 5 has been included in the following publications:

[1] J. Wu, M. Xiao, C. Wang, Y. Wu, J. Chen, J. Chen, T. Sun, "Fluid-structure interaction analysis endorses ascending aortic length as a surgical indication for thoracic aortic aneurysm", *Phenomics*, **submitted for review**.

I (M. Xiao) was responsible for methodology, data post-processing, performing simulation, and helped with manuscript composition. J. Wu was responsible for concept formation, formal analysis, and manuscript composition. C. Wang, Y. Wu, and J. Chen were responsible for patient data collection. J. Chen and T. Sun were the supervisory author, provided funding, and were involved with concept formation. J. Chen was also involved in manuscript edit and review.

[2] M. Xiao, J. Wu, C. Wang, Y. Wu, T. Sun, J. Chen "Ascending Aortic Volume: A Feasible Indicator for Ascending Aortic Aneurysm Elective Surgery?", *Acta Biomaterialia*, **submitted for review**.

I (M. Xiao) was responsible for methodology, data post-processing, performing simulation, formal analysis, and manuscript composition. J. Wu was responsible for concept formation and helped with formal analysis and manuscript composition. C. Wang and Y. Wu were responsible for patient data collection. J. Chen and T. Sun were the supervisory author, provided funding, and were involved with concept formation. J. Chen was also involved in manuscript edit and review.

ACKNOWLEDGEMENTS

First and foremost, I would like to thank my supervisor, Dr. Jie Chen, for his support and guidance throughout the entire period of my thesis program. I would like to thank Dr. Jinlin Wu for being willing to give me suggestions and valuable advice on the medical aspect of this project. I would also like to thank Dr. Di Niu and Dr. Jie Han for being my examiner for my thesis defence and Dr. Dileepan Joseph for chairing this event.

I am grateful to my colleagues and friends for their assistance and suggestions. Thank you for your constant encouragement and willingness to listen to my endless complaints.

Finally, I am sincerely grateful to my parents for always being understanding and supportive. I would not have done anything without their support.

TABLE OF CONTENTS

LIST OF TABLES

LIST OF FIGURES

LIST OF ABBREVIATIONS

AAA	abdominal aortic aneurysm
AAE	adverse aortic event
AAL	ascending aortic length
AAV	ascending aortic volume
ATAA	ascending thoracic aortic aneurysm
ATI	aortic tortuosity index
BAV	bicuspid aortic valve
BC	boundary condition
BMI	body mass index
BSA	body surface area
CFD	computational fluid dynamics
CKD	chronic kidney disease
CT	computed tomography
CTA	computed tomography angiography
EC	endothelial cell
ECM	extracellular matrix
FBN1	fibrillin-1
FEA	finite element analysis
FDM	finite difference method
FEM	finite element method
FVM	finite volume method
FSI	fluid-structure interaction

MFS	Marfan syndrome
MMP	matrix metalloproteinase
MRA	magnetic resonance angiography
MRI	magnetic resonance imaging
OSI	oscillatory shear index
PDE	partial differential equation
PRT	particle residence time
RF	radio frequency
RRT	relative residence time
SMC	smooth muscle cell
TAA	thoracic aortic aneurysm
TAD	Type A dissection
TAV	tricuspid aortic valve
TAWSS	time-averaged wall shear stress
TEE	transesophageal echocardiography
TGF-β	Transforming growth factor beta
TTE	transthoracic echocardiography
WS	wall stress (equivalent stress)
WSS	wall shear stress

CHAPTER 1. INTRODUCTION

Ascending thoracic aortic aneurysm (ATAA) is an abnormal dilation in the ascending thoracic aorta. ATAA has a risk of dissection or rupture, creating catastrophic outcomes. To prevent dissection or rupture, surgical intervention is required for at-risk ATAA. Based on studies of the natural history of ATAAs, the diameter-based criterion for surgical intervention is well established [1] [2] . A larger diameter is found to be associated with a higher risk of dissection or rupture. It is well known that based on Laplace's law, an aorta with a larger diameter suffers from higher mechanical stress. Given the limited strength of the aortic wall, it is obvious that an aorta with a larger diameter is more prone to mechanical failure, resulting in rapture or dissection of the aneurysm. However, many studies also showed that diameter alone is not a good predictor for those adverse aortic events (AAEs), including dissection or rupture, as many aneurysms dissect at a relatively small diameter which is well below the current clinical standard [3] [4] [5].

In recent years, many studies have been focusing on finding better predictors for AAEs and cooperate them into current clinical guidelines. These include the cross-sectional area-to-height ratio [6] [7] [8] [9], ascending aortic length (AAL) [10] [11] [12], curvature [13], and tortuosity [14]. In addition to those morphological parameters that can be directly measured from medical imaging, many mechanical parameters, such as the aortic wall stress and stiffness, were also studied [15] [16]. Those parameters cannot be obtained through direct measurement. Rather, computational methods must be employed to estimate those parameters. With the development of medical imaging and simulation tools, it is possible to reconstruct patient-specific 3D geometries of the aorta and simulate the interaction between the blood flow and the aortic wall. Studies have shown that the behaviour of the cells in the aortic wall can be regulated by their environment including pressure and physical stress [17] [18]. Certain flow patterns can induce cell dysfunctions or inflammatory responses [19], accelerating tissue degeneration and weakening the aortic wall. By employing computational methods, we could characterize the flow pattern and associate them with the morphological traits of the aorta. This allows us to better identify at-risk aneurysms with commonly available medical imaging tools. A more detailed introduction of ATAA including its pathology, diagnosing, and related hemodynamic parameters will be given in later chapters.

The applications of computational methods in ATAA studies have been focusing on the following areas: biomechanical characteristics of aneurysmal aortas [20] [21] [22] [23] [24] [25] [26], the influence of the aortic valve phenotype in aneurysm development [27] [28] [29] [30] [31] [32], stent graft design [33], and treatment evaluation [34] [35] [36]. Some studies also focused on developing new numerical methods [37] and tools [38] [39] for cardiovascular simulation. Although the idea of applying computational methods in cardiovascular research with patient-specific models was proposed many years ago, the major limitation is still the number of cases. Usually, less than 10 models were included in each study [21] [22] [23] [24] [25] [26]. Those studies have demonstrated the potential of using computational methods in aneurysm risk evaluation, however, it is hard to generalize those methods and use them in clinical practice due to the high computational cost, lack of common agreement in biological material properties, variations in workflow and reconstruction process.

In this study, we propose using computational methods on 100 patient-specific models to investigate the relationship between the morphological parameters and hemodynamic parameters of ATAA. Since the hemodynamic parameters have already been proven to be closely related to the pathophysiology of ATAA and the risk of AAEs, this study enables us to determine which morphological parameter is more important in ATAA evaluation and provides future direction for natural history studies of ATAA. Since morphological parameters can be easily measured from CT or MRI images, if our results were proven by future natural history studies, they can be easily generalized and used in clinical practice.

This study contributes to the related area in the following ways. First, by employing computational methods in blood flow simulation with patient-specific models, we gained a better understanding of the relationship between morphological parameters and the hemodynamics of ATAA. Our results confirmed the hypothesis that aortic elongation was accompanied by pathological flow conditions and higher mechanical stress within the aortic wall, providing further rationale for using AAL as a surgical criterion for ATAA. Second, a stronger correlation was found between ascending aortic volume and hemodynamics, indicating that aortic volume may be a better indicator for ATAA elective surgery. This provides direction for future natural history studies of the development of ATAA. The method described in this thesis can be adapted and improved by using patient-specific material properties and boundary conditions. This allows

the direct evaluation of the mechanical stress within the aortic wall and the flow condition within the aorta, providing valuable information for decision-making in surgical intervention and ATAA treatments.

1.1. Thesis Goals

This research was initiated by Dr. Jinlin Wu as a collaboration between Guangdong Provincial People's Hospital and the BINARY lab led by Dr. Jie Chen. The purpose of this study was to better understand the relationship between morphological parameters and hemodynamic parameters in ATAAs and to provide theoretical support for incorporating other potential predictors into present clinical guidelines.

As mentioned previously, researchers are working on finding new predictors to improve upon the current clinical guidelines. One particular finding by J. Wu et al [12]. showed that ascending aortic length (AAL) was another important factor to be considered in the risk assessment of ATAA. However, the mechanism behind this is poorly understood. Many studies suggested that the hemodynamic factor plays a very important role in the pathogenesis of ATAA as well as the occurrence of AAEs. The cells in the aortic wall can sense the blood flow inside the aorta and react to environmental change when homeostasis is disturbed. This results in cell gene expression and phenotype changes, which subsequently modifies the mechanical properties of the aortic wall and makes certain areas of the wall more prone to mechanical failure.

Based on those findings, we hypothesized that the change in morphology of the aorta, such as the elongation of the ascending thoracic aorta, results in the worsening of hemodynamic conditions. This subsequently initiates aortic wall degeneration. Hence, in this study, we aim to determine the relationship between various hemodynamic parameters and morphological parameters including AAL. Hopefully, the finding of this study will provide further evidence for using AAL as a valid surgical indicator for ATAA from a biomechanical point of view. Additionally, we planned to investigate other morphological parameters such as the curvature and the volume of the ascending aorta and to determine whether those parameters are hemodynamically significant in alternating the blood flow. This guides future studies, especially the natural history study of ATAA, allowing researchers to improve the current clinical guidelines for aneurysm surgical intervention to better prevent severe AAEs.

The two main goals of this thesis are stated as follows: 1. To develop a computational analysis method and workflow for simulating the blood flow in patient-specific aortic geometries. 2. To obtain various hemodynamic parameters and to investigate their relationship with morphological parameters to provide further evidence for previous findings and directions for future studies.

1.2. Thesis outline

This thesis is organized as follows. Chapter 1 gives a brief introduction to the topic and the study design, as well as outlines the goal of this study. Chapter 2 gives background information on ATAA including its pathogenesis, diagnosis, and current clinical practices in the management of ATAA. Chapter 3 introduces the computational methods and their application in cardiovascular disease studies. Chapter 4 covers the materials and methods used in this study. Chapter 5 presents the key results of this study and discussed the significance of the results. Finally, Chapter 6 summarizes the work and findings present in this thesis and suggests future research directions.

CHAPTER 2. ATAA AND ITS MANAGEMENT

2.1. Anatomy and Functions of the Aorta

The aorta is the largest artery in the human body. It delivers oxygen-rich blood from the heart to the rest of the human body. Aorta originated in the left ventricle of the heart, and it runs through the chest and the abdomen. The section that passes the chest is called the thoracic aorta and the segment in the abdominal cavity is called the abdominal aorta. Blood vessels branch off at various locations of the aorta and deliver blood to different regions of the human body.

The aorta consists of four sections: aortic root, ascending aorta, aortic arch, and descending aorta. As shown in **Figure 1**, the aortic root is the first part of the aorta, and it is directly attached to the heart. The aortic root includes the aortic valve at the annulus and the sinus of Valsalva. The aortic valve is a three-cusps structure that separates the aorta from the left ventricle. When the heart contracts during systole, the valve opens and allows the blood flows into the aorta. The right and the left coronary arteries branch off the aortic root and supply blood to the heart muscle tissue. The ascending aorta is the second part of the aorta. It starts from the Sinotubular junction and ends at the origin of the first branched arteries. The aortic arch is the curved segment of the aorta. Three arteries branch off the aortic arch, they are the brachiocephalic artery (innominate artery), the left common carotid artery, and the left subclavian artery. The brachiocephalic artery supplies the blood to the right arm through the right subclavian artery. It also supplies the blood to the brain and the right side of the head through the right common carotid artery. The left common carotid artery supplies blood to the brain and the left side of the head. The left subclavian artery supplies the blood to the left arm and the back part of the brain. Descending aorta is the part that runs from the chest to the lower side of the body, and it is further divided into the thoracic aorta and abdominal aorta.

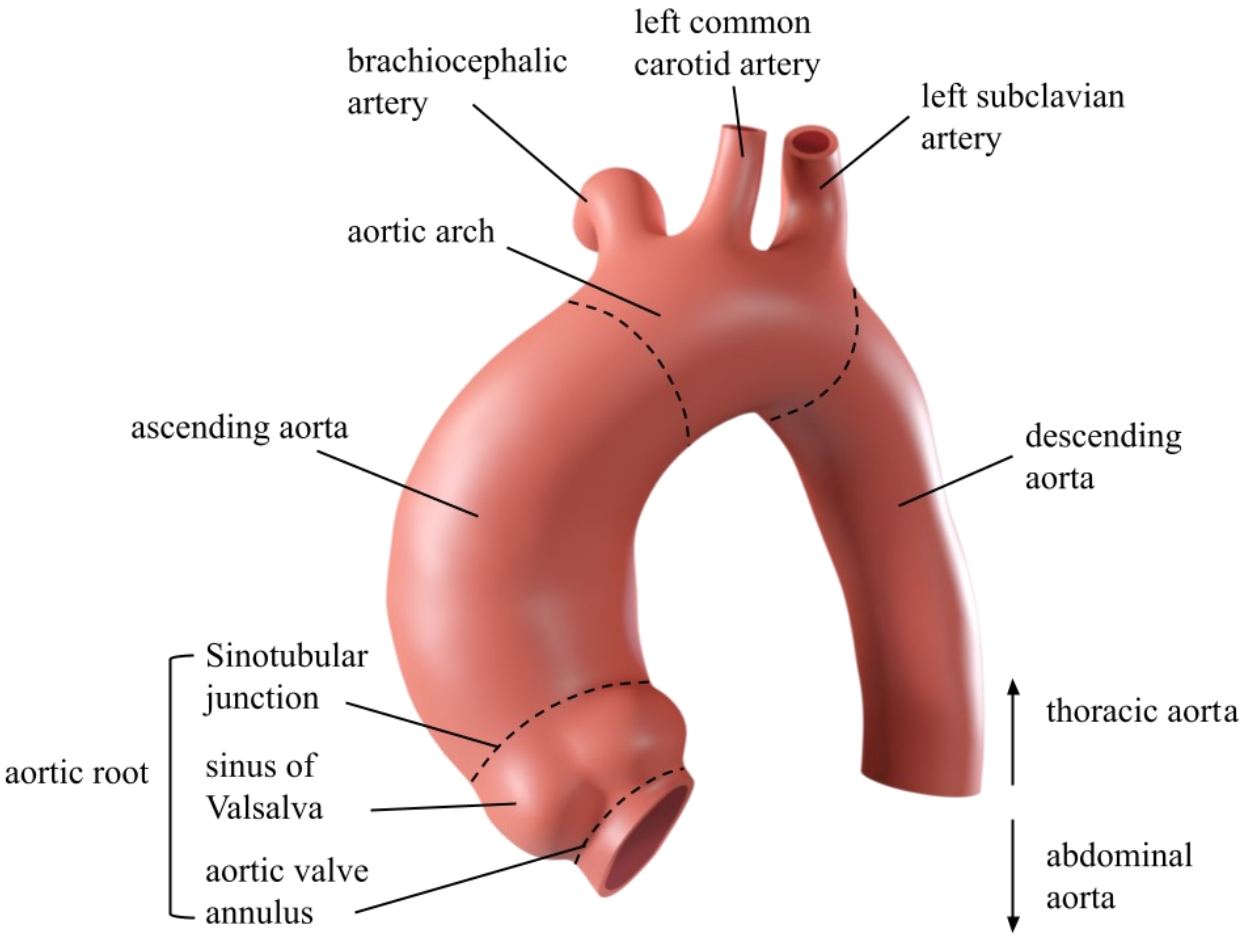

***Figure 1**. the structure of human aorta.*

The aortic wall consists of three layers: intima, media, and adventitia. Intima is the innermost layer. This layer consists of an endothelial layer, connective tissues, and smooth muscle cells (SMCs). The endothelial cells (ECs) in the endothelial layer are in direct contact with the blood. Those ECs are usually aligned and elongated along the flow direction. The media is bounded to the intima by an internal elastic lamina. The media consists of SMCs, elastin, and collagen. SMCs surrounded by collagen fibres are aligned in the circumferential direction to form a load-bearing layer [40], allowing the vessel to respond to varying pressure loads. The adventitia is the outermost layer. It is bounded to the media by the external elastic lamina. This layer consists of collagen, elastin, vasa vasorum (small blood vessels), and nerves. The collagen in this layer is typically aligned in the longitudinal direction [40]. The noncellular component of the aortic wall is called the extracellular matrix (ECM). ECM provides structural support for the cellular

component and predominantly defines the mechanical properties of the aortic wall [41]. Except for providing mechanical support, the elastin and collagens can modulate cell signalling and are ultimately responsible for regulating the behaviour of SMCs [41] [42].

The aortic size varies with age, gender, and body surface area. Aortic diameters increase with age and body surface area, and it is usually larger for men than that for women [3] [43]. Different measuring techniques and motion artifacts can also affect the measured results [43] [44]. The normal sizes for aortas measured by cardiac magnetic resonance (CMR) are given in **Tabel 1** .

Table 1*. The normal size of human aorta measured by CMR [43]*

Location	Women	Men
Sinuses of Valsalva	2.8 cm	3.2 cm
Sinotubular Junction	2.2 cm	2.5 cm
Ascending thoracic aorta	2.6 cm	2.7 cm
Proximal descending thoracic aorta	1.9 cm	2.1 cm
Mid descending thoracic aorta	2.5-2.6 cm	2.4-3.0 cm

2.2. Aortic Aneurysm and AAEs

An aortic aneurysm is an abnormal bulge in the artery. An aneurysm is usually caused by the degeneration of aortic wall tissue. The loss of SMCs and the deterioration of elastic fibres in the medial cause the wall to lose elasticity [43]. The pressure of the blood causes the degenerated part to expand and create a dilated region in the aorta. There are two different types of aortic aneurysms classified based on location: thoracic aortic aneurysm (TAA) and abdominal aortic aneurysm (AAA). Some aneurysms may involve more than one segment of the aorta. It was reported that 60% of the TAA occurred at the ascending thoracic aorta and the aortic root, 40% occurs at the descending thoracic aorta, 10% occurs at the aortic arch, and 10% involved both the thoracic and abdominal aorta (thoracoabdominal aorta aneurysm) [45]. TAA is further classified into the ascending thoracic aortic aneurysm (ATAA), the aortic arch aneurysm, and the descending thoracic aortic aneurysm based on its location.

The aneurysm has a great risk of dissection or rupture, creating a life-threatening condition. These events are sometimes referred to as adverse aortic events (AAEs). Dissection happens when a tear occurs in the inner layer of the aorta. Blood surges into the tear, disrupting the media layer. A false lumen will be created between the separated layers, disrupting the normal blood flow. The aorta may also rupture completely, causing lethal internal bleeding. The aortic dissections involving the ascending aorta are classified as Type A dissections (TADs), and the dissections that do not involve the ascending part are classified as Type B dissections (Stanford scheme). Approximately 67% of the aortic dissection was reported to be TADs [46]. Alternatively, aortic dissections can be classified based on the origin using the DeBakey scheme. Type I dissection originated in the ascending aorta and then propagate to the downstream part of the aorta. Whereas Type II originated and was confined in the ascending part of the aorta. Type III dissections originated in the descending aorta.

Patients with acute aortic dissection have high mortality. Reports showed that 40% of the patient died immediately, 1% per hour increase in mortality after the dissection [3]. 5% to 20% mortality during or after the surgery and only 50% to 70% of the patients will be alive 5 years after the surgery [3]. Although TAA is less common than AAA, the prognosis of TAA is usually worse than that of AAA with 2-3 times higher rupture-related mortality [47]. The dilation of the ascending aorta can cause compressive syndrome on adjacent tissue, and the dilation of the aortic root can also result in aortic valve regurgitation and heart failure [3]. Surgical intervention and replacement of the aorta are recommended for patients with high risk factors to prevent acute aortic dissection.

2.3. Pathogenesis of TAA

As mentioned in previous sections, the aortic wall consists of three layers: intima, media, and adventitia. The elastin in the aortic wall allows the aorta to expand and contract in response to the change in blood pressure, while the collagen provides mechanical strength to the aortic wall [41] [48]. The media layer plays a key role in the development of TAA. Medial degenerations are characterized by medial elastic fibre fragmentation and vascular SMC loss. Medial degeneration is commonly associated with aortic aging [45] [49] [50]. However, more profound medial degeneration was observed in patients with TAA than in healthy people [51]. Medial

degeneration causes the vessel to lose elasticity, resulting in aortic dilation and aneurysm formation.

In healthy people, the elastin and collagen are degenerated by matrix metalloproteinase (MMPs) and replaced by newly synthesized proteins. This physiological process is tightly regulated by various inhibitors to maintain a balance between the synthesis and the decomposition of the ECM proteins [47]. Studies have shown that the synthesis of elastin is sustained in ATAA patients, whereas the increase in activity of MMP-2 and MMP-9 contributes to the elastic fibre loss in the aortic wall [52]. The transforming growth factor beta1 (TFG-β1) plays a key role in ATAA formation as it promotes the release of MMP-2 and MMP-9 in the ECM [53]. Fibrillin-1 (FBN1) is also a critical component in microfibrils which provide structural support and regulatory functions in ECM. The FBN1 deficiency could promote the production of MMP-2 by SMCs and cause subsequent medial degeneration [54]. FBN1 also acts as an inhibitor for TFG-β1. The mutations in the gene encoding FBN1 increase the activity of TFG-β1 and result in subsequent ECM degeneration [53].

The formation of ATAA was also associated with inflammatory responses. Tang et al. found that the expression of Th1 cytokine was higher in some ATAA specimens than in non-aneurysm specimens, showing that the Th1-related transmural inflammatory response may facilitate vascular remodeling and the initial dilation of ATAAs [55]. He et al. showed that the infiltration of T-lymphocytes and macrophages into the medial layer may contribute to medial degeneration in TAA and TAD patients [56]. Inflammatory cells can produce a wide variety of MMPs, cleaving elastin and collagens in the aortic wall and contributing to the degeneration of ECM [47] [57]. The signaling factors secreted by T-lymphocytes may cause the apoptosis of SMCs [56]. Hence, inflammatory cells play an important role in TAA formation by producing MMPs and proinflammatory cytokine. In addition, the up-regulated of MMP-2 found in non-inflammatory tissue in patients with Marfan syndrome (MFS) or bicuspid aortic valve (BAV) suggests that the increase in MMP-2 may also play a role in SMC apoptosis [58]. Besides MMPs, the expressions of a destringing and metalloproteinases with thrombospondin motifs (ADAMTS) are found to be higher in TAA and TAD tissue, suggesting that upregulated ADAMTS expression may also contribute to TAA formation by promoting macrophage infiltration and degrading ECM [59].

Oxidative stress is linked to the pathogenesis of TAA. The reactive oxygen species induce an increase in the expression of MMPs and SMC apoptosis, leading to ECM degradation [53]. Yang et al. studied the oxidative stress in Marfan thoracic aortic tissue from mice and found that there was a significant increase in the oxidative species, rising the possibility that the accumulation of oxidative stress could be a potential cause for the decrease in contractibility in aneurysmal tissue [60]. It is known that oxidative stress plays a central role in the development of AAA. The increase in reactive oxygen species upregulates the proinflammatory gene expression, causes SMC apoptosis, and activates MMPs, which in turn leads to AAA formation [53]. However, the role of reactive oxygen species in the pathogenesis of TAA was less studied and understood.

The lack of collagen can cause the weakening of the mechanical strength of the aortic wall and make the wall more susceptible to rapture [61]. Research on genetically modified mice showed that the increase in uncleavable collagen and the change in collagen fibre alignment direction in the adventitia layer are associated with the increase in stiffness of the aorta [62]. This also makes the aorta more susceptible to mechanical failure. Carmo et al. showed that the aged collagen cross-links accumulate in aneurysm tissue while the synthesis of new collagen ceased, resulting in a decrease of the total collagen content in the aortic wall [63].

Vascular SMCs also play an important role in aortic wall remodeling and ATAA formation. SMCs have an elongated shape and align along two intermingled helices within the aortic wall [64]. The contractile units in SMCs are linked with ECM to form an elastin-contractile unit, allowing the vessel to respond to the pulsatile pressure exerted by the blood flow [65]. SMCs are sensitive the environmental stress and they act accordingly in response to environmental change. The disruption of SMCs' homeostasis cause SMCs to switch to more synthetic phenotypes and lose contractility. The SMCs with a synthetic phenotype tend to synthesize ECM components and MMPs to degenerate the ECM components, promoting aortic wall remodeling [66]. The leukocyte activity is inhibited by healthy SMCs in aortic tissue and the infiltration of lymphocytes was only observed in areas devoid of SMCs [67]. This makes the degenerated area in the aortic wall more prone to inflammatory responses. Guo et al. proposed a two-step model for the pathogenesis of TAAs based on earlier findings. In the two-step model, the environmental or genetic factor causes the initial damage of the ECs and aortic wall components. To mitigate these damages, SMCs switch to a synthetic phenotype in order to repair the damaged tissue [51].

This subsequentially triggers inflammatory responses, initiating atherosclerosis or medial degeneration and hence TAA [51].

TAA is often associated with genetic disorders. MFS is the most studied genetic disorder associated with aortic aneurysms. MFS is a connective tissue disorder caused by the mutation of the FBN1 gene. MFS cause the aortic wall tissue to lose distensibility and dilates, which then causes an increase in wall stress [68]. This forms a positive feedback cycle that results in the continuous progress of the dilation and eventually causes the formation of aortic aneurysms. Coady et al. found that patients who had a family history of TAA presented at a significantly younger age and had a significantly higher aneurysm growth rate than patients with MFS or sporadic TAA [69]. This suggests that genetic factors may play a key role in ATAA formation. Several gene mutations that disrupt the function of the elastin-contractile units and the mechanosensing of SMCs can lead to ECM dysfunction and hence ATAA [65].

Except for genetic causes, several other factors can also lead to ATAA formation. Hypertension causes an increase in the force exerted on the SMCs, thus potentially triggering a pathogenic signaling pathway [65] [70]. Cigarette smoking and atherosclerosis are also strong risk factors for sporadic TAA with atherosclerotic disease sharing many common mechanisms with TAA formation [53]. BAV is often associated with ATAA. Fedak et al. found that FBN1 content in ECM was significantly reduced in BAV patients [54]. Whether ATAA is caused by the altered hemodynamic or both the ATAA and BAV have the same genetic origin is unclear. Both the altered hemodynamic and the genetic factor may contribute to the development of ATAA in BAV patients. Nkomo et al. showed that BAV is associated with aortic dilation regardless of whether BAV-related stenosis or regurgitation is present [71]. However, the peak flow velocity is higher in BAV patients compared with the control group, suggesting that turbulent flow and other hemodynamic factors could also contribute to aortic dilation [71].

Studies have also demonstrated that the shear force applied by the blood blow on the ECs can potentially alter the gene expression of the ECs, resulting in elastic fibre degeneration, SMC loss, atherosclerosis, and inflammatory response [72]. The direction and magnitude of the shear force are greatly associated with the flow pattern. Liu et al. showed that a helical blood flow in the

ascending aorta may help to prevent the formation of atherosclerotic plaques and to reduce the adhesion of blood cells on the luminal surface of the artery [73].

2.4. Imaging and Diagnosing of Aortic Aneurysm

Patients with ATAA are often asymptomatic or occasionally present with acute chest pain. Only about 5% of TAAs are symptomatic and 95% of TAAs were not detected until a severe AAE happens [74]. Asymptotic ATAAs are usually discovered by incidents when the patients are diagnosed with other diseases or conditions with imaging techniques.

Computed tomography (CT) is the most widely used imaging technique for monitoring and diagnosis of aortic diseases including ATAA. CT scans utilize the different absorbance of X-rays in different tissues to create contrast in images. Single-detector spiral CT was introduced in the early 1990s into clinical imaging [75]. In the late 1990s, Multidetector-row computed tomography (MDCT) was introduced for extended coverage and better image quality [75]. Nowadays, the new generation CTs allow the evaluation of the entire geometry of the aorta with sensitivities up to 100% and specificities of 99% [76]. There are two different types of CT scans, noncontract CT and contrast CT (or CT angiography, CTA). During CTA scan, a contrast agent is slowly injected into the patient's blood during a specific interval to aid the image formation. The use of contract agents allows the inner wall and lumen of the aorta to form sharp images. It is usually used to examine the intimal flap and the false lumen in aortic dissection patients. During the imaging process, ECG gating technique is usually employed to minimize the artifacts caused by the pulsatile movement of the aortic root and the ascending aorta [76]. In retrospective ECG-gated CT imaging, the acquisition time duration lasts the entire cardiac cycle. The final image is selected based on the ECG reading in the diastolic phase. In prospective ECG-gated imaging, the scan is only triggered during a specific interval of the cardiac cycle where the movement is minimum to minimize radiation exposure. The scan is usually triggered at the end of the diastolic phase [76]. The reported mean ascending aortic diameter is larger from CT images without ECG-gating due to motion artifacts [77].

Transthoracic echocardiography (TTE) and magnetic resonance imaging (MRI) were also used for aneurysm screening, diagnosis, and surveillance. TTE utilizes ultrasound waves and the Doppler effect to provide real-time images of the aorta and its movements. In addition to the

aorta, it also provides information about the heart and the heart valves. It is commonly used in clinical screening, diagnosis, and surveillance for people with suspected or known heart diseases. TTE is good at imaging the aortic root and the proximal segment of the aorta. However, due to the obstacles and the distance to the transducer, the image quality of the aortic arch and the distal part of the ascending thoracic aorta is usually compromised. Hence TTE cannot be used for the characterization of the whole ATAA geometry. Transesophageal echocardiography (TEE), a semi-invasive imaging method, can improve the range of imaging by inserting a probe with a transducer down the esophagus. However, TEE is still not able to image the distal part of the thoracic aorta and is not commonly used in TAA screening or surveillance [78].

MRI has several advantages including its ability to provide high soft tissue contrast and to measure the flow of the blood inside the vessel [79]. Radio waves are employed to excite hydrogen nuclei inside the human body in an oscillating magnetic field. The hydrogen nuclei in different tissue respond to the radio frequency (RF) signal differently. The resultant RF signal is then received and analyzed. The contrast can be determined by the nuclei density and the time it takes for the excited nuclei to return to their equilibrium state. During the measurement, no contract agent is required, and no ionizing radiation is received by the patient. However, the cost of the MRI scan is significantly higher than the other techniques and the examination time is also longer. To reduce the acquisition time and motion artifacts, gadolinium contrast agents can be used to aid the imaging process and improve the signal-to-noise ratio. This process is known as MR angiography (MRA) [79]. MRI can also be employed to measure blood flow. The MRI signal phase along a magnetic field gradient is directly related to the flow velocity [80]. By measuring the phase change between two acquisitions, the flow velocity can be calculated. Recent advances allow more comprehensive acquisitions to be performed and analyzed. By collecting a series of time-resolved volumetric data in different directions, a 3D velocity field can be obtained. This technique is known as the four-dimensional (4D) flow MRI and is often used to evaluate the flow condition inside the aorta and valve function.

In addition to imaging techniques, several plasma biomarkers in relation to the pathogenesis of aortic aneurysm can be used as potential indicators for TAA and predictors for acute aortic dissection. These biomarkers include MMPs, TGF-β, D-dimers, and Inflammatory markers [81] [82] [83]. But in general, they are more often used in the diagnosis of acute aortic dissections

instead of in the screening for aortic aneurysms. The 2014 European guideline has incorporated D-dimers into the laboratory test for patients suspicious of aortic dissection [2]. However, these biomarkers have not yet been used in the routinely clinical diagnosis of aortic aneurysms.

2.5. Surgical Intervention Criterion

Surgical interventions are required for at-risk aneurysms to prevent AAEs. Depending on the location of the aneurysm and its affected area, different procedures can be performed to replace part of the ascending aorta with a prosthetic graft. The maximum diameter of the ascending aorta has been the most commonly used criterion and the gold standard for surgical intervention. Early natural history studies on ATAAs have shown that the hinge point of ascending aortic aneurysm dissection or rupture risk was 6.0 cm, with a 31% rupture or dissection rate [84]. Based on the strong association between the maximum diameter of ATAA and the increased risk of nature complications [44] [85] [86] [87], a diameter-based surgical criterion was established. Surgical replacement of the aorta is recommended for patients with an ATAA diameter of 5.5 cm as a good balance of the risk of AAEs and the surgical risk [2]. A lower threshold of 5.0 cm can be used for patients with family histories, high rate of diameter increases or other risk factors like BAV or MFS [2].

Nevertheless, there are still a significant number of cases of rupture or dissection in patients with ATAA diameters well below 5.5 cm [3] [4] [5]. Approximately 60% of the patient had a diameter less than 5.5 cm and 40% with a diameter less than 5.0 cm [4]. Evidence from previous studies also suggests that the size of an ATAA can significantly increase during dissection [88] [89] [90], suggesting a “left-shift” of the current clinical standard might be necessary. In the meantime, many researchers are actively investigating other potential risk predictors for AAE such as other morphological parameters, hemodynamic parameters, and biomechanical parameters.

Asvin et al. showed that for patients with a maximum diameter < 5.5cm, acute type A dissection happened at a smaller diameter for patients who have a dilated aortic root than patients who have a dilated ascending aorta, suggesting that the location of the dilation may play an important role in predicting aortic dissection [91]. Sharma et al. investigated the relationship between multiple size ratios and type A aortic dissection, showing that an abnormal maximum diameter to aortic

root diameter ratio (>1.06) is 4.5 times more likely to be in the group of patients with ATAA dissection [92]. However, the measurements were taken after the ATAA dissection happened and may not reflect the actual shape before the AAE occurred.

The aortic cross-sectional area-to-height ratio was proposed by several studies as a potential risk factor for AAE [6] [7] [8] [9]. Masri et al. analyzed the patients with dilated aortic roots, suggesting that aortic root cross-sectional area to height ratio >$10cm^2/m$ can be considered abnormal and associated with high mortality [6]. Studies on the cross-sectional area measured at multiple locations also showed similar results, suggesting that cross-sectional area to height ratio >$10cm^2/m$ may be considered as a potential risk factor [7] [8] [9].

In addition to the indexed cross-sectional area, the ascending aortic length (AAL) was also investigated in recent studies. Krüger et al. showed that the AAL (measured from the Sinotubular junction to the origin of the brachiocephalic artery) was significantly longer for patients in the pre-dissection and the dissection groups when compared with the control [10]. The combination of the AAL and the diameter can better identify pre-dissection patients compared to using the maximum diameter alone. Heuts et al. used a multivariable regression model with various influencing factors, showing that both the aortic dilation and the aortic elongation were associated with the increase in dissection risk [11]. A comprehensive study by Wu et al. showed that the average yearly risk of ATAA with length (measured from the aortic annulus to the base of the brachiocephalic artery) above 13 cm increase more than 5-fold compared to the ATAA with length below 9 cm [12]. Two hinge points were found between 11.5 cm to 12.0 cm and 12.5 cm to 13 cm, suggesting that AAL>11cm may serve as a potential risk predictor for AAE [12].

Except for the diameter and the length, other morphological parameters such as the curvature (the angle between the plane perpendicular to the aortic valve, and the plane perpendicular to the cross-section at the origin of the innominate artery) and tortuosity (ratio of AAL to the Cartesian distance between the aortic annulus and the aortic bifurcation) were also explored in several studies. A study based on a mathematical model of the ascending aorta demonstrated that the increases in aortic curvature significantly increase the force exerted by the blood flow on the aortic wall [13]. Compared with diameter, blood pressure, and cardiac output, the aortic curvature was relatively more important and may be considered a potential predictor for AAEs

[13]. However, the relationship between aortic curvature and the risk of AAEs has not yet been analyzed statistically using clinical data. A study on a group of patients with MFS showed that the aorta with aortic tortuosity index (ATI) > 1.95 is more likely to dissect than the arteries with lower ATI [14]. Yet, this study was limited to AAAs and Type B dissections.

Morphological and size-based parameters can be easily measured from CT and MRI images, and they are the most commonly used and accepted predictors for AAEs in current clinical practice. In addition to those parameters, non-size-based parameters were also studied. Mechanical properties and hemodynamic factors are also important factors to be considered in the development of aneurysms and the prediction of AAEs. Unlike morphological parameters, those parameters can be directly associated with the pathophysiology of AAEs. Studying those parameters can give researchers insights into why some morphological parameters are more important than others. Furthermore, those parameters can also be used as a direct risk predictor for AAEs.

Mechanical stress is one of the important parameters. When the wall stress exceeds the strength of the aortic wall, mechanical failure occurs. It could be the reason that cause the initial tear in the intima. Based on Laplace's law, ATAAs with a larger diameter are likely to experience higher wall stress. Hence ATAAs with larger diameters are more susceptible to dissection or rupture. Elefteriades et al. determined the mechanical properties of the aortic wall using blood pressure, diameter and the wall thickness of the aorta measured in systole and diastole, showing that distensibility of the aortic wall decreases with the increase in aortic size [44]. As the aortic wall loses elasticity, the blood pressure causes the vessel to dilate and increase in diameter. This also makes the wall more prone to dissection or rupture.

However, it is difficult to characterize the properties of the aortic tissue and to measure the mechanical stress inside the human body. With the development of computation and simulation technology, it is possible to simulate the blood flow in the aorta and the mechanical stress within the aortic wall. This allows researchers to determine the mechanical properties of the wall tissue indirectly and use the estimated properties in the risk assessment of ATAA. For example, Disseldorp et al. used 3D ultrasound data and finite element analysis (FEA) to estimate the peak wall stress and the tissue stiffness [15]. Farzaneh et al. used the gated CT scan data and FEA to

estimate aortic stiffness and achieved a good correlation between the estimated stiffness and the directly measured stiffness from the tissue collected after surgery [16]. Although the stiffness and the stress can be determined by the use of FEAs, the wall strength can not be easily obtained without taking tissue samples from the patients.

Aortic hemodynamics and altered flow patterns were also linked to the degeneration of the aortic wall [93]. 4D flow MRI is often used to measure the flow field, the obtained flow field can then be used to calculate relevant hemodynamic parameters such as the wall shear stress (WSS) and the flow eccentricity [93] [94]. Alternatively, computational methods can be employed to estimate the hemodynamic parameters and to study the relationship between the morphological feature and the flow pattern. These methods will be introduced in the next chapter.

CHAPTER 3. COMPUTATIONAL METHOD IN THE STUDY OF ATAA

3.1. Computational Methods

Finite element analysis (FEA), computational fluid dynamics (CFD), and fluid-structure interaction (FSI) studies have emerged in recent years as useful computational methods in the study of blood flow, its interaction with the aortic wall, and the biomechanical stress within the aortic wall.

FEA is a process in which the finite element method (FEM) is employed to numerically solve the governing equations of various physical phenomena such as electromagnetic interaction and heat transfer. Those equations are often in the form of partial differential equations (PDEs) or ordinary differential equations (ODEs). With complex geometries and boundary conditions, the governing equations cannot be solved analytically. Hence, FEM can be used to obtain approximate solutions of those differential equations with known boundary conditions. FEM is based on the discretization of the computational domain by dividing it into smaller elements called finite elements. By solving equations at each discrete point (node) and combining the results together, the approximate solution of the entire structure can be obtained. Researchers could estimate the mechanical properties of the aortic wall and the stress within the wall using FEA, allowing them to better predict the aneurysm progression and the risk of AAEs.

In CFD analysis, the Navier-Stokes equation and continuity equation, which govern the fluid motion, are solved using computational algorithms. By solving those equations with predetermined boundary conditions, researchers could compute hemodynamic parameters that are hard or impossible to measure *in vivo*. finite volume method (FVM) and finite difference method (FDM) are the most often used method in CFD. Simulations allow the characterization of the complex flow field and various hemodynamic parameters such as the wall shear stress (WSS). The simulation results can give researchers insight into the pathology of aortic aneurysms and can also be used in risk assessment.

By combining FEA and CFD, researchers could study the interaction of the blood flow and the structure (i.e. the aortic wall) around it in an FSI analysis. There are two coupling methods for

FSI: one-way FSI and two-way FSI. In a one-way FSI simulation, the fluid domain and the solid domain are solved separately. The solution of one domain is used as the boundary condition of the other. Usually, the CFD analysis is performed first to determine the force applied by the blood flow on the aortic wall. Then FEA can be employed to predict the stress and the deformation of the aortic wall. In a two-way FSI, the two domains are solved together. The results are transferred from one domain to another in each iteration and a converged solution will be obtained for each time step.

The main benefit of the one-way FSI is its low computational cost. The results are accurate if the deformation of the solid domain is small. In addition, the mesh quality will be constant during the entire simulation since the mesh will not deform during the simulation period [95]. Significant mesh deformation can result in mesh elements with high skewness, making the simulation unstable and difficult to converge [96]. A two-way FSI solution will be more accurate and can capture the transient behaviour of both the fluid flow and the solid structure. But it requires significantly higher computational power. Hence, two-way FSI is only recommended when the one-way FSI is not accurate enough to capture the transient behaviour of the simulation domain, such as to simulate the motion of heart valves [96].

3.1.1. Governing Equations

The motion of the fluid is governed by the conservation of mass, conservation of momentum and the conservation of energy. Since the flow does not involve heat transfer or compressibility, only the conservation equation of mass and momentum need to be solved. The conservation of mass equation can be written as follows:

$$\frac{\partial \rho}{\partial t} + \nabla \cdot (\rho \vec{u}) = S_m$$

Where u is the fluid velocity vector, ρ is the fluid density, and S_m is the source term. Navier-Stokes equation is a equation that describes the conservation of momentum in fluid dynamics. The general form of Navier-Stokes equation takes the form:

$$\frac{\partial}{\partial t}(\rho \vec{u}) + \nabla \cdot (\rho \vec{u}\vec{u}) = -\nabla \mathrm{P} + \nabla \cdot \left(\bar{\bar{r}}\right) + \rho \vec{g} + \vec{F}$$

Where P is the static pressure, $\rho\vec{g}$ is the gravitational body force (due to gravitational acceleration), $\vec{F}$ is the external body force, and $\bar{\bar{r}}$ is the stress tensor given by:

$$\bar{\bar{r}} = \mu\left[(\nabla\vec{u} + \nabla\vec{u}^T) - \frac{2}{3}\nabla\cdot\vec{u}I\right]$$

Where μ is the dynamic viscosity, I is the unit tensor. In a cardiovascular simulation, there is no phase change in the system. Hence the conservation of mass equation can be simplified to:

$$\nabla\cdot\vec{u} = 0$$

Usually, blood is assumed to an incompressible liquid. Where the no-slip boundary condition applies, the Navier-Stokes equation takes the following form:

$$\frac{\partial}{\partial t}(\vec{u}) + (\vec{u}\cdot\nabla)\vec{u} = -\frac{\nabla \mathrm{P}}{\rho} + v\nabla^2\vec{u} + \vec{g}$$

Where $v = \frac{\mu}{\rho}$ is the kinematic viscosity. The term $v\nabla^2\vec{u}$ is the diffusion term.

3.1.2. Hemodynamic Parameters of Interest

The behavior of ECs and SMCs in the aortic wall is regulated by their environment including the physical force sensed by those cells. Different mechanical stress applied to the vascular cells can trigger different signaling pathways and subsequently influence the composition and mechanical properties of the aortic wall.

The response and behaviors of the ECs are regulated by wall shear stress (WSS). WSS is the tangential force per unit area exerted by the blood on the inner wall of the aorta raised from the viscous nature of the blood. WSS τ can be expressed as:

$$WSS = \tau = \mu\left(\frac{\partial u}{\partial y}\right)_{y=0}$$

Where μ is the dynamic viscosity, u is the fluid velocity, and y is the distance to the wall.

To characterize the overall stress level exerted by the blood during the entire cardiac cycle, the time averaged WSS (TAWSS) can be calculated by taking the time average of the WSS at the given location:

$$TAWSS = \frac{1}{T}\int_0^T |WSS| dt$$

Where T is the period of the cardiac cycle.

Early studies on atherosclerosis associate low WSS with atherogenesis and plaque formation. A negative correlation was found between intimal layer thickness and the wall shear rate, suggesting that a high wall shear rate within the physiological range could inhibit intimal thickening [97]. Zarins et al. found that atherosclerosis is more likely to form at a location with low shear stress and diverging flows [98]. Chien et al. found that exposure to shear stress promotes vessel dilation and reduces monocyte adhesion, suggesting that exposure to shear stress might be protective and antiatherogenic [99]. Many other findings suggest that the signal transduction and behaviors of the ECs can be regulated by shear stress [17] [18]. High WSS is shown to be beneficial as it promotes vascular adaptive dilation and prevents ECs dysfunction [19]. ECs dysfunction is an early sign of many cardiovascular diseases such as hypertension and inflammatory disorders [19].

Several studies showed that an abnormally high and asymmetric WSS was found in BAV patients [28] [29] [30]. Bissell et al. found that a combination of high WSS and a disturbed flow pattern is associated with aortic dilation, suggesting that the flow pattern may play an important role in aneurysm formation in BAV patients [100]. More recent findings showed that altered gene expression is associated with high WSS in BAV patients, resulting in medial degeneration in the regions with high WSS [101, 102]. Pasta et al. studied the relation between simulated WSS and the activity of the MMPs and they found that the activity of certain MMPs was positively correlated to systolic WSS in ascending aorta [103]. These findings suggest that a high level of WSS exceeding the physiological range can potentially lead to vascular remodeling and medial degeneration.

Besides the magnitude, the changing in directions of WSS can be characterized by oscillatory sear index (OSI). OSI is calculated as [104]:

$$OSI = \frac{1}{2}\left(1 - \frac{\left|\int_0^T WSSdt\right|}{\int_0^T |WSS|dt}\right)$$

OSI is used to describe the oscillating nature of physiological blood flow. It varies from 0 to 0.5. When the flow is unidirectional in the near wall region, OSI will be 0 for the period. When the blood flow is oscillating and keep changing directions, an OSI close to 0.5 will be observed. Although OSI is a good description of the variation in the flow direction, it is insensitive to the magnitude of the shear stress [105]. Himburg et al. introduced a new parameter called relative resident time (RRT) or particle resident time (PRT) to characterize the residence time of particles [105]. It is the relative time a solute particle spends at the given location. RRT is calculated as:

$$RRT = \frac{1}{(1 - 2 \times OSI) \times TAWSS}$$

A disturbed wall shear stress characterized by high OSI can upregulate the expression of certain genes and cause aortic wall degeneration, whereas a unidirectional laminar flow was shown to be protective [19] [106]. The regional phenotype of ECs can be regulated by local shear stress and demonstrate an anti-inflammatory, anti-proliferation form or atherosclerosis susceptible form [19]. Hwang et al. found that oscillatory shear stress can result in higher oxidative stress in ECs [107]. Himburg et al. found that an increase in OSI can upregulate endothelial permeability [105]. Chen et al. found that disturbed flow characterized by increased OSI results in vascular remodeling [108]. Numata et al. analyzed six patient-specific models and showed that the aneurysm induces a turbulent flow characterized by high OSI [21]. Regions with high OSI are found to be at locations close to the favorite site for entry tear in aortic dissection, relating a high OSI with aortic dissection caused by medial degeneration [21]. Jayendiran et al. analyzed the geometries from two ATAA patients and two healthy patients using CFD and 4D MRI data and showed that there is a strong connection between the hemodynamic parameters and the morphological traits [109]. ATAA patients were found to have lower WSS and higher RRT, and the difference between the patient group and the control group was predicted to increase

continuously over time [109]. Due to those findings, WSS, TAWSS, OSI, and RRT are the most important and recognized hemodynamic parameters used in the evaluation of the flow condition inside the aorta. These parameters were also used in intracranial aneurysm studies and intracranial aneurysm rupture risk predictions [110] [111].

3.1.3. Mechanical Parameters of Interest

Laplace's Law is commonly used in physiology to describe the relationship between the vessel diameter and the wall tension. Laplace's Law for a cylindrical chamber can be written as follows:

$$T = \frac{PR}{h}$$

Where T is the wall tension, P is the pressure, R is the radius, and h is the thickness of the chamber wall. According to this law, a larger diameter means higher stress within the aortic wall. The aortic wall will rupture when the wall stress (WS) exceeds the wall strength. However, due to its complex geometry, Laplace's law cannot accurately predict the stress distribution within the aortic wall. To obtain the stress distribution and assess the risk, FEA can be employed to estimate the WS. Many studies have applied FEA in calculating the stress distribution and found that the initial intimal tears are likely to occur in regions with high WS [112] [31]. Many proposed using the WS estimated by FEA as a viable surgical indicator. To obtain a good estimation, the mechanical property of the aortic wall must be determined. The mechanical property of the aortic wall varies a lot from patient to patient. Usually, an average material property was used in FEA studies. Those properties are usually obtained from direct measurements of tissue obtained in surgeries or estimated from 4D imaging data through parameter optimization. Azadani et al. used biaxial stretch tests to measure the aortic tissue stiffness and found that tissue obtained from ATAA patients was much stiffer than normal controls [113]. ATAA tissue stiffness was positively correlated with diameter [113]. The wall stiffness and WS can also be obtained using 4D imaging and FEA [15] [16]. Usually, a model was established using the reconstructed 3D geometries and simulated with different parameters until the output results match the *in vivo* measurement. By optimizing the model parameter, a good estimation of the aortic wall properties can be obtained.

The wall strength is another parameter of interest although it cannot be measured or estimated in vivo. Studies showed that aortic wall strength can have large variations from one region to another [114]. But in general, tissue from ATAA patients was stiffer and less strong than tissue from non-aneurysmal aortas [115]. It is reasonable to assume that higher regions with high WS have a higher risk of rupture or dissection.

3.2. Computational Methods with Patient-Specific Model

To apply those computational methods in the study of ATAA and to calculate the parameters of interest, a patient-specific model of the computational domain must be established. Then by applying *in vivo* measured boundary conditions or idealized boundary conditions, the biomechanical and hemodynamic parameters of interest can be obtained.

The patient-specific geometry is usually reconstructed from medical images acquired by CT or cardiovascular MRI. These images are usually in the format of DICOM (Digital Imaging and Communication in Medicine) format with a predetermined slice thickness. Then, segmentation software can be employed to convert the sequenced images into 3D models. Commonly use commercial segmentation software includes Materialize Mimics (Materialise, Leuven, Belgium) and ImFusion Suite (ImFusion GmbH, Munich, Germany). There are also open-source packages such as SimVascular [38]. After translating the 2D images to 3D geometries, the reconstructed geometries need to be discretized into finite elements. This step is called meshing. Before discretizing, the converted geometries need to be fixed and optimized to eliminate small protrusions or defects. Those small defects are often due to motion or imaging artifacts, and they will affect the mesh quality and final results. Segmentation software has built-in tools to minimize or eliminate those artifacts. The fix can also be done in the meshing software or other CAD tools.

After optimizing the geometry, commercial CFD and FEA packages can then be used to generate meshes from the reconstructed geometries and mathematically solve the governing equations of the physical processes with appropriate boundary conditions and material properties applied. Ansys Fluent (Ansys Inc, Canonsburg, U.S.), Ansys Mechanical (Ansys Inc, Canonsburg, U.S.), OpenFOAM (The OpenFOAM Foundation, London, U.K.), Abaqus (ABAQUS Inc., Providence, U.S.), and SimVascular are the most used simulation tools in cardiovascular research. Most

packages have integrated post-processing tools for parameter calculation and visualization. The contour plots for each parameter and velocity streamlines can then be generated and analyzed or compared with *in vivo* measurements.

CHAPTER 4. MATERIALS AND METHODS

A flow chart for the process used in this study is shown in **Figure 2**. CT scans of the patient were first obtained from the hospital's database. The sequenced imaging data was first imported into Materialise Mimics (Materialise, Leuven, Belgium) for surface reconstruction. Next, the converted surface model in STL format was imported to Ansys SpaceClaim (Ansys, Canonsburg, U.S.) for pose processing. The processed model can then be used to generate meshes for simulation.

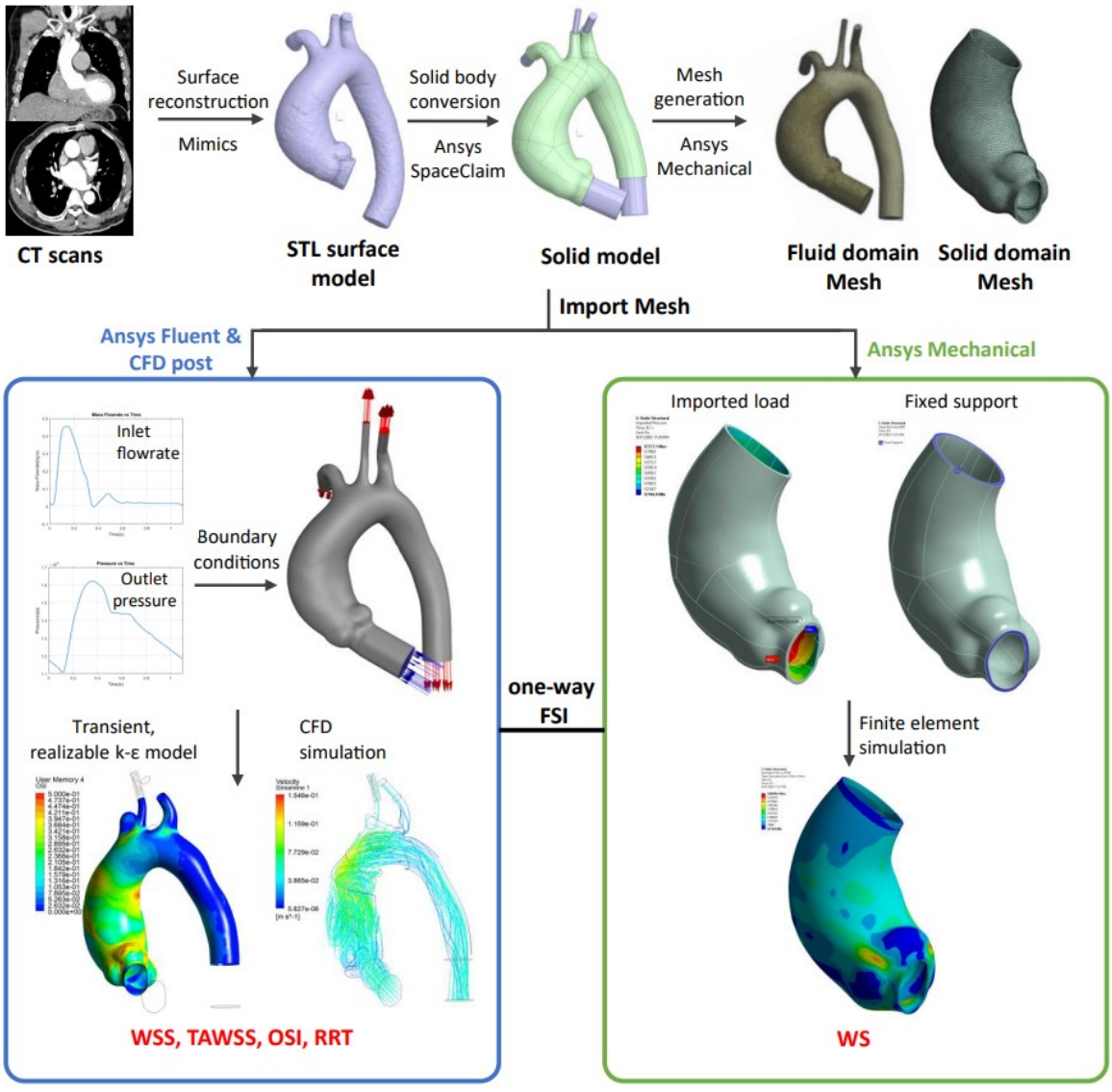

Figure 2. The fluid-structure interaction flow chart

One-way FSI was performed in this study. The mesh of the fluid domain was first imported to Ansys Fluent 2022R1 (Ansys, Canonsburg, U.S.). General boundary conditions were applied to the model. The transient simulation was run over the entire cardiac cycle to obtain the key hemodynamic parameters including WSS, TAWSS, OSI, and RRT. The contour plots for each parameter and the streamlines for the blood flow were also generated. Then the load obtained in Ansys Fluent was imported into Ansys Mechanical (Ansys, Canonsburg, U.S.) as boundary conditions. FEA was then performed with the applied boundary conditions to obtain the mechanical stress within the aortic wall.

4.1. Patient Data Acquisition

This study was approved by the Institutional Review Board of Guangdong Provincial People's Hospital (ID number: KY-Z-2022-218-01). The study cohort included 100 consecutive patients with no past aortic intervention in the CTA database (2019-2021) of Guangdong Provincial People's Hospital. Patient data labeled with thoracic aortic dilatation and/or thoracic aortic aneurysm were included in the search criterion. Patients with age under 18 years or with acute aortic syndrome were excluded from this study. In this cohort, 68 patients received cardiovascular surgery. The CT image data were obtained through ECG-gated CT scanning. Patient data was stored in DICOM format in the database.

4.2. Data Preprocessing

4.2.1. Reconstruction of Patient Specific Geometries

The geometry of the aorta is generated from DICOM data obtained via CT scans. Commercial segmentation software Mimics was used to extract the contours and generate the 3D surface of the entire aorta including a small segment of the brachiocephalic artery, the left subclavian artery, and the left common carotid artery. The coronary arteries were omitted since they are not of interest to this study. This process is semiautomatic. To convert the stacked CT images to a 3D geometry, first, a mask was created based on the selected grey scale threshold. Then, the region growing tool in Mimics was used to isolate the masked regions. Only the main aortic lumen needs to be preserved; Whereas other small parts or unconnected parts were excluded. After the mask for the aortic lumen was finalized, it was then converted to a 3D geometry by

Mimics automatically. The contours of the converted geometry were adjusted manually to better fit the actual geometry. After the adjustments, the converted 3D geometry was exported in STL format for further processing. This process was applied to all 100 cases.

Although the Mimics package includes built-in tools for model postprocessing like smoothing, they were not used in this process. Instead, the exported STL files were processed using another commercial solid modelling CAD package Ansys SpaceClaim 2022 R1. In SpaceClaim, defects of the STL files were manually fixed, and small peaks and protrusions were smoothed out to create a model with a smooth surface. As shown in **Figure 3**, (a) is the original STL file imported into SpaceClaim and (b) is the smoothed surface model. Some CT image sets have more artifacts, resulting in a less smooth surface than others. Manual fixes were required to ensure that all models have the same quality for mesh generation.

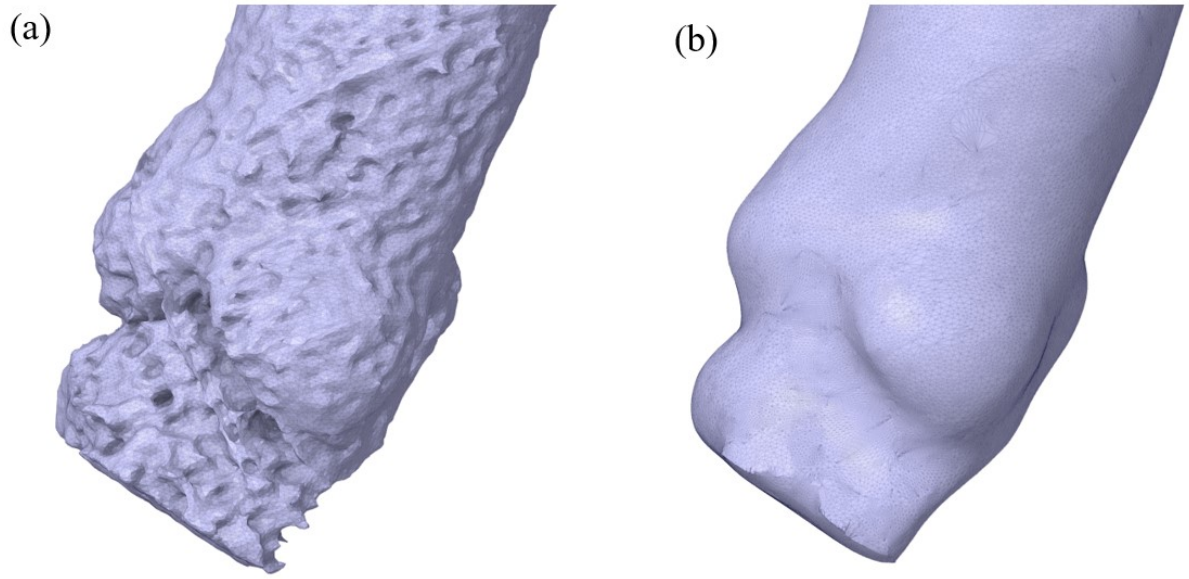

Figure 3. *Comparison between the surface of the automatically generated geometry (a) and the smoothed geometry (b).*

The flow chart of the optimization process is shown in **Figure 4**. First, the STL file was imported SpaceClaim as a faceted body. Obvious holes or protrusions were manually fixed. Then, the smoothing tool was used to smooth the surface out. Next, the auto-fixing tool was employed to fix overlapped faces and holes so the thicken tool can be applied to the model to create the aortic wall in the following steps. The lower part of the descending thoracic aorta was removed to reduce the computational cost since the lower part of the descending thoracic aorta is not of

interest to this study. The inlet and the outlets at the branched arteries were cut open. The artery wall with a uniform thickness of 1.5mm [23] [116] was created using the thicken tool in SpaceClaim. The extrusion direction was outward since the inner wall of the aorta was used during segmentation (the inner wall is more clearly imaged during CTA scans).

Then, the aortic wall was shrink-wrapped which eliminates sharp edges and makes the entire surface smooth by unifying the face size. The shrink-wrap face size was set to 0.7mm to 0.8mm depending on the distance between branched arteries. Auto skin tool was then employed to convert the faceted body to a solid body (shown in green in **Figure 4**) consisting of spline surfaces. The inlets and the outlets were trimmed to create flat surfaces. Volume extraction tools were then used to create the fluid domain for CFD analysis by constructing another solid (shown in orange in **Figure 4**) body for the aortic lumen.

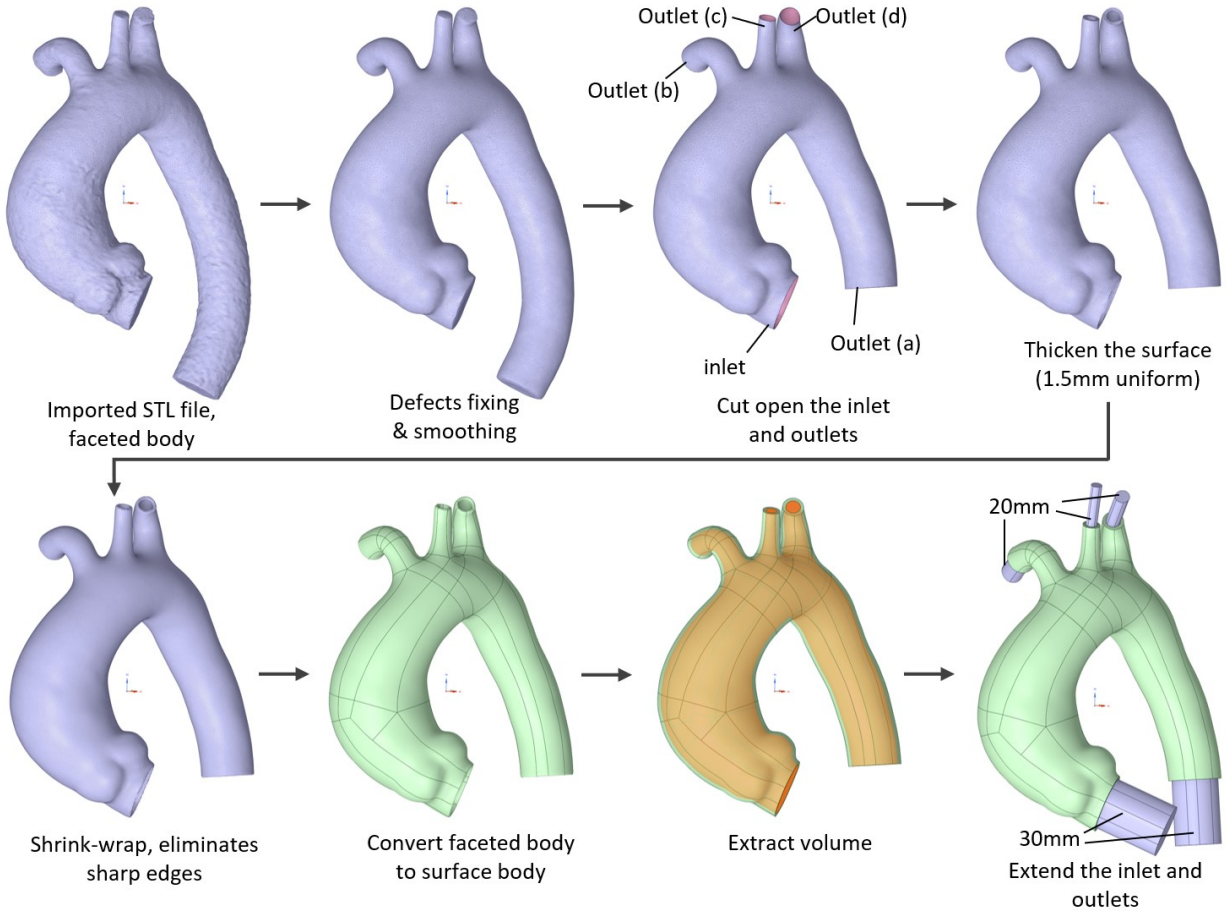

Figure 4. *Fow chart of the geometry post-process.*

The inlet and the outlet of the fluid domain were extended in directions perpendicular to the trimmed surfaces. The inlet and the outlet at the descending aorta were extended by 30 mm and the outlets at the brachiocephalic artery, the left common carotid artery, and the left subclavian artery were extended by 20 mm. The flow extensions are required to obtain a full development flow as the flow enters the simulation domain of interest. The outlet flow extensions also help to prevent recirculation and the backflow of the fluid. This improves the convergence of the solution.

The fluid domain and the solid domain were then divided into the ascending part and the part containing the aortic arc, the descending part, and the branched arteries. Since we were more interested in the results related to the ascending part of the artery. Splitting the geometries allow easy calculation for TAWSS, OSI, and RRT of the ascending aorta. Each part of the model was then named and saved in a single SCDOC file (SpaceClaim document file).

4.2.2. Determination of Morphological Parameters

The morphological parameters of the ascending aorta were obtained after the geometry reconstruction. For each case, the maximum diameter of the ascending part, the diameter of the Sinuses of Valsalva, the diameter of the Sinotubular junction, AAL, ascending aortic curvature, ascending aortic volume (AAV), and maximum cross-sectional area of the ATAA were measured from the 3D model as shown in **Figure 5**. The maximum diameter and the maximum cross-sectional area were measured at the location where the aortic perimeter was at its maximum (plane 2). The length of the perimeter was measured using the measurement tool in SpaceClaim and the diameter was calculated based on the measured value. Similarly, the diameter of the Sinuses of Valsalva and the diameter of the Sinotubular junction were calculated based on the perimeter measured at the Sinuses of Valsalva (plane 4) and the Sinotubular junction (plane 3). AAL was measured from the origin of the innominate artery (plane 1) to the aortic annulus (plane 5). Ascending aortic curvature can be obtained by measuring the angle between plane 1 and plane 5. To measure AAL, a spline was first created by connecting the center point of a serious cross-sectional plane as the approximate centerline of the aorta. The length of the spline was directly measured using the measurement tool. AAV was the volume of

the segment containing the ascending thoracic aorta and the Sinuses of Valsalva, as shown in **Figure 5** (c). AAV was directly measured using the mass properties tool in SpaceClaim.

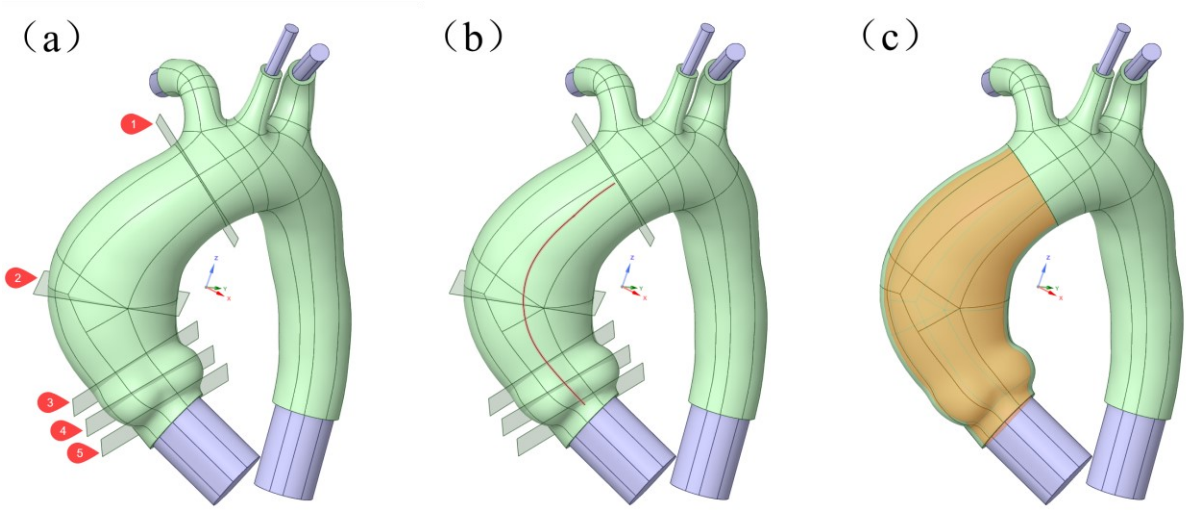

Figure 5. *Locations where morphological parameters were obtained. (a) Plane 1: Cross-sectional plane at the origin of the innominate artery; Plane 2: Cross-sectional plane at the location where the diameter is maximum; Plane 3: Cross-sectional plane at Sinotubular junction; Plane 4: Cross-sectional plane at Sinuses of Valsalva; Plane 5: Cross-sectional plane at aortic annulus; (b) center line of the aorta; (c) The AAV measurement range is highlighted in orange.*

In clinical practice, the maximum diameter is defined as the maximum diameter of the entire ascending aorta including the aortic root. So, the values measured at plane 2 were compared with the value measured at plane 4 and the larger one was taken to be the maximum diameter of the entire ascending aorta.

The measurements of the key morphological parameters were performed by two people, and the results were compared to determine consistency. The maximum diameter was measured from the original CT data and the reconstructed geometries. There were no significant discrepancies between the measurements. This means that the reconstruction process did not introduce significant morphological changes to the aortic geometries.

4.3. Meshing

After the STL files were converted to SCDOC files, the simulation domains need to be discretized into finite elements. Tetrahedron elements were generated for both the fluid and the solid domains in Ansys Mechanical 2022 R1 (Ansys, Pennsylvania, U.S.). Meshing is critical in CFD and FEA as the element size and structure must be carefully selected to obtain accurate results.

4.3.1. Wall y+ and Boundary Layer

Since in the CFD simulation, we were interested in the variation of properties associated with the aortic wall such as the WSS and the pressure, a prism boundary layer needs to be created at the aortic wall to capture the near-wall physics. The thickness of the prism layer was determined based on the wall y+ value.

The boundary layer of the turbulent flow consists of three layers: the viscous sublayer (viscous shear dominates), the log layer (highly turbulent), and the outer layer (turbulent shear dominates). The velocity profile in the near wall region takes a predictable form if scaled variables were used. Wall y+ is a dimensionless value used to measure the distance to the wall. Wall y+ is defined as:

$$y^+ = \frac{yu_\tau}{v}$$

Where y is the absolute distance to the wall, u_τ is the friction velocity, and v is the kinematic viscosity. The friction velocity can be calculated by:

$$u_\tau = \sqrt{\frac{\tau_w}{\rho}}$$

Where τ_w is the WSS, ρ is the fluid density.

The velocity profile changes rapidly in the region close to the wall. Since we were interested in obtaining WSS and several parameters calculated based on WSS, the velocity gradient must be resolved accurately in the near-wall region. Two methods can be used to obtain an accurate

velocity profile: using standard wall functions or fully resolving the viscous sublayer. Since the velocity profile takes a predictable form in the boundary layer, wall functions can be used to determine the velocity gradient at the wall. To use wall functions, the centroid of the cell adjacent to the wall needs to be in the log layer. It is recommended to have a y+ value between 30 to 300 [117]. Another method is to fully resolve the viscous sublayer. The first cell adjacent to the wall needs to be close to 1 with the prism layers having a growth ratio smaller than or equal to 1.2 [117].

Due to the small size of the aorta, it was not possible to use wall functions to obtain the velocity gradient. Hence, the thickness of the first layer of cell must be selected to make sure they have a y+ value approximately equals to 1. A randomly chosen case was simulated with a very fine mesh at peak inlet flow rate. According to the definition of y+, the absolute distance y needs to be smaller for larger u_τ to make sure that y+ equals to 1. By using the peak inlet flowrate in simulation, we can make sure that the y+ for the cells near the first layer is close to 1. Then first layer cell thickness can be calculated using the simulation results.

The thickness of the first layer cells of the inflation layer was determined to be 0.15 mm. By selecting this value, most cells in the first inflation layer will have a wall y+ value approximately equal to 1, which ensures good velocity gradient profile resolution near the wall. 7 prism layers were generated with a growth ratio of 1.2. The wall y+ value for the first layer cells near the wall for a representative case at t = 0.1s is shown in **Figure 6**.

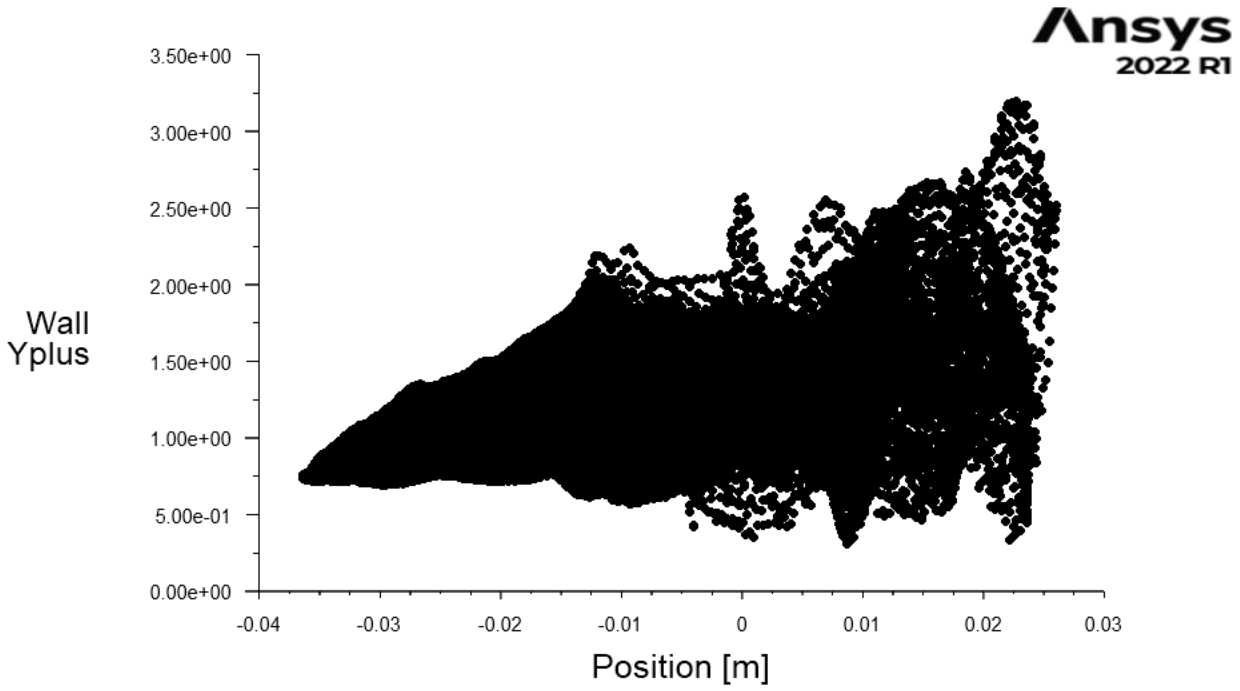

***Figure 6**. Plots of wall y+ value of the first layer cells at t = 0.1s.*

4.3.2. Mesh Independent Test

A mesh independence study was performed to find the optimal size of the mesh. In general, the size of the mesh will affect the computation time and the accuracy of the simulation results. A coarse mesh has a lower computational cost, but it will introduce discretization error to the simulation results. A finer mesh allows the simulation results to be more accurate, but it will increase the computation time significantly. Hence, a mesh independence test is required to find the optimal size of the mesh which allows the model to have a minimized number of cells without introducing a significant discretization error in the simulation results [118]. Since the shapes and features of the human aortas are similar, a randomly selected aortic geometry from the 100 cases was used in the mesh-independent test.

For the fluid domain, the body size and the surface size of the mesh were varied. Whereas the parameters related to the inflation layer were fixed since those parameters were derived from the wall y+ value (first layer thickness 0.15mm, inflation ratio 1.2). The brachiocephalic artery, the left subclavian artery, and the left common carotid artery have small diameters. Depending on the geometry, the diameter of the branched artery can be as small as 2~3mm. Hence, a finer

mesh was created for the three branched arteries and the bifurcation region for better resolution. 1.2 mm fixed element size was used in the bifurcation region and for the branched arteries. Meshes with consecutive element numbers were generated, with approximately 0.4 to 4.6 million elements for the fluid domain. The settings for each mesh were given in **Table 2**.

Transient simulations were run for 0.1s using a timestep of 0.005s. Average WSS, maximum WSS, average pressure, and maximum pressure were monitored during the process. The result at the last time step (t = 0.1s) was used for comparison between different meshes. The simulation results including average WSS, maximum WSS, average pressure, and maximum pressure (**Table 2**).

Table 2. *Mesh settings, element numbers and simulated hemodynamic parameters at t = 0.1s for the mesh independent test*

Mesh number	Body Size (mm)	Face Size (mm)	Element number (*10^6)	Average WSS (Pa)	Maximum WSS (Pa)	Average pressure (Pa)	maximum pressure (Pa)
1	1	0.6	4.6	1.861	28.62	13800	13890
2	1.2	0.6	3.3	1.861	28.8	13770	13860
3	1.5	0.6	2.5	1.862	28.62	13800	13900
4	1.6	0.6	2.3	1.861	28.81	13790	13880
5	1.8	0.6	2.1	1.861	28.8	13780	13880
6	2	0.6	1.9	1.861	28.8	13800	13900
7	2.5	0.8	1.8	1.861	28.61	13810	13900
8	3	0.8	1.7	1.861	28.8	13810	13900
9	2	0.7	1.6	1.929	27.19	13800	13900
10	2	0.8	1.4	1.929	27.19	13800	13890
11	2	1	1	1.926	25.47	13800	13900
12	2	1.5	0.8	1.864	27.01	13770	13870
13	2	2	0.7	1.782	19.25	13770	13870
14	2.5	2.5	0.5	1.694	17.26	13730	13830
15	2.3	3	0.4	1.347	9.821	13790	13880

The results of the test are shown in **Figure 7**. Average WSS and maximum WSS converged to a fixed value. Average pressure and maximum pressure showed some fluctuation, but the fluctuation is relatively small compared to the overall pressure value.

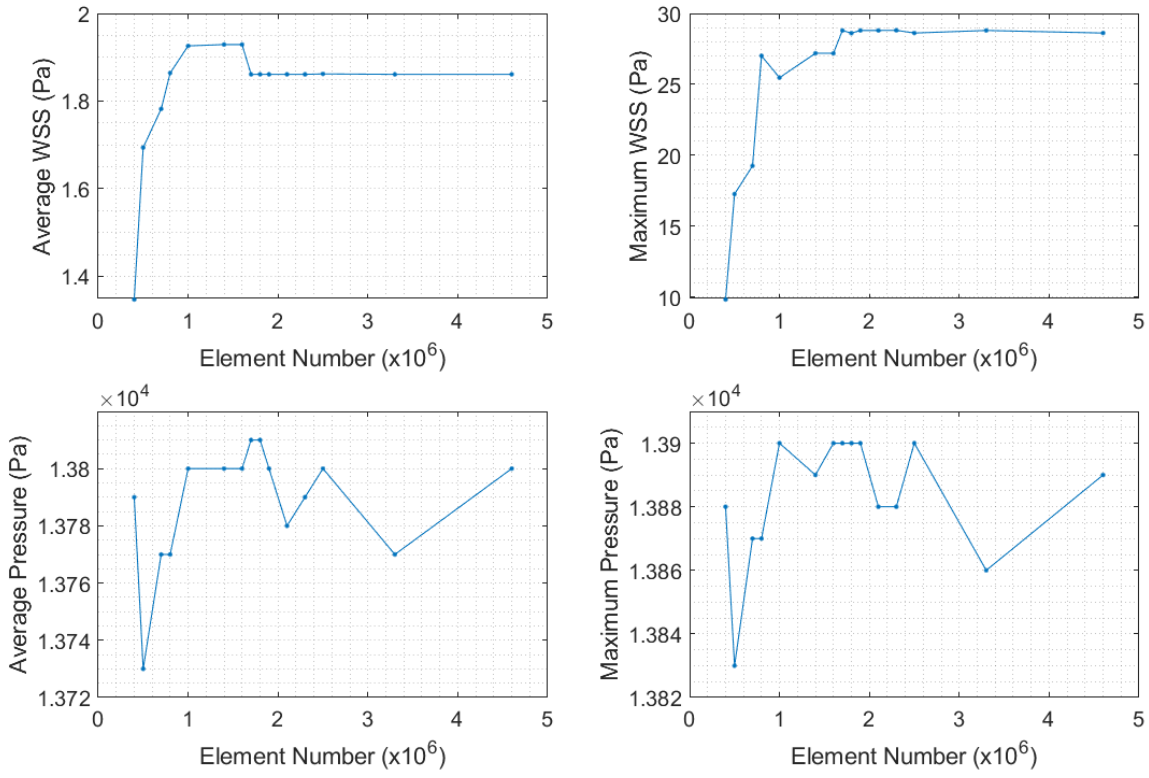

Figure 7. *Average WSS, Maximum WSS, average pressure, and maximum pressure obtained when meshes with different elements number were used.*

The percentage difference between the results obtained using coarser mesh and the result obtained using the finest mesh was then calculated (**Figure 8**). The effect of changing mesh size reduces with the increase in element count. The percentage variations of the pressure and WSS between the mesh with elements > 1 million were relatively small. The percentage variation in pressure was always smaller than 1%. Since the same mesh settings need to be generalized to other geometries, the mesh with approximately 1.9 million elements was selected as a good balance between the computational cost and the result accuracy. Since the geometries were different for different cases, approximately 0.8 to 2 million elements were generated for different cases depending on the volume of the simulation domain (~1 million on average).

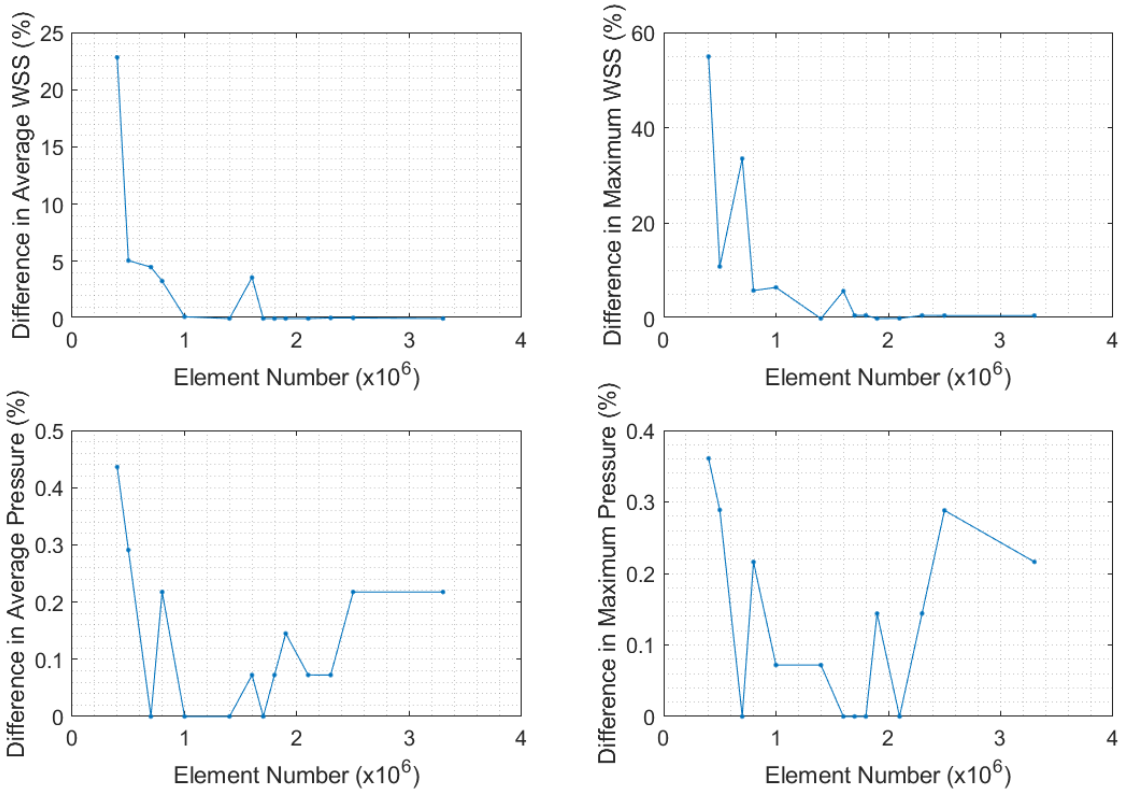

Figure 8. *percentage difference in average WSS, Maximum WSS, average pressure, and maximum pressure between meshes with consecutive element numbers.*

For the solid domain, uniform tetrahedron mesh with different sizes was generated. Meshes with approximately 10000 to 0.4 million elements were generated for the solid domain. The CFD simulation was first performed using the selected mesh setting where the body size is set to 2 mm, and the face size is set to 0.6 mm. The load obtained from the CFD simulation with the selected mesh size was imported and used in the mesh-independent test. Maximum WS and average WS were reported in **Table 3**.

Table 3. *Mesh settings, element numbers and simulated biomechanical parameters at t = 0.1s for the mesh independent test*

Mesh number	Body Size (mm)	Element number (*10^6)	Average Equivalent Stress (Pa)	Maximum Equivalent Stress (Pa)
1	1	357005	2.25E+05	8.58E+05
2	1.2	221540	2.25E+05	8.46E+05
3	1.5	98373	2.25E+05	8.36E+05

4	2	43159	2.26E+05	8.24E+05
5	3	37943	2.25E+05	7.85E+05
6	3.5	14082	2.25E+05	7.71E+05
7	4	11041	2.24E+05	7.61E+05

WS and its percentage variation were plotted in **Figure 9** and **Figure 10**, respectively. The mesh with 0.1 million elements was selected to make the percentage variation smaller than 1%. Depending on the geometry, approximately 0.04 to 0.11 million elements can be generated for different cases depending on the volume of the simulation domain (~0.05 million on average).

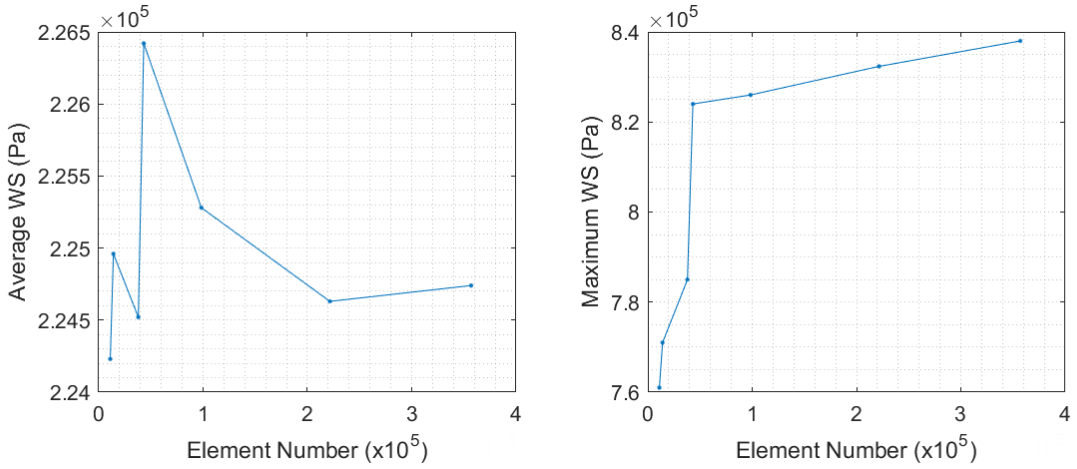

Figure 9. *Average WS and Maximum WS obtained when meshes with different elements number were used.*

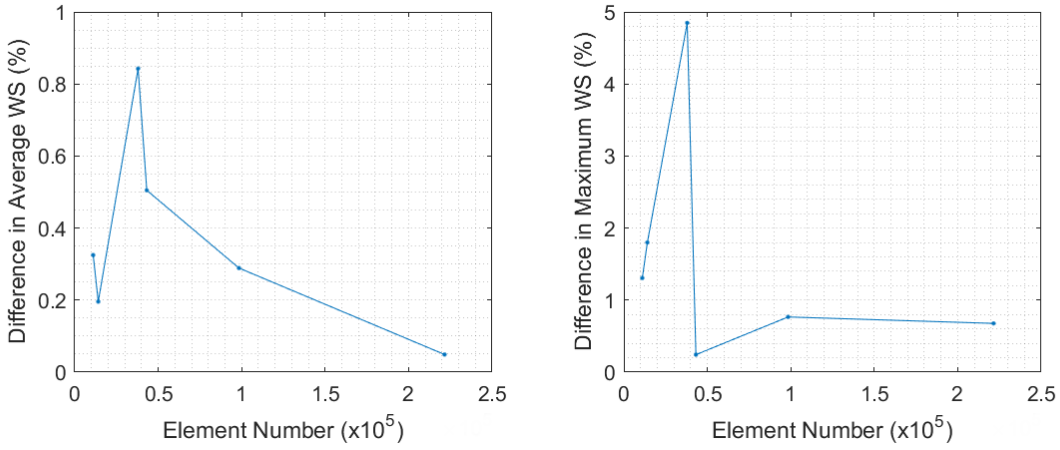

Figure 10. *Percentage difference in average WS and Maximum WS between meshes with consecutive element numbers.*

4.3.3. Mesh Generation for Patient Specific Geometries

For the ascending part of the aorta, 7 prism layers were generated with a first layer thickness of 0.15 mm and a growth ratio of 1.2. The surface element size was set to 0.6 mm. The body element size was 2 mm for both the ascending and the descending parts. 1.2 mm element size was used for the bifurcation region and small branches. **Figure 11** shows the fluid domain mesh. **Figure 12** is a cross-sectional view of the mesh for the ascending aorta, showing the prism layers. **Figure 13** is the mesh for the branched arteries, showing the smaller elements near the bifurcation region. For aortic wall, the mesh size was set to 1.5 mm uniform. **Figure 14** shows the mesh generated for the ascending aortic wall.

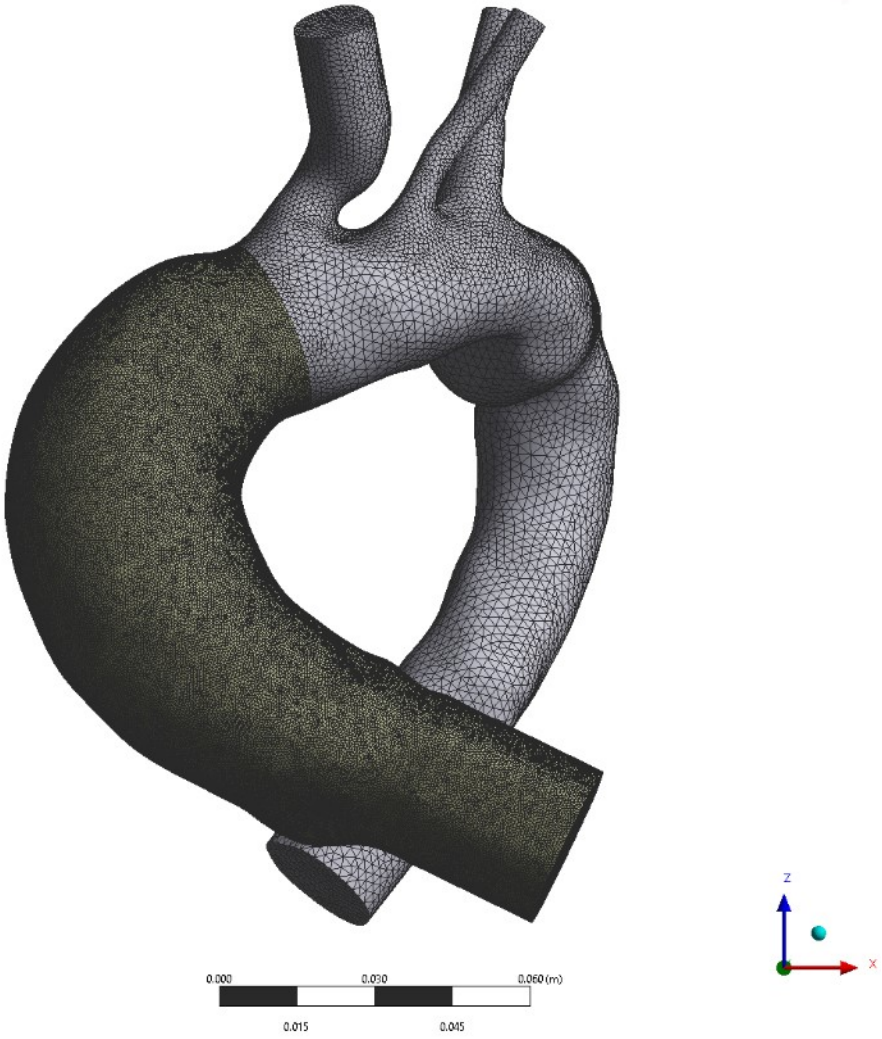

Figure 11. *Generated mesh for the entire fluid domain including the extended inlet and outlets. The mesh was divided into the ascending part (yellow) and the descending part (gray).*

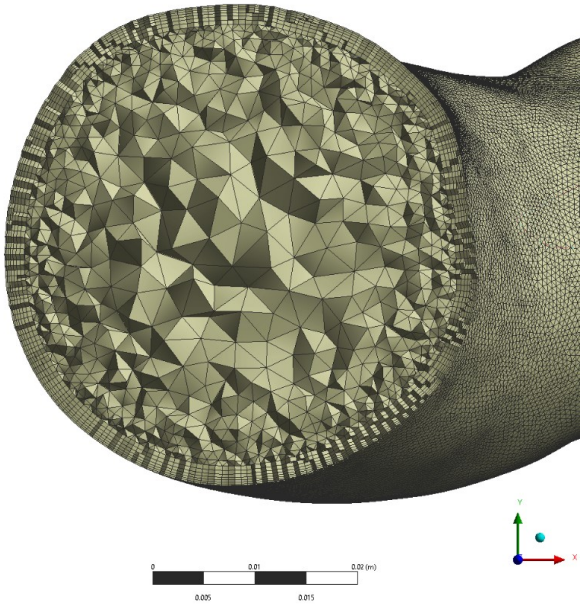

Figure 12. *Cross-sectional view of the mesh for the ascending part of the aorta.*

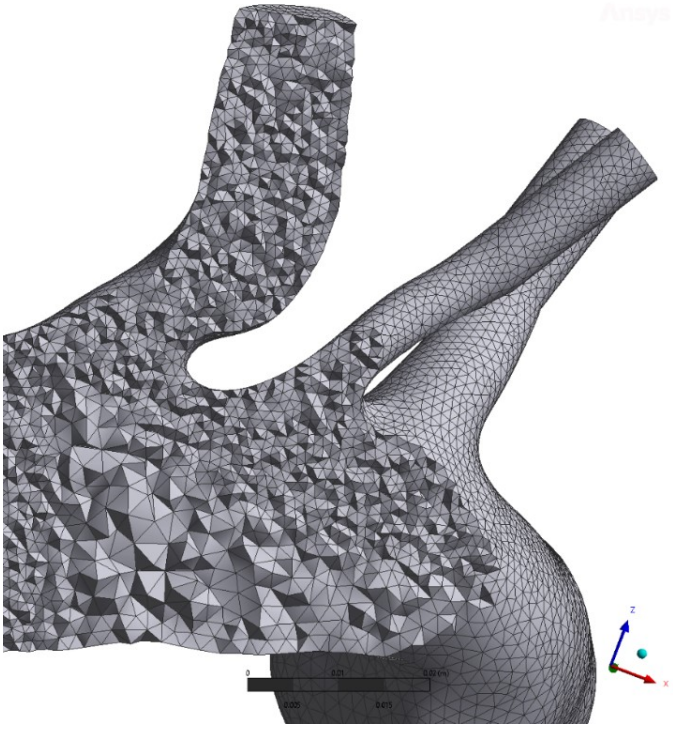

Figure 13. *Mesh near the bifurcation region.*

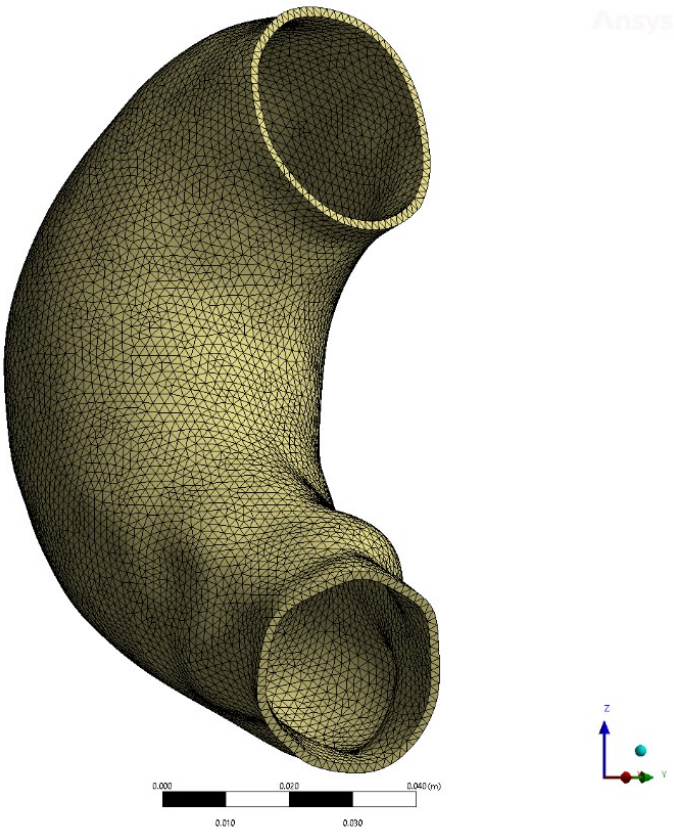

Figure 14. *Mesh for the ascending aortic wall.*

Orthogonality, skewness, and aspect ratio are the three most important parameters in measuring mesh quality. Orthogonality refers to the angle between adjacent surfaces of one finite element. The skewness of an element is a measure of the deviation of the actual cell size from the optimal cell size. The aspect ratio is defined as the radius ratio of circumscribed to inscribed circles. Meshing with highly skewed cells may result in inaccurate or even divergent solutions. Hence, the generated meshes were refined iteratively to improve elements with low quality. The orthogonality of the generated mesh was kept above ~0.2 and the skewness was kept below ~0.8 whenever possible for each generated mesh. Mesh refining function was employed to improve mesh quality.

4.4. Computational Modeling of ATAA

The fluid flow was simulated using the Ansys Fluent 2022 R1 and the static structural simulation was performed in Ansys Mechanical 2022 R1. The two systems were one-way coupled through

Ansys Workbench 2022R1. The solution of the fluid domain was transferred as boundary conditions to the solid domain.

4.4.1. Fluid Model

To mathematically simulate the blood flow, assumptions on the physical properties and the boundary conditions have to be made. Blood rheology is one of the most important factors in building the fluid model. Blood is a mixture suspending blood cells, platelets, and plasma. The properties of the blood are largely affected by blood cells. The dynamic viscosity of blood increases with the hematocrit which is the volume percentage of red blood cells in blood [72].

There are two popular models for blood. One is the Newtonian model, and another is the shear-thinning model. The Newtonian model assumes the blood has constant viscosity, which means that there is a linear relationship between the shear stress and strain. The shear thinning model describes a changing viscosity with the shear rate. At a low shear rate (typically lower than $100\ s^{-1}$ [119]), red blood cells aggregate and stack (rouleaux formation), resulting in a high blood viscosity. Whereas with the increase in shear rate, rouleaux formation reduces and the blood viscosity decreases. This behaviour is known as shear-thinning. The Carreau model and Ballyk model are the two most used non-Newtonian models for blood flow simulation.

Although non-Newtonian is a more accurate description for blood rheology, the non-Newtonian behaviour is only significant in small capillaries where the shear rate is relatively low, and the dimension of the vessel is comparable to the blood cells [120]. In large vessels, the non-Newtonian behaviour of blood can be neglected, and the blood can be assumed to be a Newtonian fluid [120]. Long et al. showed that at a shear rate higher $50\ s^{-1}$, which is approximately the physiological flow rate in large arteries, blood behaved like Newtonian fluid [121]. Additionally, rouleaux formation requires a relatively long time (a few seconds) after the shear rate drop, whereas the disaggregate process is relatively fast [122], suggesting that rouleaux formation is unlike to occur in large arteries with a pulsatile blood flow. An image-based CFD simulation on carotid artery bifurcation compared the simple Newtonian model and two other shear-thinning models (Carreau-Yasuda Model and Ballyk Model), showing that the Newtonian model is a reasonable assumption for large arteries [123]. Soulis et al. Compared the Newtonian model and non-Newtonian model in CFD analysis of a reconstructed aortic model

and showed that both models produced consistent patterns for TAWSS, OSI, and RRT, suggesting that the Newtonian model is a good approximation in CFD analysis of ATAA [124]. Hence in our analysis, blood was assumed to be a Newtonian and incompressible fluid with a density of $1060 kg/m^3$ and a dynamic viscosity of 0.0035 [125] [126, 127]. This assumption is valid since the shear rate is sufficiently high and the blood vessel diameter is much larger than the blood cells [128].

4.4.2. Boundary Conditions

Transient analysis was performed to capture the pulsatile nature of the blood flow. Flowrate measured by MRI is often used as boundary conditions. However, in this study, patient-specific flow rate measurements were not available. Hence, a general inlet flow rate and outlet pressure were used in this analysis. The inlet volumetric flow rate was measured in the ascending aorta of a healthy male with no known cardiac disease using MRI during a 1.1s period (one cardiac cycle) [129]. The outlet pressure is the pressure measured during the same period of time [129]. These boundary conditions were used in multiple similar studies [125] [130]. The measured inlet volumetric flow rate was converted to the mass flow rate. The inlet mass flow rate and the outlet pressure are shown in **Figure 15**. A uniform mass flow rate was assumed across the inlet and the flow direction was assumed perpendicular to the inlet plane. The expended inlet makes sure a fully developed parabolic velocity profile is achieved before the blood enters the simulation domain of interest. Similarly, the measured pressure was imposed on the outlets. A non-slip wall boundary condition was used, and the aortic wall was assumed to be rigid in this one-way FSI analysis.

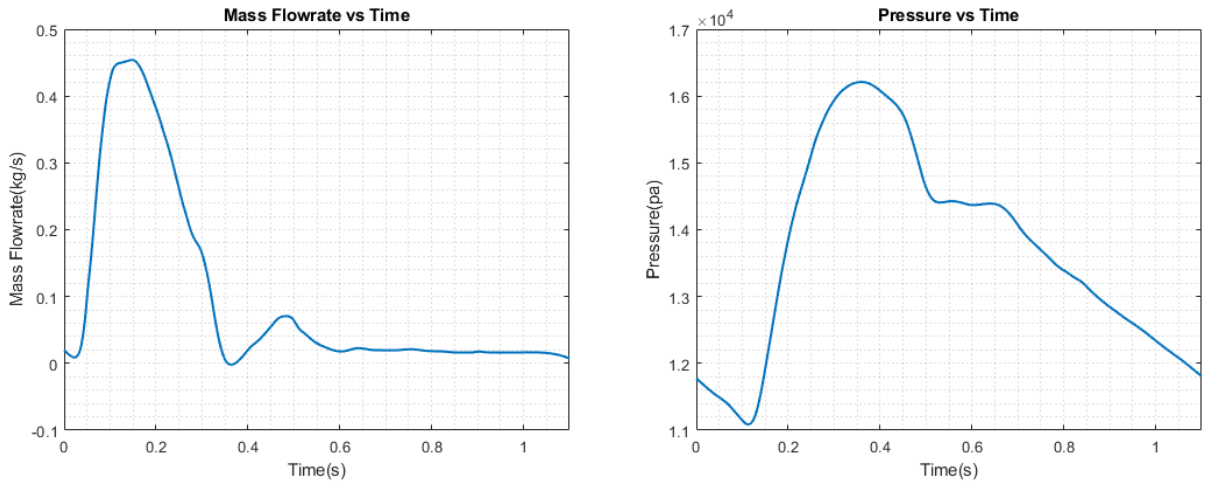

Figure 15. *Inlet mass flowrate (kg/s) and outlet pressure (pa) during the 1.1s cardiac cycle.*

4.4.3. Solver Configuration

Ansys uses the FVM to solve the governing equations of fluid motions. The default pressure-based solver was used. For a pressure-based solver, the way that pressure and velocity are updated is controlled by the pressure-velocity coupling scheme. The Pressure-Implicit with Splitting of Operators (PISO) algorithm with neighbour correction was used as it is recommended for all transient flow simulations [117].

Flow can be classified as either laminar, transitional, or turbulent. The type of flow depends on the speed of the flow and the dimensions of the fluid domain. Reynolds number is a dimensionless parameter which is often used as the criterion to determine whether the flow is laminar or turbulent. The Reynolds number is defined as:

$$Re = \frac{\rho L u}{\mu}$$

Where ρ is the mass density of the fluid, L is the characteristic dimension of the system, u is the fluid velocity, and μ is the dynamic viscosity of the fluid. A system with a Reynolds number smaller than 2300 is likely dominated by laminar flow. Whereas a Reynolds number greater or equal to 2300 usually indicates that the system is dominated by transitional or turbulent flow. The estimated Reynold number at the peak systole velocity is larger than 2300. Hence a turbulent model must be used to capture the nature of the high-velocity turbulent flow.

Three methods can be used to solve a turbulent flow. They are the direct numerical simulation (DNS), large eddy simulation (LES), and the Reynolds averaged Navier-Stokes (RANS) simulation [117]. The DNS method numerically solves the unsteady Navier-Stokes equation with the whole spectrum of turbulence resolved. However, this usually requires an excessive amount of computing power and is practically unattainable. The LES method solves a filtered Navier-Stokes equation where a portion of the turbulence is filtered out. In the RANS simulation, all the turbulence is time-averaged to obtain a velocity field and pressure field varying smoothly. In this method, all the turbulent motions are modeled, and an averaged behavior is obtained. Since in most applications, we only care about the average behavior of the turbulent flow, this method is widely used in many commercial CFD packages including Fluent. To obtain the RANS equation, the variables are decomposed into the average component and the fluctuating component. By substituting these expressions into the instantaneous continuity and momentum equation and taking the average, the RANS equation with an additional Reynolds stress tensor term can be obtained [131]. The Reynolds stress tensor term can be modeled in different ways. In this study, the realizable k-ε was selected. Since the viscous sublayer needs to be fully resolved, the Enhanced Wall Treatment (EWT) option was enabled to resolve the viscous sublayer.

The transient simulation was selected. The time step used in the simulation is 0.001s constant. The Courant-Friedrich-Lewy condition requires that any information travels during one timestep within the mesh must be smaller than the distance between two adjacent mesh elements. This leads to the definition of the Courant number C:

$$C = \frac{u\Delta t}{\Delta x}$$

Where u is the velocity, Δt is the time step size, and Δx is the distance between two adjacent cells. To satisfy the CFL condition, the Courant number must be kept below 1. A Courant number exceeding 1 may result in the divergence of the solution. The maximum velocity is estimated to be $1.1 m/s$ in the inlet flow extension region. The element size is 2mm in the center of the domain and 1.2mm in the region closer to the wall. All the other regions in the simulation domain will have lower velocities than the inlet region. So, a time step of size 0.001s is small enough to keep the Courant number below 1.

Finally, the convergence criteria must be selected for the solver to judge the convergence of the solution. The absolute convergence criteria were 10^{-6} for velocities and 10^{-3} for continuity, k, and epsilon. Since it is possible that a poor initial guess will result in a very high residue and a 10^{-3} drop in residual does not guarantee convergence, the residuals were monitored during the solving process to make sure that they decrease for tens of iterations before the solver conclude that the solution has converged [117]. According to the observation, for most time steps, the solution converges within approximately 150 iterations, so the maximum iteration is set to 200.

4.4.4. Solid Model

In the solid domain simulation, fixed supports were applied at the cross section at the aortic annulus and the region near the brachiocephalic artery. Other parts were unconstrained. The aortic wall was assumed to be uniform and incompressible. An isotropic elastic model was used for the aortic wall. The Young's modulus was set to 1.7 MPa and the Poisson's ratio was 0.45 [116]. The load applied by the fluid inside the blood vessel to the artery wall was directly transferred from the fluid domain simulation. Figure 12 shows the transferred load from the fluid domain. The equivalent stress and the total deformation were reported.

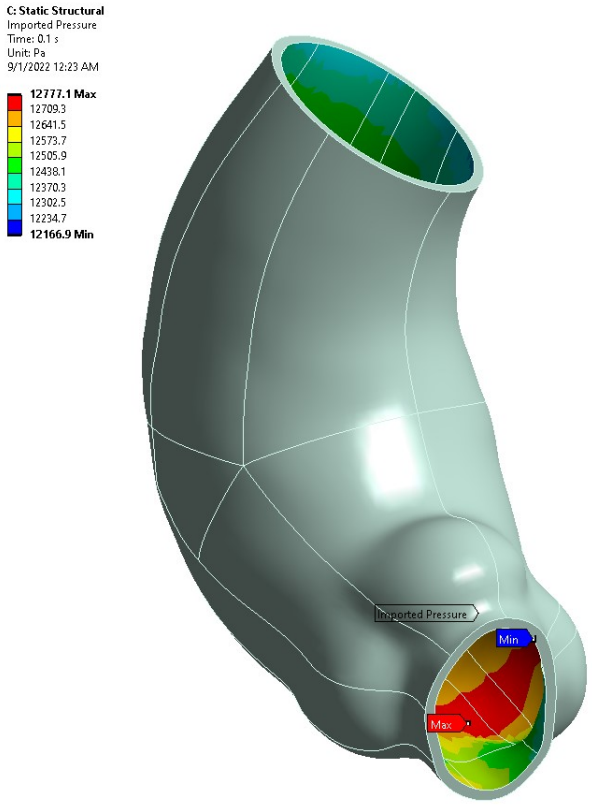

Figure 16. *Transferred load from the fluid domain at t=0.1s.*

4.4.5. Parameter Calculation

In addition to the default parameters solved by Fluent, we are also interested in calculating TAWSS, OSI, and RRT. A user-defined function (UDF) was set up to calculate these variables over the entire cardiac cycle. User-defined memories (UDMs) were created for each cell at the artery wall to store the intermediate values and the calculated results. The results saved in UDMs can then be accessed through Ansys CFD-post.

4.5. Statistical Analysis

Continuous patient baseline characteristics were reported as the mean with standard deviation (SD) for normally distributed data and median with interquartile range (IQR) for data with a nonnormal distribution. Categorical data were reported as frequencies with percentages. First, a correlation matrix was generated to visualize the whole dataset. Based on the results, the

parameters AAL and AAV were selected and analyzed further as they demonstrated a strong correlation with the hemodynamic and biomechanical parameters.

For the two-group comparison, Shapiro–Wilk test was performed on continuous variables to determine whether they were normally distributed. Independent t-tests were performed for variables with normal distribution. Mann-Whitney U tests were performed for variables with non-normal distributions. The cohort was further divided into four groups based on quantiles. One-way ANOVA was used to compare the means of parameters among different intervals for variables with normal distribution. Otherwise, Kruskal–Wallis H test was used. Pearson correlation coefficients were calculated to determine the relationship between morphological, hemodynamic and biomechanical parameters. P-values were reported for each pair of parameters. Statistical significance was taken as $P<0.05$ (two-tailed). Statistical analyses were performed using R-4.2.2 (The R Foundation, Vienna, Austria).

CHAPTER 5. RESULTS AND DISCUSSION

5.1. Preliminary Analysis

First, a correlation matrix (**Figure 17**) was generated for the entire dataset to determine the direction of further analysis. Diameter, AAL, AAV, maximum cross-sectional area, diameter of the Sinuses of Valsalva, and the diameter of the Sinotubular junction showed significant correlation with hemodynamic parameters.

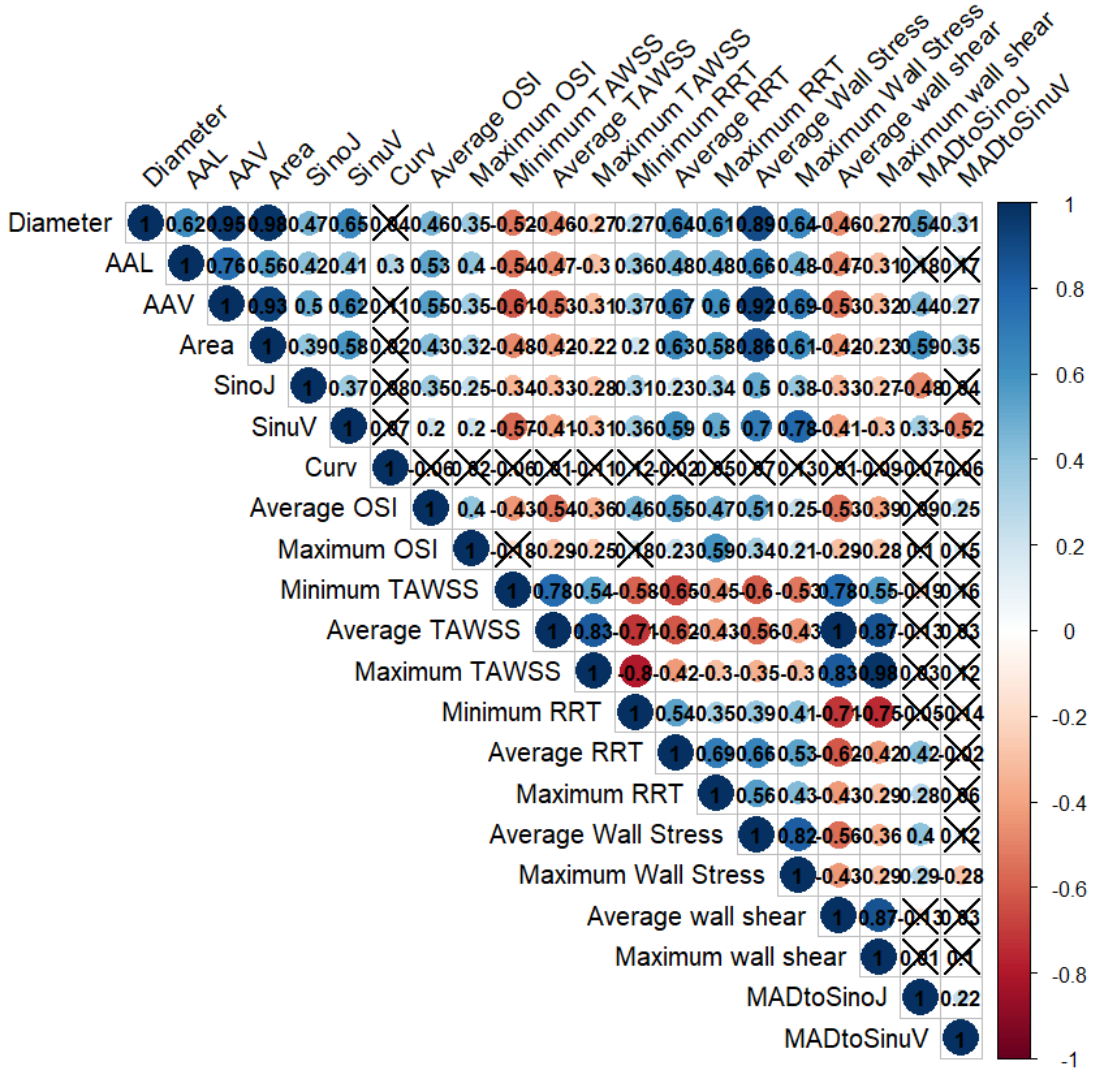

Figure 17. Correlation matrix of all the parameters. Area: maximum cross-sectianl area. SinoJ: diameter of the Sinotubular junction. SinoV: diameter of the Sinuses of Valsalva. MADtoSinoJ: the ratio of the maximum diameter to the diameter of the Sinotubular junction. MADtoSinuV: the ratio of the maximum diameter to the diameter of the Sinuses of Valsalva.

Previous studies found that the aortic ratios showed correlations with Type A dissection [92]. However, our findings indicated that there was no significant correlation between the aortic ratios and hemodynamic parameters. Curvature showed no significant correlation with any of the hemodynamic parameters, indicating that curvature does not impact the overall hemodynamic condition. But it is possible that the curvature can affect the local distribution of the hemodynamical parameters and the mechanical stress. Since the one-dimensional parameter diameter does not account for the elliptical and irregular shape of the aorta, several studies suggested that the maximum cross-sectional area may be a more valid measurement of the aorta [6] [7]. In this cohort, we found that the square of the maximum diameter is highly correlated to the maximum cross-sectional area with a correlation coefficient of 0.98, indicating that the aortic cross-sections were very close to circular shapes. Comparing the correlation coefficients related to the diameter and maximum cross-sectional, no significant difference was found between the two groups. From a hemodynamic point of view, the cross-sectional area showed no significant advantage in evaluating the hemodynamic conditions of ATAA. Many studies showed that AAL, the previously neglected dimension in the early natural history study of ATAA, can be important in ATAA risk evaluation [10] [11] [12]. AAL showed a relatively strong correlation with various hemodynamic parameters, suggesting that the change in AAL can significantly alter the flow conditions. A similar trend was also observed for AAV.

Based on the preliminary analysis, we decided to focus on the study of AAL and AAV. AAL, as a recently proposed ATAA indicator, showed great potential in risk evaluation. It was hypothesized that aortic elongation causes the worsening of aortic flow conditions, however, evidence was still missing. AAV, as a 3D parameter, overcomes the limitation of 1D parameters such as the irregular shape of the aorta. It also showed a relatively strong correlation with hemodynamic conditions. Hopefully, our findings can provide further evidence for using AAL as an indicator for ATAA and provide future directions for the natural history study of ATAA.

5.2. Patient Demographics

The baseline characteristics include gender, age, height, weight, body mass index (BMI), body surface area (BSA), hypertension, family history, diabetes, chronic kidney disease (CKD), smoking, Marfan syndrome (MFS), and root aneurysm were shown in **Table 4**. The mean age

was 63.500 [54.0, 69.2] years. 60% of the patients were male. Patients were classified based on diameter, AAL, and AAV. The cut-off values were 50mm, 110mm, and 197 mL respectively. The cut-off values for diameter and AAL were selected based on the previous study of Wu et al. [12]. Since no previous natural history study of AAV was found, the third quartile was selected as the cut-off value for enlarged aortas.

Table 4. *Demographic and clinical characteristic of the cohort.*

Variables	Overall
Male (%)	60 (60.0)
Age, year (median [IQR])	63.5 [54.0, 69.2]
Height, cm (median [IQR])	164.0 [158.0, 170.0]
Weight, kg (median [IQR])	63.0 [56.750, 70.0]
BMI, kg/m^2 (median [IQR])	23.4 [22.3, 26.0]
BSA, m^2 (Mean ± SD)	1.6 ± 0.1
Hypertension (%)	44 (44.0)
Family history (%)	10 (10.0)
Diabetes (%)	11 (11.0)
CKD (%)	4 (4.0)
Smoking (%)	11 (11.0)
MFS (%)	1 (1.0)
Root Aneurysm (%)	19 (19.0)

The characteristics of patient classified by diameter are given in **Table 5**. No significant difference in characteristic variables was found between the control group and the dilated group. The distribution of diameter was shown in **Figure 18**, with an average diameter of 50.1±8.8 mm.

The characteristics of patient classified by AAL is given in **Table 6**. Compared to controls, patients with elongated aorta were more frequently seen in males (68% vs. 45%, p=0.035). Increases in weight (66.000 [60.000, 70.500] vs 58.000 [52.000, 65.000] kg, p=0.002) and BSA (1.701±0.155 vs 1.611±0.208 m^2, p=0.015) were also observed in patients with elongated ascending aortas. No significant difference was found between the two groups among the other variables including age, height, BMI, pretension, family history, diabetes, CKD, smoking, MFS, and root aneurysm. The distribution of AAL was shown in **Figure 19**. The distribution is overall normal with an average of 114.2±13.4 mm.

Table 5. Characteristics of the cohort classified by the maximum diameter with the cut-off diameter of 50 mm.

Variables	Controls	Dilated	p value
n	59	41	-
Male (%)	34 (57.627)	26 (63.415)	0.679
Age, year (median [IQR])	65.000 [55.500, 70.000]	61.000 [51.000, 69.000]	0.353
Height, cm (median [IQR])	164.000 [157.000, 170.000]	165.000 [160.000, 168.000]	0.676
Weight, kg (median [IQR])	63.000 [57.000, 68.250]	63.500 [59.000, 70.000]	0.400
BMI, kg/m^2 (median [IQR])	23.333 [22.349, 26.346]	23.571 [22.500, 26.000]	0.952
BSA, m^2 (Mean ± SD)	1.661 ± 0.191	1.680 ± 0.158	0.593
Hypertension (%)	28 (47.458)	16 (39.024)	0.421
Family history (%)	5 (8.475)	4 (9.756)	1.000
Diabetes (%)	7 (11.864)	6 (14.634)	0.766
CKD (%)	3 (5.085)	1 (2.439)	0.642
Smoking (%)	6 (10.169)	6 (14.634)	0.543
MFS (%)	0 (0.000)	1 (2.439)	0.410
Root Aneurysm (%)	10 (16.949)	9 (21.951)	0.608

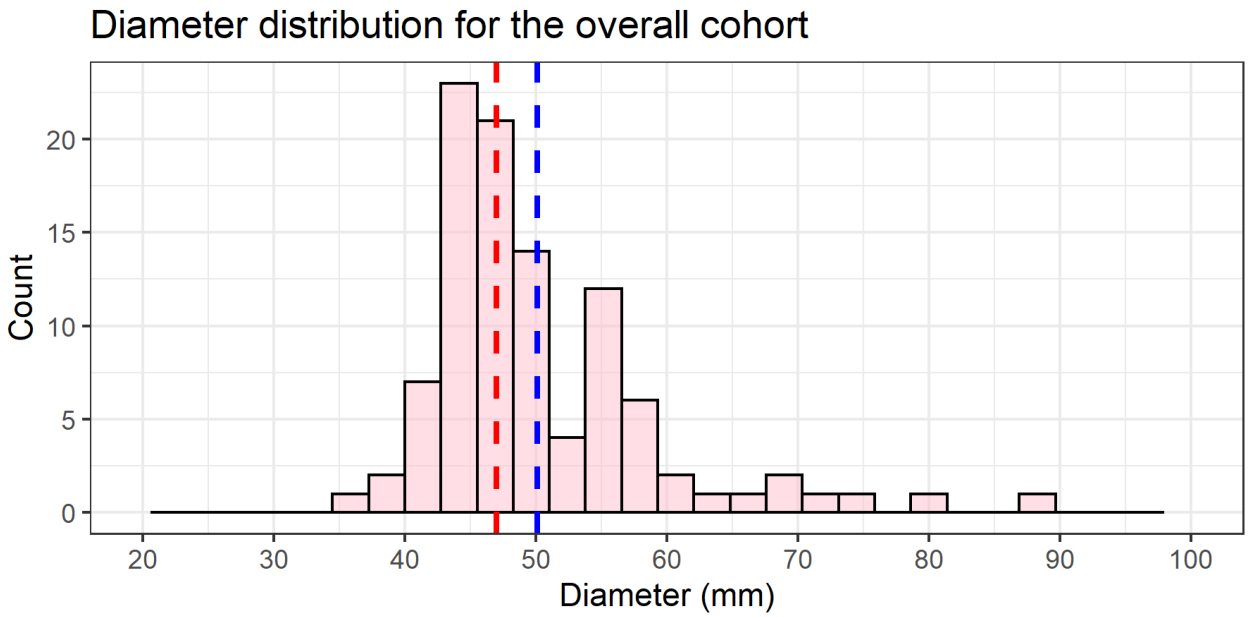

Figure 18. Diameter distribution of the overall cohort. The red line shows the median value, and the blue line shows the mean value of diameter.

Table 6. Characteristics of the cohort classified by AAL with the cut-off AAL of 110 mm.

Variables	Controls	Elongated	p value
n	37	63	-
Male (%)	17 (45.9)	43 (68.2)	0.035
Age, year (median [IQR])	65.0 [58.0, 72.0]	62.0 [54.0, 69.0]	0.260
Height, cm (median [IQR])	161.0 [154.0, 170.0]	166.0 [160.0, 170.0]	0.069
Weight, kg (median [IQR])	58.0 [52.0, 65.0]	66.0 [60.0, 70.5]	0.002
BMI, kg/m^2 (median [IQR])	23.0 [21.7, 24.7]	23.9 [22.5, 26.6]	0.132
BSA, m^2 (Mean ± SD)	1.6 ± 0.2	1.7 ± 0.1	0.015
Hypertension (%)	16 (43.2)	28 (44.4)	1.000
Family history (%)	3 (8.1)	7 (11.1)	0.741
Diabetes (%)	4 (10.8)	7 (11.1)	1.000
CKD (%)	1 (2.7)	3 (4.7)	1.000
Smoking (%)	3 (8.1)	8 (12.6)	0.742
MFS (%)	0 (0.0)	1 (1.5)	1.000
Root Aneurysm (%)	6 (16.2)	13 (20.6)	0.792

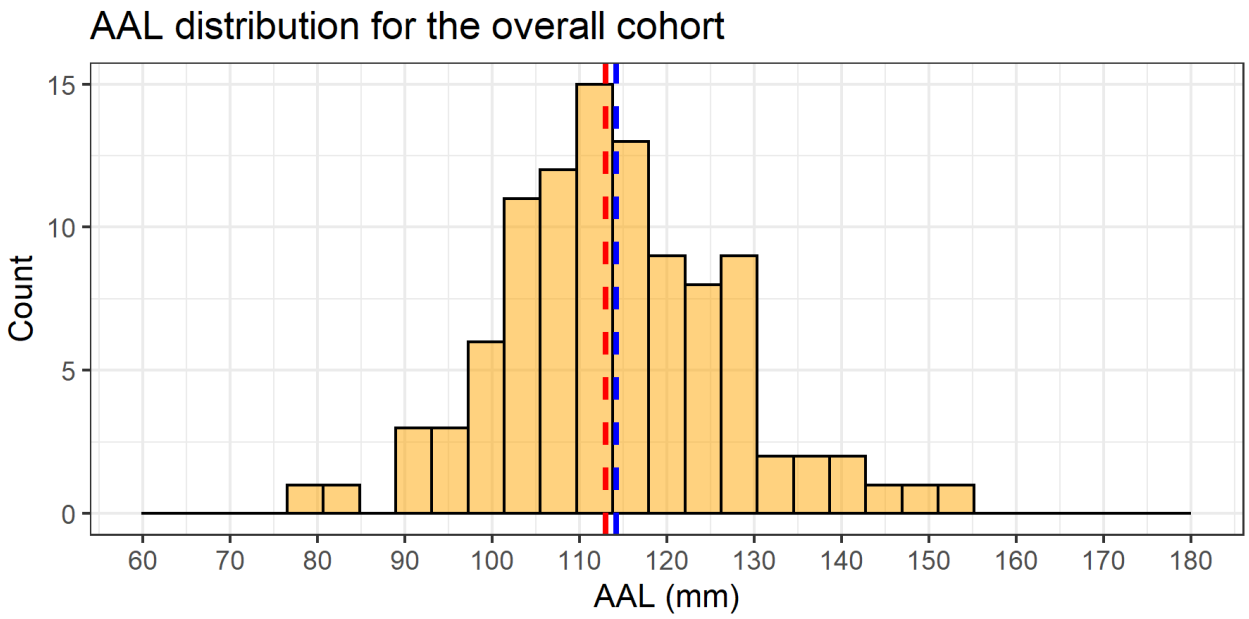

Figure 19. AAL distribution of the overall cohort. The red line shows the median value, and the blue line shows the mean value of AAL.

Table 7. Characteristics of the cohort classified by AAV with the cut-off AAV of 197 mL.

Variables	Controls	Enlarged	p value
n	75	25	-
Male (%)	40 (53.3)	20 (80.0)	0.020
Age (median [IQR])	64.0 [55.0, 69.5]	63.0 [49.0, 69.0]	0.521
Height (median [IQR])	162.0 [157.0, 170.0]	167.0 [163.0, 172.0]	0.042
Weight (median [IQR])	63.0 [55.0, 68.0]	70.0 [61.0, 74.0]	0.010
BMI (median [IQR])	23.3 [22.2, 26.0]	24.1 [22.6, 26.4]	0.476
BSA (Mean ± SD)	1.6±0.2	1.7±0.2	0.022
Hypertension (%)	34 (45.3)	10 (40.0)	0.816
Family history (%)	9 (12.0)	1 (4.0)	0.444
Diabetes (%)	8 (10.7)	3 (12.0)	1.000
CKD (%)	3 (4.0)	1 (4.0)	1.000
Smoking (%)	6 (8.0)	5 (20.0)	0.136
MFS (%)	0 (0.0)	1 (4.0)	0.250
Root Aneurysm (%)	12 (16.0)	7 (28.0)	0.239

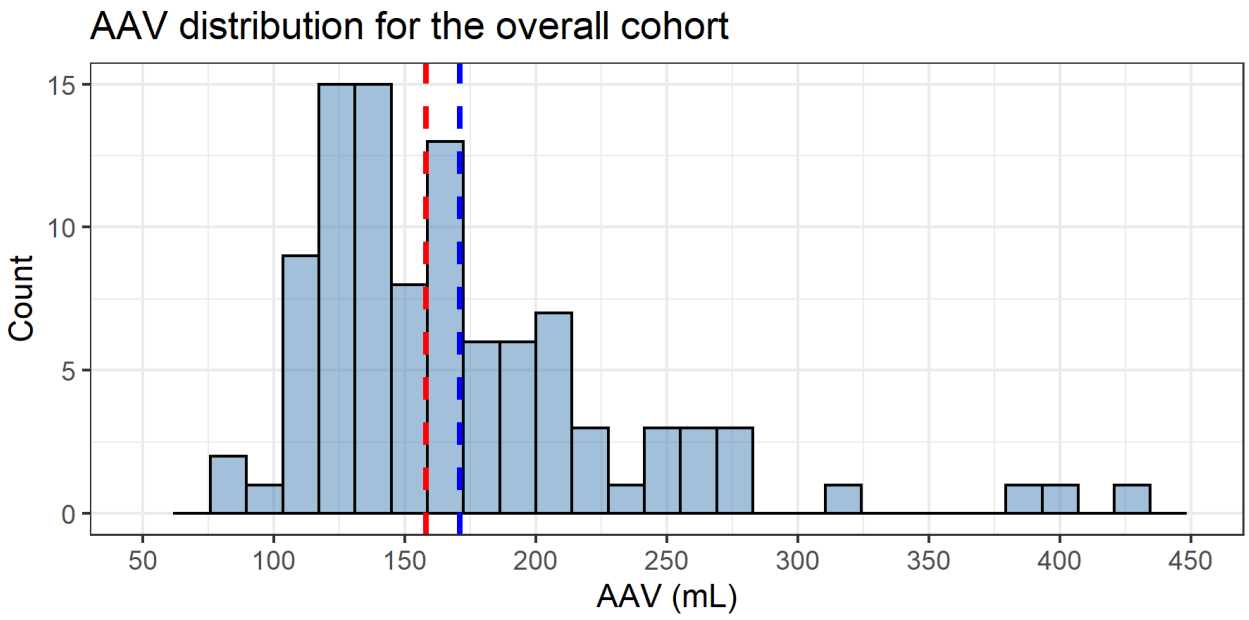

Figure 20. *AAV distribution of the overall cohort. The red line shows the median value, and the blue line shows the mean value of AAV.*

The characteristics of patient classified by AAV is shown in **Table 7**. Similar to AAL, patients with enlarged AAV tend to have higher weight (70.0 [61.0, 74.0] vs. 63.0 [55.0, 68.0] kg, p=0.010) and BSA (1.7±0.2 vs. 1.6±0.2 m^2, p=0.022). Patients with enlarged AAV were more frequently found to be male in the enlarged group than in the control group (80.0% vs. 53.3%, p=0.020). There are no significant differences between the control group and the enlarged group among the other parameters. The distribution of AAV is shown in **Figure 20**.

5.3. Results

5.3.1. Correlation between Diameter, AAL, and AAV

Figure. 20 shows the scatter plot of AAL vs. diameter. Most ATAAs meet the current clinical surgery criterion (diameter ≥ 5.5 cm) and were classified as enlarged based on AAV. A moderate positive correlation was found between AAL and diameter. The correlation coefficient between AAL and diameter is 0.623 ($P < 0.001$). A positive correlation was also found between AAL and AAV with a correlation coefficient of 0.761 ($P < 0.001$). Diameter and AAV are highly correlated with a correlation coefficient of 0.950 ($P < 0.001$).

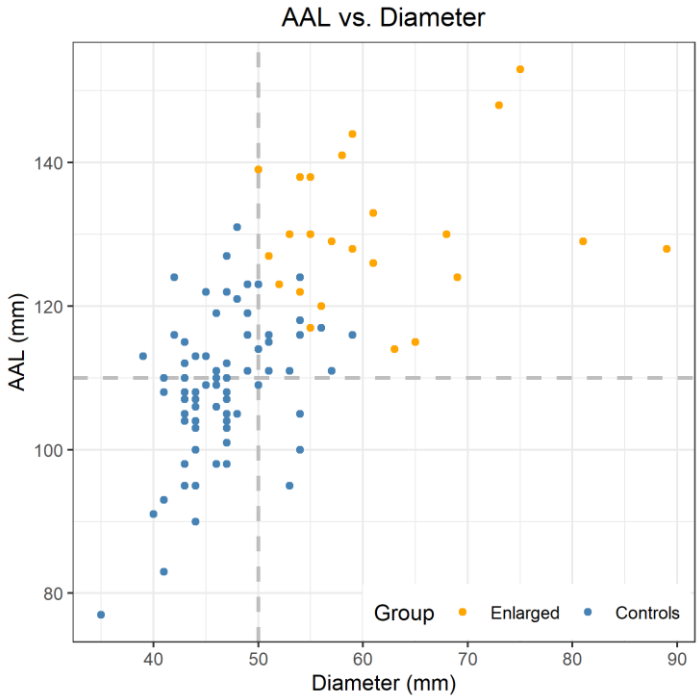

Figure 21. Scatter plot of AAL vs. diameter. The cut-off AAL and diameter are shown in grey dashed lines. For AAL the cut of value is 110mm. For diameter, the cut off value is 50mm. The geometries classified as Enlarged based on AAV is shown in orange (>197mL), and the geometries in the control group are shown in blue.

5.3.2. Two-Group Comparison

Dilatated Group vs. Control Group

Considering diameter remains the gold standard for elective surgery criterion, we first find the connection between diameter and various hemodynamic parameters for comparison. The distribution of hemodynamic parameters differs significantly between the control group and the dilated group (**Figure 22**). The patients with dilated aorta had significantly compromised hemodynamics. Compared to controls, the patients with aortic aneurysms had a decreased TAWSS (0.822 [0.607, 0.945] vs. 1.120 [0.908, 1.454] Pa, $p<0.001$), decreased maximum WSS (20.345 [18.875, 26.336] vs. 26.194 [21.089, 36.213] Pa, $p=0.009$), increased average OSI (0.202±0.021 vs. 0.172±0.023, $p<0.001$), increased maximum OSI (0.499 [0.498, 0.499] vs. 0.498 [0.497, 0.499], $p=0.001$), increased average PRT (3.113 [2.602, 4.240] vs. 2.023 [1.567, 2.535], $p <0.001$), and increased maximum PRT (762.375 [373.914, 1336.230] vs. 287.949 [192.053, 438.692], $p<0.001$). The average WS and maximum WS was also found to be higher for patients in the dilated group (186.673 [177.279, 204.158] vs. 160.590[152.032, 168.144] kPa, $p<0.001$), increased maximum WS (864.740 [719.880, 1086.800] vs. 779.350 [702.650, 910.370] kPa, $p=0.047$). The increase in diameter is confirmed to be associated with the change in hemodynamic conditions inside the aorta.

Elongated Group vs. Control Group

A similar trend was observed for AAL (**Figure 23**). The patients with elongated AAL also had significantly compromised hemodynamics. Compared to controls, the patients with elongated AAL had a decreased TAWSS (0.895 [0.664, 1.155] vs. 1.125 [0.860, 1.491] Pa, $p=0.002$), decreased maximum WSS (22.764 [19.106, 28.754] vs. 24.778 [19.810, 37.863] Pa, $p=0.15$), increased average OSI (0.190±0.026 vs. 0.174±0.024, $p=0.002$), increased maximum OSI (0.499 [0.498, 0.499] vs. 0.498 [0.497, 0.499], $p=0.006$), increased average PRT (2.769 [2.163, 4.070] vs. 1.957 [1.531, 2.647], $p <0.001$), increased maximum PRT (552.389 [303.996, 957.753] vs. 287.949 [169.617, 446.761], $p=0.001$), increased average WS (177.645 [165.141, 196.812] vs 158.343 [149.141, 168.385] kPa, $p<0.001$), and increased maximum WS (876.760 [729.965, 1063.550] vs 770.420 [703.890, 822.250] kPa, $p=0.013$).

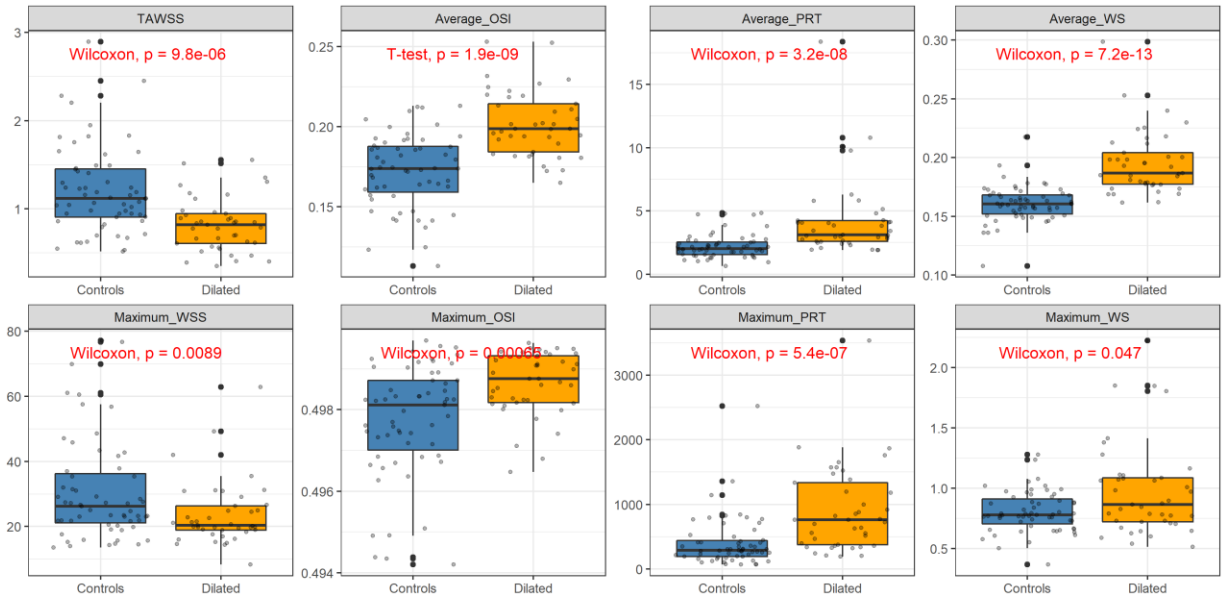

***Figure 22**. Boxplot comparing the hemodynamic and biomechanical parameters in the control group and the dilated group. The values of TAWSS and maximum WSS are expressed in Pa. The values of average WS and maximum WS are in kPa. The exact p values for the T-Test or the Mann-Whitney U tests are shown in red. The solid line indicates the median value. The upper and lower edge correspond to the first and third quartiles.*

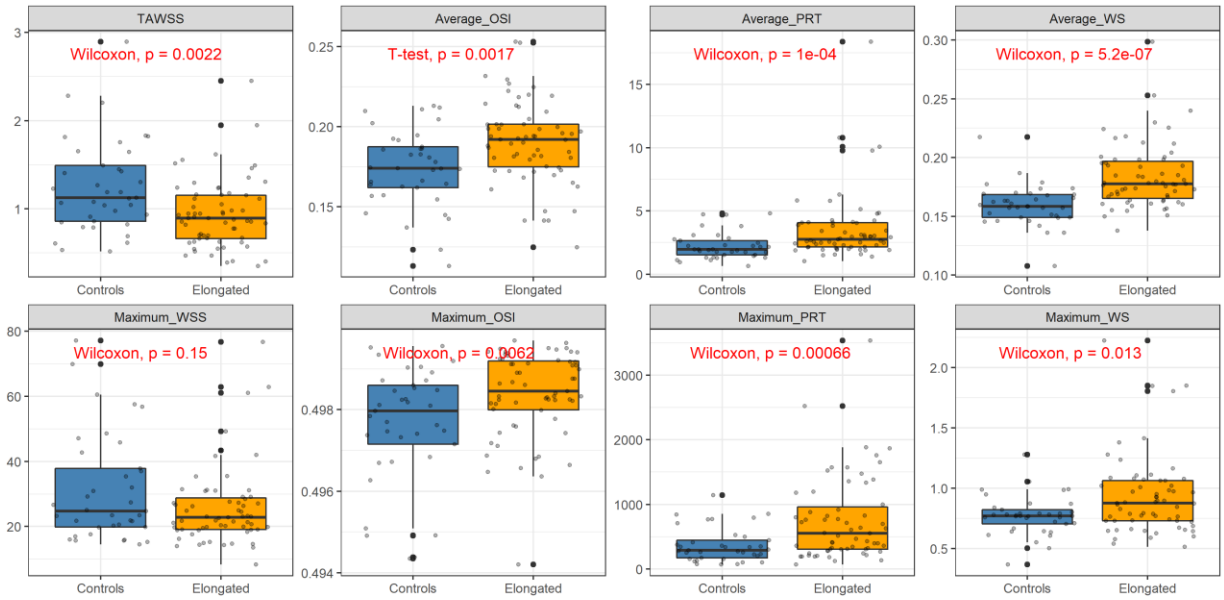

***Figure 23.** Boxplot comparing the hemodynamic and biomechanical parameters in the control group and the elongated group. The values of TAWSS and maximum WSS are expressed in Pa. The values of average WS and maximum WS are in kPa. The exact p values for the T-Test or the Mann-Whitney U tests are shown in red. The solid line indicates the median value. The upper and lower edge correspond to the first and third quartiles.*

Enlarged Group vs. Control Group

Figure 24 shows the comparison between the enlarged group and the control group. Compared to the control group, patients with enlarged ascending aorta had decreased TAWSS (1.081 [0.858, 1.329] Pa vs. 0.666 [0.543, 0.855] Pa, $p < 0.001$), decreased maximum WSS (24.778 [19.744, 35.410] Pa vs. 21.139 [18.326, 24.851] Pa, $p = 0.030$), increased average OSI (0.178±0.025 vs. 0.203±0.022, $p < 0.001$), increased maximum OSI (0.498 [0.497, 0.499] vs. 0.499 [0.498, 0.499], $p = 0.002$), increased average PRT (2.163 [1.772, 2.758] vs. 4.082 [2.952, 5.808], $p < 0.001$), increased maximum PRT (312.847 [207.445, 519.391] vs. 996.047 [640.644, 1573.140], $p < 0.001$), increased average WS (163.317 [156.246, 173.206] kPa vs. 200.489 [193.076, 218.122] kPa, $p < 0.001$), and increased maximum WS (769.680 [668.745, 879.795] kPa vs. 1072.000 [873.060, 1280.000] kPa, $p < 0.001$). Compared with the groups classified based on diameter and AAL, the difference between the two groups classified based on AAV is more profound.

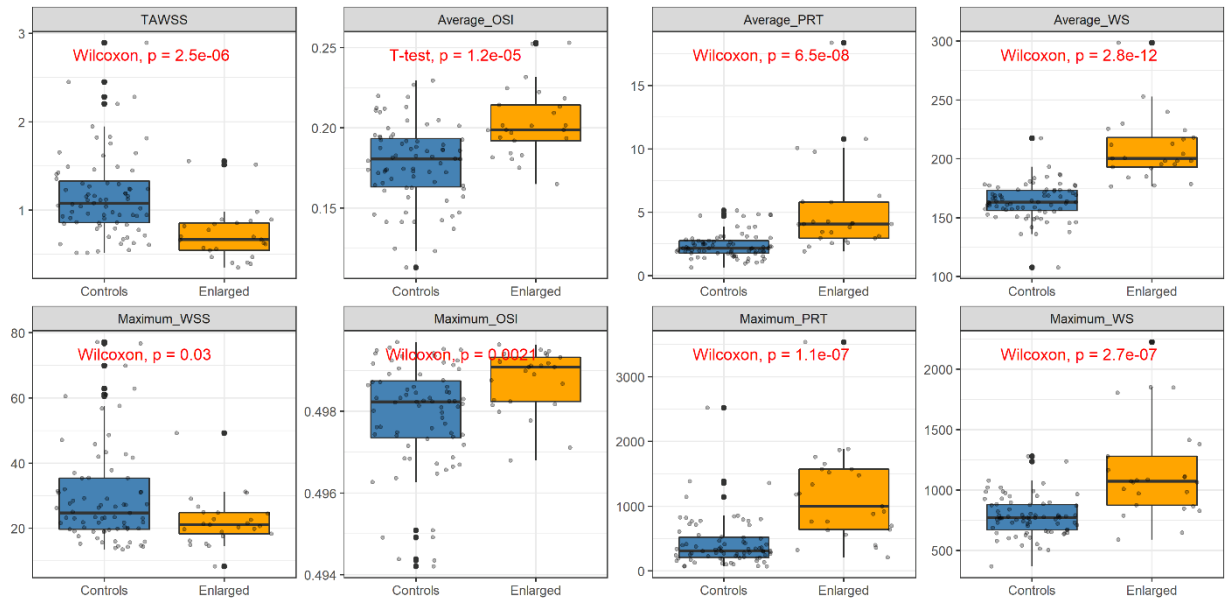

Figure 24. *Boxplot comparing the hemodynamic and biomechanical parameters in the control group and the enlarged group. The values of TAWSS and maximum WSS are expressed in Pa. The values of average WS and maximum WS are in kPa. The exact p values for the T-Test or the Mann-Whitney U tests are shown in red. The solid line indicates the median value. The upper and lower edge correspond to the first and third quartiles.*

5.3.3. Dose-response Relationship

Diameter

The diameter was then divided into four intervals based on quartiles: Q1 (35-44, n=30), Q2 (45-47, n=21), Q3 (48-54, n=28), and Q4 (55-89, n=21) mm. The median or mean value with IQR or SD of each parameter among different groups is given in **Table 8**. A strong dose-response relationship was found between diameter and various hemodynamical parameters (**Figure 25**).

Table 8. *Table comparing the mean with SD or median with IQR between Q1, Q2, Q3, and Q4 classified based on diameter. The values of TAWSS and maximum WSS are expressed in Pa. The values of average WS and maximum WS are expressed in kPa.*

Variables	Q1	Q2	Q3	Q4	p value
Maximum WSS (median [IQR])	27.505 [22.980, 37.648]	26.194 [18.871, 31.061]	20.074 [17.414, 28.127]	20.640 [18.875, 24.851]	p=0.010
TAWSS (median [IQR])	1.141 [0.946, 1.480]	1.153 [0.794, 1.296]	0.843 [0.624, 1.115]	0.775 [0.543, 0.895]	p<0.001
Average WS (median [IQR])	153.636[146.790, 163.006]	164.375[157.437, 172.980]	177.894 [169.044, 184. 300]	204.158 [195.317, 224.312]	p<0.001
Maximum WS (median [IQR])	762.830 [652.015, 853.245]	839.860 [770.420, 974.340]	767.260 [669.100, 887.020]	1063.700 [827.390, 1379.800]	p<0.001
Average OSI (Mean ± SD)	0.164±0.022	0.178±0.023	0.199±0.016	0.200±0.025	p<0.001
Maximum OSI (median [IQR])	0.498 [0.497, 0.498]	0.498 [0.497, 0.499]	0.499 [0.498, 0.499]	0.499 [0.498, 0.499]	p=0.004
Average PRT (median [IQR])	1.960 [1.388, 2.165]	2.231 [1.877, 2.843]	3.003 [2.461, 4.131]	3.443 [2.576, 5.808]	p<0.001
Maximum PRT (median [IQR])	273.903 [160.704, 381.431]	312.847 [253.377, 498.242]	488.568 [336.149, 831.872]	996.047 [557.554, 1574.010]	p<0.001

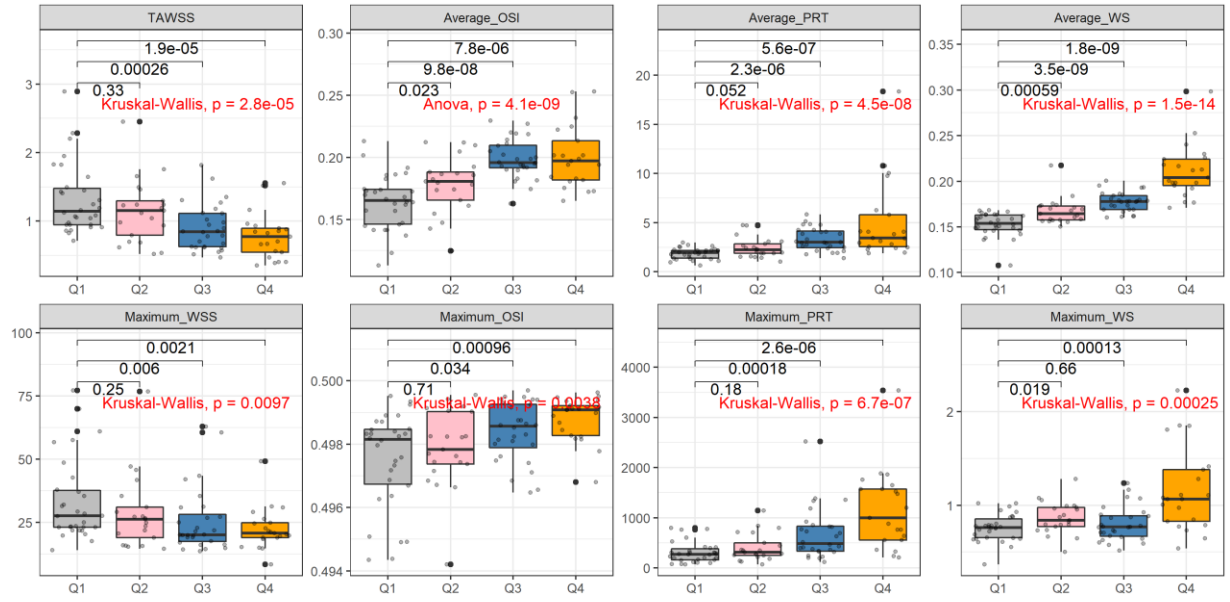

Figure 25. *Boxplot comparing the hemodynamic and biomechanical parameters in the four groups divided based on diameter quartiles. The values of TAWSS and maximum WSS are expressed in Pa. The values of average WS and maximum WS are expressed in kPa. The exact p values for the Kruskal-Wallis Test or the ANOVA are shown in red.*

AAL

Similarly, we divided AAL into Q1-Q4 groups based on quartiles: Q1 (77-106), Q2 (107-113), Q3 (114-123), and Q4 (124-153) mm. The median or mean value with IQR or SD of each parameter among different groups is given in **Table 9**. Similar to diameter, a strong dose-response relationship was observed between diameter and various hemodynamical parameters (**Figure 26**).

Table 9. *Table comparing the mean with SD or median with IQR between Q1, Q2, Q3, and Q4 classified based on AAL. The values of TAWSS and maximum WSS are expressed in Pa. The values of average WS and maximum WS are expressed in kPa.*

Variables	Q1	Q2	Q3	Q4	p value
Maximum WSS (median [IQR])	24.778 [21.614, 37.863]	26.336 [19.839, 31.270]	22.980 [19.461, 27.636]	20.640 [16.879, 23.965]	p=0.086
TAWSS (median [IQR])	1.187 [0.909, 1.645]	1.153 [0.857, 1.436]	0.946 [0.855, 1.115]	0.627 [0.507, 0.832]	p<0.001
Average WS (median [IQR])	157.495 [148.889, 167.800]	162.274 [157.020, 169.938]	176.990 [166.491, 184.982]	198.307 [178.308, 220.463]	p<0.001
Maximum WS (median [IQR])	770.420 [703.890, 791.140]	771.990 [719.445, 879.795]	771.450 [645.720, 928.250]	1063.700 [918.345, 1271.800]	p<0.001
Average OSI (Mean ± SD)	0.170±0.022	0.177±0.025	0.191±0.020	0.201±0.029	p<0.001
Maximum OSI (median [IQR])	0.498 [0.497, 0.498]	0.498 [0.497, 0.499]	0.498 [0.498, 0.499]	0.499 [0.498, 0.499]	p=0.010
Average PRT (median [IQR])	1.879 [1.340, 2.230]	2.231 [1.850, 2.758]	2.602 [2.385, 2.952]	4.085 [3.426, 5.818]	p<0.001
Maximum PRT (median [IQR])	261.607 [127.340, 373.914]	346.712 [233.910, 578.320]	464.040 [281.715, 820.061]	919.459 [494.485, 1548.040]	p<0.001

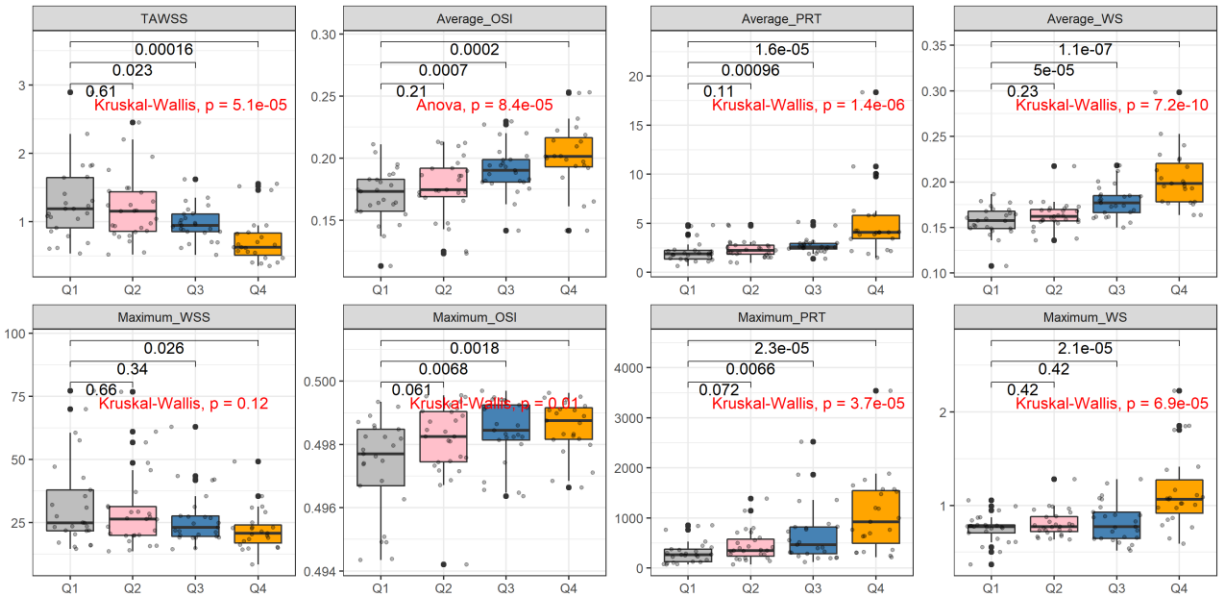

Figure 26. *Boxplot comparing the hemodynamic and biomechanical parameters in the four groups divided based on AAL quartiles. The values of TAWSS and maximum WSS are expressed in Pa. The values of average WS and maximum WS are expressed in kPa. The exact p values for the Kruskal-Wallis Test or the ANOVA are shown in red.*

AAV

The same analysis was repeated for AAV. The four intervals divided based on quartiles were [54.1 mL, 127 mL] (Q1), (127 mL, 158 mL] (Q2), (158 mL,197 mL] (Q3), and (197 mL, 429 mL] (Q4). The mean with SD or median with IQR for each group is given in **Table 10**. **Figure 27** demonstrates the relationship between AAV and hemodynamic parameters. Strong dose-response relationships were confirmed, especially for average OSI, average PRT, and average WS.

Table 10. *Table comparing the mean with SD or median with IQR between Q1, Q2, Q3, and Q4 classified based on AAV. The values of TAWSS and maximum WSS are expressed in Pa. The values of average WS and maximum WS are expressed in kPa.*

Variables	Q1	Q2	Q3	Q4	p value
Maximum WSS (median [IQR])	29.210 [22.980, 42.691]	24.778 [19.810, 27.636]	19.868 [16.928, 31.061]	21.139 [18.326, 24.851]	0.002
TAWSS (median [IQR])	1.304 [0.946, 1.655]	1.081 [0.935, 1.228]	0.928 [0.671, 1.237]	0.666 [0.543, 0.855]	<0.001
Average WS (median [IQR])	150.780 [145.939, 159.665]	162.973 [158.327, 169.342]	176.990 [169.082, 179.693]	200.489 [193.076, 218.122]	<0.001
Maximum WS (median [IQR])	754.180 [642.130, 781.970]	802.260 [733.380, 895.910]	764.840 [672.090, 793.290]	1072.000 [873.060, 1280.000]	<0.001
Average OSI (Mean ± SD)	0.184±0.026	0.184±0.026	0.184±0.026	0.184±0.026	<0.001
Maximum OSI (median [IQR])	0.498 [0.497, 0.498]	0.498 [0.497, 0.499]	0.498 [0.497, 0.499]	0.499 [0.498, 0.499]	0.004
Average PRT (median [IQR])	1.756 [1.295, 2.163]	2.230 [1.926, 2.675]	2.769 [2.385, 3.853]	4.082 [2.952, 5.808]	<0.001
Maximum PRT (median [IQR])	269.259 [115.123, 303.996]	312.847 [194.891, 604.250]	409.925 [326.625, 770.270]	996.047 [640.644, 1573.140]	<0.001

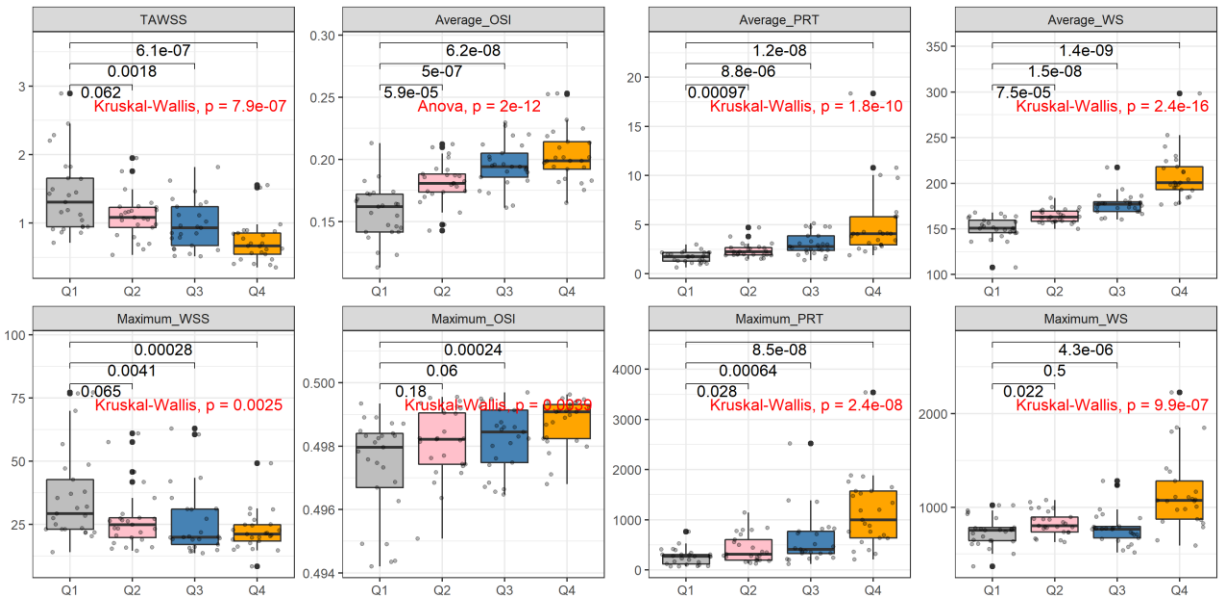

Figure 27. *Boxplot comparing the hemodynamic and biomechanical parameters in the four groups divided based on AAV quartiles. The values of TAWSS and maximum WSS are expressed in Pa. The values of average WS and maximum WS are expressed in kPa. The exact p values for the Kruskal-Wallis Test or the ANOVA are shown in red.*

5.3.4. Correlation between Morphological Parameter and Hemodynamic Parameters

Diameter

As shown in **Figure 28** diameter correlates significantly with most of the hemodynamic parameters and mechanical parameters investigated in this study. A very strong positive correlation was found between diameter and average WS, with a correlation coefficient of 0.89 ($p < 0.001$). The diameter showed strong correlations with average PRT, maximum PRT, and maximum WS, with correlation coefficients of 0.64 ($p < 0.001$), 0.61 ($p < 0.001$), and 0.64 ($p < 0.001$), respectively. The diameter is negatively correlated with TAWSS (-0.46, $p< 0.001$). A relatively weak positive correlation was found between diameter and maximum OSI (0.35, $p < 0.001$). No significant linear correlation was found between diameter and maximum WSS.

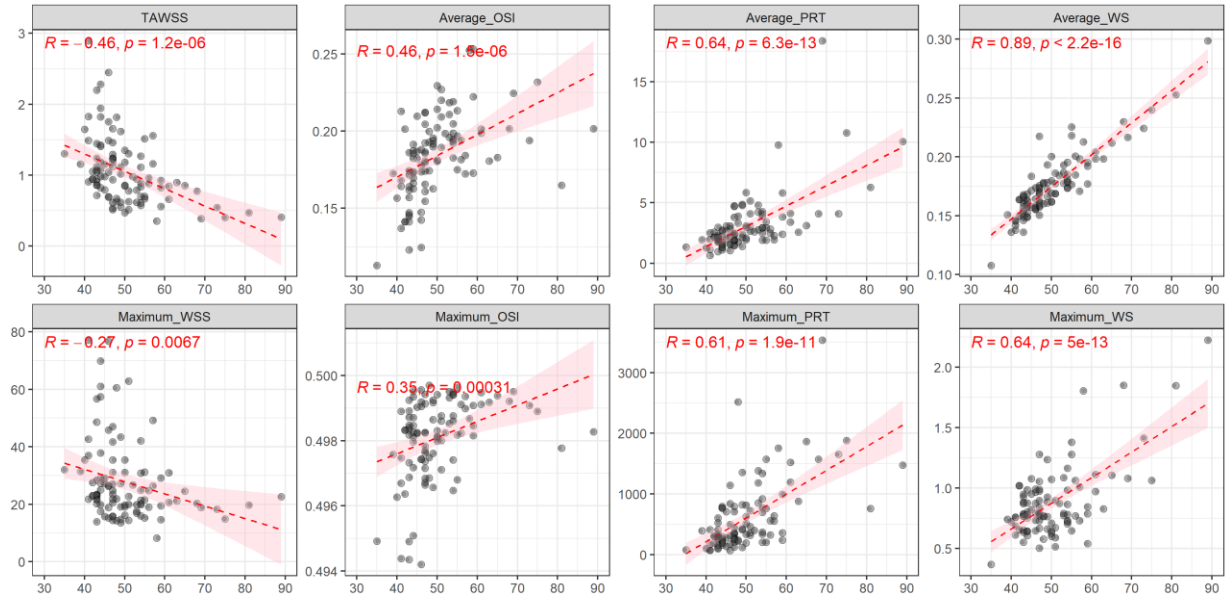

Figure 28. *Scatter plots of hemodynamic and biomechanical parameters vs. diameter. The values of TAWSS and maximum WSS are expressed in Pa. The values of average WS and maximum WS are expressed in kPa. The values of diameter are expressed in mm. The fitted results are shown red dashed lines and the confidence intervals are shown in pink.*

AAL

AAL was found to be significantly correlated to hemodynamic parameters linearly as shown in **Figure 29**. The correlation coefficient for AAL with TAWSS, maximum WSS, average OSI,

maximum OSI, average PRT, maximum PRT, average WS, and maximum WS were -0.47 ($p<0.001$), -0.31 ($p=0.002$), 0.53 ($p<0.001$), 0.40 ($p<0.001$), 0.48 ($p<0.001$), and 0.48 ($p<0.001$), 0.66 ($p<0.001$), and 0.48 ($p<0.001$), respectively.

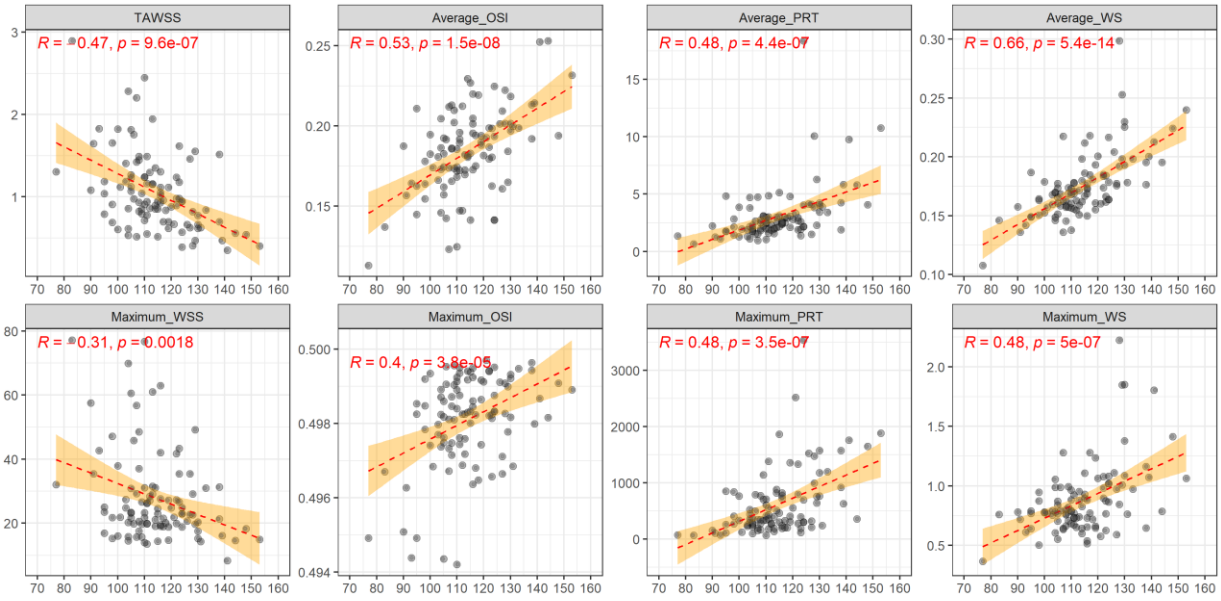

Figure 29. *Scatter plots of hemodynamic and biomechanical parameters vs. AAL. The values of TAWSS and maximum WSS are expressed in Pa. The values of average WS and maximum WS are expressed in kPa. The values of AAV are expressed in mm. The fitted results are shown red dashed lines and the confidence intervals are shown in yellow.*

AAV

AAV correlates significantly with hemodynamics, as shown in **Figure 30**. A very strong positive correlation was found between AAV and average WS, with a correlation coefficient of 0.92 ($p < 0.001$). AAV also showed significant correlations with TAWSS, maximum WSS, average OSI, maximum OSI, average PRT, maximum PRT, and maximum WS. The correlation coefficients were -0.53 ($p < 0.001$), -0.32 ($p < 0.001$), 0.55 ($p < 0.001$), 0.35 ($p < 0.001$), 0.67 ($p < 0.001$), 0.60 ($p < 0.001$), and 0.69 ($p < 0.001$), respectively.

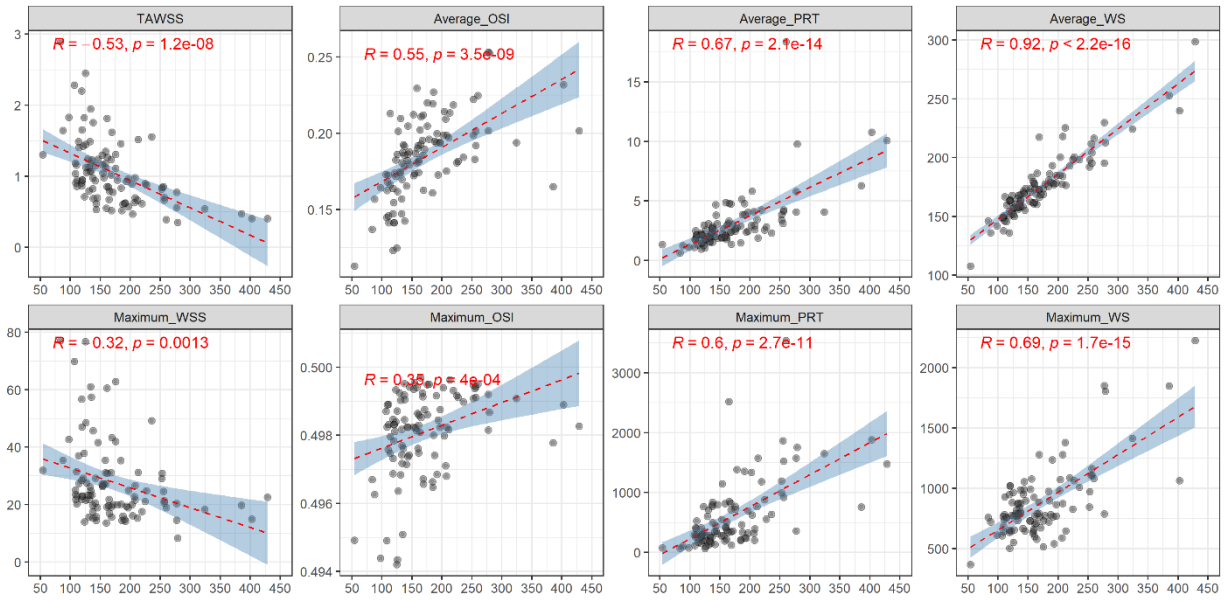

Figure 30. *Scatter plots of hemodynamic and biomechanical parameters vs. AAV. The values of TAWSS and maximum WSS are expressed in Pa. The values of average WS and maximum WS are expressed in kPa. The values of AAV are expressed in mL. The fitted results are shown red dashed lines and the confidence intervals are shown in blue.*

5.4. Discussion

5.4.1. AAL and Hemodynamics

As mentioned in the introduction, both the American and European clinical guidelines recommend patients with ATAA diameter ≥ 5.5 cm for surgical repair [2, 3]. These recommendations are primarily based on early natural history studies of ATAA where a strong relationship between the maximum diameter of ATAA and AAEs was found [44] [85] [86]. A hinge point at 6.0 cm was found at which the risk of AAEs increases abruptly [86]. However, there are still a significant number AAEs happened in patients with small to moderate-sized ATAAs [3] [4] [5]. A study on the International Registry of Acute Aortic Dissection (IRAD) data showed that 59% of patients with Type A aortic dissection had aortic diameters smaller than 5.5 cm [4]. A more recent study showed that there are two hinge points, one at 5.25 cm and another one at 5.75 cm, at which the risk abruptly increases [132]. Both hinge points are smaller than the one found earlier. Evidence from previous studies also showed that the size of an ATAA can significantly increase during dissection [88] [89] [90]. The inclusion of dissected cases

within early natural history studies may result in an overestimated surgical threshold. Those factors suggest a downward modification of the current clinical guidelines for ATAA surgery.

To improve the current clinical standard, researchers are also trying to find other promising predictors for AAEs such as family history and other morphological parameters. Krüger et al. first associated dissection risk with aortic elongation and published multiple studies about aortic elongation [133] [134] [10]. One particularly important finding by Wu et al. on the natural history study of ATAA proposed using the AAL of 11 cm as a potential surgical indicator [12]. This clinical finding has been confirmed by a growing number of studies. Heuts et al. found that AAL is significantly larger in the pre-dissection patient group, resulting in a higher diagnostic accuracy using AAL compared with using diameter [135]. Eliathamby et al. found AAL can be very useful in discriminating patients with type A dissection from stable ATAAs [136]. However, the mechanism behind aortic elongation and high AAE risk is poorly understood.

In this study, we tried to relate AAL with the flow conditions inside the aorta. Our results confirmed our hypothesis that aortic elongation is accompanied by a change in flow condition. This provides supporting evidence for using AAL as an indicator for ATAA elective surgery. The compromised hemodynamics may form a feedback loop with progressively degraded aortic wall tissue. As discussed earlier, we selected WS, WSS, OSI, and RRT as measurements of the biomechanical stress within the aortic wall and the flow condition inside the aorta. Aortic dissection can be seen as a mechanical failure when the WS exceeds the wall strength [115]. Aortic wall strength and other properties vary from patient to patient. Due to the limitation of this study, only CT images were available, and it was not possible to obtain or estimate patient-specific material properties. Nevertheless, higher WS generally means a higher risk of dissection or rupture. It has also been shown that the magnitude and direction of WSS play a key role in regulating ECs gene expression and aortic wall remodeling. As discussed earlier, research showed that a high shear rate characterized by high TAWSS is protective and antiatherogenic [97] [99] [19]. Whereas, both low WSS and high OSI have been associated with atherosclerosis and plaque formation [137]. A disturbed flow (high OSI) with low WSS can induce EC dysfunction and contribute to atherogenesis and inflammatory response, whereas a unidirectional laminar flow was shown to be protective [72] [98] [106]. A disturbed flow can also upregulate the expression of certain genes and cause subsequent tissue degeneration and wall remodeling

[19] [106] [108]. A similar hemodynamic study also found that regions with high OSI were close to the favorite site for entry tears in aortic dissection [21]. Regions with high PRT were found near the recirculation zone in stenotic coronary arteries [138]. High PRT was also associated with vascular wall thickening [108].

When comparing the elongated group with the control group, significantly higher OSI, RRT, WS, and lower TAWSS were reported, meaning that there is a strong association between aortic elongation and pathological flow conditions and higher mechanical stress within the wall. The dose-response effects between AAL and hemodynamics also showed a similar trend. The curve fitting also suggested a significant linear relationship between AAL and hemodynamic parameters. To better evaluate the relationship between AAL and flow conditions, we compared the effect of aortic dilation and aortic elongation. Overall, diameter showed higher significance levels and stronger correlations with hemodynamic and biomechanical parameters. It is worth noticing that the correlation coefficient between diameter and average WS is 0.89 ($p<0.001$), which is considered to be a very strong linear correlation. This is consistent with Laplace's law that the wall stress increases proportionally with diameter. Whereas when correlating AAL and average WS linearly, only a moderate correlation was found (0.66, $p<0.001$).

Noticeably, the correlation coefficient between AAL and diameter is 0.623 ($P < 0.001$). A similar correlation coefficient of 0.752 ($P < 0.001$) was reported earlier by Krüger et al. [10]. Although a significant correlation exists between AAL and diameter, the correlation is not perfect. A patient can have a significantly elongated but only slightly dilated aorta (**Figure 21**). This suggests that the two parameters should be considered separately. The previous nature history study conducted by Wu. et al. confirmed this and showed that taking the arithmetic sum of indexed diameter and AAL can significantly improve the model discrimination [12]. Similar observations were previously reported by Krüger et al. [133]. Krüger et al. recommended a scoring system called TAIPAN for surgical intervention. In this system, two points will be given for patients with aortic diameters of ≥ 5.5 cm; one point will be given for patients with aortic diameters between 4.5 to 5.4 cm; and one point will be given for patients with AAL ≥ 12cm [10] [134]. Surgical intervention is recommended for any patient with a total score of ≥ 2. Based on their dataset, the TAIPAN demonstrated greater sensitivity in predicting aortic dissection than the diameter-only prediction criteria [10] [134]. Despite the fact that incorporating AAL into the

evaluation criteria did improve the discrimination, the autocorrelation between the two parameters cannot be ignored. Ideally, we would perform the analysis among diameter-matched groups. But due to the limitation of available cases, not enough data can be gathered to produce a statistically significant result. In future studies, a more comprehensive diameter-matched group comparison can be performed to explore this relationship further.

In future studies, the aortic tissue of the patient with different AAL can also be obtained. By studying the characteristic of the aortic tissue, we could confirm the relationship between the hemodynamic characteristic and tissue remodeling.

5.4.2. High WSS or Low WSS

Aortic elongation and dilation are associated with the increase in OSI, RRT, and WS. This result agrees with many other CFD studies that higher OSI, RRT and WS are associated with aortic wall degeneration and greater AAE risk. However, aortic elongation and dilation are also associated with lower WSS. This is as expected since given the same initial conditions, a larger aortic diameter will result in a lower overall flow rate and hence a lower WSS. Many CFD studies have suggested the connection between WSS and aortic remodeling. However, conflict findings were present regarding whether a high WSS or a low WSS is a risk factor.

High WSS is beneficial as it prevents ECs dysfunction [19]. Low WSS has been associated with the loss in ECs and the alternation in ECs shapes [139]. ECs exposed to low WSS become less elongated than normal ECs [139]. Low WSS is also associated with wall remodeling as Low WSS dysregulates the antioxidant and anti-inflammatory mediators [18]. Boussel et al. studied the hemodynamic characteristic of intracranial aneurysms and found that aneurysm growth is likely to occur at locations with low TAWSS [140]. Kiema et al. found that WSS is negatively correlated to media degeneration and wall strength [141]. Also, macrophage infiltrations were predominantly found in the inner curves of TAA where WSS was lower [141]. A study also showed that rapture occurs predominantly at the recirculation zone with low WSS [142].

On the contrary, studies on BAV patients showed that an abnormally high WSS can also negatively impact the aorta. Bissell et al. found that a combination of high WSS and a disturbed flow pattern is associated with aortic dilation [100]. Atkins et al. and Guzzardi et al showed that

altered gene expression was associated with high WSS in BAV patients, which in turn led to medial degeneration in the regions with high WSS [101] [102]. Mahadevia et al. found that the site of aortic dilation coincides with the location of increased WSS in patients with BAV [143]. Pasta et al. found that the activities of certain MMPs were positively correlated to systolic WSS in ascending aorta [103]. Salmasi et al. found that WSS was negatively correlated to wall thickness, elastin levels and SMC count, showing that elevated WSS was related to aortic wall degeneration [144]. These findings suggest that a high level of WSS exceeding the physiological range can lead to medial degeneration and aortic dilation.

Meng et al. proposed two different pathways for aneurysm formation, one is the inflammatory-cell-mediated pathway associated with low WSS and high OSI, and another one is the mural-cell-mediated pathway associated with high WSS and positive WSS gradient [145]. A disturbed flow characterized by low WSS, high OSI, and high blood cell resident time promotes inflammatory cell infiltration. The MMPs produced by macrophage lead to matrix degeneration and subsequent vessel dilation. On the contrary, high WSS and positive WSS gradient caused by impinging flow sensed by SMCs and fibroblasts upregulate the production and activation of MMP-2 and MMP-9, leading to ECM degeneration [145]. This hypothesis explains why both high WSS and low WSS are associated with intracranial aneurysm formation. Overall, most studies associated aneurysm development with low WSS, which is consistent with our study. Many studies associating aneurysm formation with high WSS were focusing on BAV patients. In this study, we did not model the aortic valve. A healthy aortic valve with three leaflets will fully open during systole. However, a BAV with leaflet fusion will not fully open during systole. This results in a smaller inlet size and an altered direction of the blood flow. Hence WSS may be even higher in patients with BAV, triggering a different biologic pathway. The role of WSS in ATAA formation deserves further exploration.

The association between aortic dilation and the decrease in maximum WSS is consistent with in vivo measurements. Bürk et al. applied 4D flow cardiovascular MR to patients with dilated aortas, age-matched controls and healthy volunteers and found that the increase in ascending aortic diameter is significantly associated with the decrease in systolic WSS and the increase in OSI. CFD studies with patient-specific models also showed similar results that aortic dilation is associated with low WSS and high OSI [21].

5.4.3. AAV and Hemodynamics

With the recent developments in imaging and image processing technologies, accurate 3D reconstruction of the aorta can be easily achieved. Segmentation software like Mimics can quickly convert stacks of CT images into 3D models. The segmentation process is semi-automatic and can be performed with minimal training. Hence it is possible to introduce 3D parameters, such as AAV, into the clinical practice in evaluating the risk of ATAA. Previous studies have showed the advantage of combining multiple 1D parameters in evaluating the risk of ATAA [10] [12] [134]. We have already demonstrated that both aortic elongation and aortic dilation were related to compromises flow conditions and higher mechanical stress. The significant correlation between hemodynamic change, aortic dilation, and aortic elongation suggests that the morphological change in aortic shape can significantly alter the flow pattern and result in a pathogenic flow condition.

In this study, we also compared hemodynamic parameters among different groups of patients based on AAV and calculated the correlation coefficient between those parameters with AAV. A similar pattern was observed for AAV. We found that increasing AAV was strongly associated with worsening hemodynamics. Hemodynamic parameters were significantly different among groups of ATAAs classified based on AAV. Mechanical stress is higher in the aortic wall when AAV is large. Compared with diameter and AAL, smaller p values were reported when associating hemodynamic parameters with AAV. Furthermore, stronger correlations were found between all hemodynamic parameters, biomechanical parameters and AAV. These findings suggest that AAV can better reflect the flow condition inside the ATAA and the mechanical stress in the aortic wall. A significant linear correlation was observed between diameter and AAV with a correlation coefficient of 0.92, but the correlation is not perfect. By using AAV instead of diameter, increases in the magnitude of correlation coefficients and significance levels were noticeable, especially for average WS and AAV.

Compared to the correlation between average WS and diameter (0.89, $p<0.001$) and the correlation between average WS and AAL (0.66, $p<0.001$) as reported in our previous work, AAV showed an even stronger correlation with average WS (0.92, $P<0.001$). The correlation coefficient of maximum WS and AAV (0.69, $p<0.001$) was also higher compared to maximum

WS and diameter (0.64, $p<0.001$), and maximum WS and AAL (0.48, $p<0.001$). This suggests that AAV better reflects the overall mechanical stress within the aortic wall. In this study, an isotropic material was applied to the aortic wall. Since many studies showed that the aortic wall demonstrates anisotropic elastic properties, future studies are required to investigate this relationship further by applying an anisotropic hyperplastic material to the aortic wall. The longitudinal and circumferential stress can also be calculated separately since the aortic wall strength is not the same in all directions.

Due to difficulties in measurements, there are not many clinical studies on the relationship between AAV and AAEs. A recent study of 358 patients evaluated the prediction accuracy of Type A dissection based on diameter, AAL, and AAV using receiver operating characteristic (ROC) analysis. At the same specificity level, both AAL and AAV showed higher sensitivities in predicting Type A dissection than using the diameter, suggesting that both AAV and AAL can better identify patients at higher risk of dissection [135]. AAV showed a stronger correlation to pathological flow conditions and higher biomechanical stress based on our study. This may explain the high sensitivity of AAV in ROC analysis.

Another advantage of using AAV is that AAV is expected to be more sensitive than diameter alone since it can capture any small size change in the entire 3D geometry. Although according to the Laplace Law, higher diameter means a higher mechanical stress, hence is likely that the segment with the largest diameter undergoes the most rapid change. However, as discussed earlier, hemodynamical factors also play an important role in aortic wall remodeling. The regions with high OSI or RRT do not necessarily coincide with the region with the highest mechanical stress. As a result, remodeling can also happen in different locations. It is possible that an aneurysm can undergo remodeling without a change in maximum diameter [146]. Both diameter and AAL are 1D parameters and they are not able to capture subtle morphology variations in ATAA. For example, the non-circular shape of the aorta cross-section and size change in a segment with a smaller diameter.

Due to the shorter length of ATAA, this phenomenon is not profound in ATAA compared with AAA. This is why the parameter volume has been proposed and studied more frequently in the evaluation of AAA. Similar to ATAA, the current clinical standard for AAA surgical

intervention is based on early natural history studies. These studies showed that AAAs with larger diameters have a higher chance of rupture [1] [147]. However, evidence also showed that diameter alone is not sufficient in evaluating the risk of AAA dissection [148]. Furthermore, due to the elliptical cross-sections and tortuosity of the abdominal aorta, accurate diameter measurement can be difficult [149]. Hence many researchers have proposed using AAA volume as a potential indicator. Renapurkar et al. studied the infrarenal AAA and showed that aortic volume change can occur even when the diameter remains relatively constant [146]. Their findings suggest that volume is a better indicator of aneurysm growth [146]. Kauffmann et al. showed that volume measurements were more sensitive than diameter measurements in AAA development [150]. At the same time, the volume measurements have comparable reproducibility compared with the maximum diameter, with repeatability coefficients of <6 mL for volume measurement and <6 % for relative volume growth [150]. Parr et al. and den Hartog et al. also reported high reproducibility and sensitivity of AAA volume measurements and suggested that measuring AAA volume might be a better method of detecting aortic expansion [151] [152]. Liljeqvist et al. studied the relationship between AAA volume and AAA growth rate. A positive correlation was found between the baseline AAA volume and the volume growth rate [153]. Similar correlations were not found between baseline diameter and diameter growth rate [153]. It is not yet known whether a similar relationship exists between AAV and the ATAA growth rate, suggesting that further studies on the ATAA volume are necessary. Besides, the study on the measurement reproducibility and sensitivity of AAV is still missing.

In diameter measurements of ATAA, discrepancies were often seen in clinical practice. The discrepancies usually arose from the complex geometries of the ATAA such as non-circular cross-section, the curvature of the ATAA, the asymmetric shape of the aortic root, and the measurement method (hand measurement or centerline measurement) [154]. Due to the curvature of ATAA, diameters measured from the axial images tend to be larger than the diameters measured using the automated centerline method [155] [154]. The size measurements of the aortic root can also have large variations depending on the method used (sinus-to-commissure or sinus-to-sinus) [154]. AAV measurement does not suffer from these problems since AAV accounts for all the morphological variations in ATAA including the elliptical cross-section and the complex shape of the aortic root.

5.4.4. Limitations

In this study, patient-specific wall material properties were not used. The elastic modulus can have large variations and a high degree of anisotropy depending on the patient. Previous studies have shown that aneurysm tissue is stiffer than normal aortic tissue [156] and tissue stiffness is loosely correlated with ATAA diameter [113]. The actual stress might be underestimated for ATAAs with larger diameters or overestimated for ATAAs with smaller diameters. Because it is practically impossible to determine patient-specific aortic wall properties based on available data and this study focuses only on the influence of aortic morphology on hemodynamic characteristics, the use of a more complex model is unnecessary. The simulated results of the simplified model have already confirmed the validity of using AAL as an additional surgical indicator and demonstrated the potential of using AAV as an elective surgery criterion. To improve upon the current model, an anisotropic material can be used to model the aortic wall since the longitudinal and circumferential elastic modulus and strength were shown to the different [157].

Another limitation is that the movement of the heart and hence the movement of the aortic root is not modeled. Fix support was applied at the annulus as it is a common treatment for the aortic model and has been used in many similar studies. As a comparative study, this should not affect the stability of the conclusions.

CHAPTER 6. CONCLUSION

First, our results showed that aortic elongation was associated with the worsening in hemodynamics in ATAA, consolidating the role of AAL as a valid surgical indicator. The correlations between AAL and various hemodynamic parameters were comparable to the correlations between diameter and those parameters. Considering many patients with larger AAL only showed slight aortic dilation, AAL in combination with diameter is expected to provide higher prediction accuracy and selectivity for AAEs.

Second, a strong association was found between the increase in AAV and compromised hemodynamic conditions. Hence, we proposed to incorporate AAV, a 3D parameter, into the current clinical elective surgery criterion. AAV is expected to have a higher sensitivity to aneurysm growth because it reflects the size of the entire ascending part of the aorta instead of just the largest part, thereby accounting for both the dilation and elongation of the aorta. Additionally, AAV can also be measured easily with current clinical imaging processing tools, and the measurements are semi-automatic and expected to have high reproducibility. Compared with 1D surgical indicators like diameter and AAL, AAV showed higher statistical significance and stronger associations with hemodynamic and biomechanical parameters. Hence, by using AAV as an independent or in combination with AAL and AAV, a better prediction might be achieved. Future studies, especially natural history studies, on the role of AAV as a potential indicator for ATAA development or as a risk predictor for AAE are warranted.

In conclusion, the two main goals of this thesis were successfully met. We developed a computational analysis method and workflow for simulating the blood flow in patient-specific aortic geometries. We also obtained various hemodynamic and biomechanical parameters using the one-way FSI analysis workflow we developed. Finally, we investigated the relationship between the hemodynamics and morphological parameters, confirmed that AAL is indeed a valid surgical indicator and suggested direction for future ATAA nature history studies.

To improve upon the current method, patient-specific material properties can be incorporated into the computational model. Aortic wall properties and boundary conditions can be obtained or estimated using 4D MRI. This allows the patient-specific hemodynamic parameters and

mechanical stress to be calculated. Those results can help evaluate the conditions and risks for ATAAs. Instead of using dimensions measured from the geometry, mechanical stress and estimated wall properties can be used in surgical decision-making, effectively preventing severe AAEs from happening.

REFERENCE

[1] A. T Hirsch et al., "ACC/AHA 2005 Practice Guidelines for the management of patients with peripheral arterial disease (lower extremity, renal, mesenteric, and abdominal aortic)," *Circulation,* vol. 113, no. 11, pp. e463-654, 2006.

[2] R. Erbel et al., "2014 ESC Guidelines on the diagnosis and treatment of aortic diseases," *Eur. Heart. J.,* vol. 35, no. 41, p. 2873–2926, 2014.

[3] L. F. Hiratzka et al., "2010 ACCF/AHA/AATS/ACR/ASA/SCA/SCAI/SIR/STS/SVM Guidelines for the Diagnosis and Management of Patients With Thoracic Aortic Disease," *Circulation,* vol. 121, no. 13, p. e266–e369, 2012.

[4] L. A. Pape et al., "Aortic diameter >or = 5.5 cm is not a good predictor of type A aortic dissection: observations from the International Registry of Acute Aortic Dissection (IRAD)," *Circulation,* vol. 116, no. 10, p. 1120–1127, 2007.

[5] L. M. Parish, J. H. Gorman, S. Kahn, P. Plappert, M. G. John-Sutton, J. E. Bavaria and R. C. Gorman, "Aortic size in acute type A dissection: implications for preventive ascending aortic replacement," *European Journal of Cardio-Thoracic Surgery,* vol. 35, no. 6, pp. 941-946, 2009.

[6] A. Masri et al., "Aortic cross-sectional area/height ratio and outcomes in patients with a trileaflet aortic valve and a dilated aorta," *Circulation,* vol. 134, no. 22, pp. 1724-1731, 2016.

[7] M. N. Acharya et al., "Analysis of aortic area/height ratio in patients with thoracic aortic aneurysm and Type A dissection," *Eur. J. Cardiothorac. Surg.,* vol. 54, no. 4, pp. 696-701, 2018.

[8] M. Acharya et al., "Relationship between indexed aortic area and aortic diameter in bicuspid aortic valve aortopathy: A retrospective cohort study," *Ann. Med. Surg. (Lond),* vol. 65, no. 2021, p. 102342, 2021.

[9] A. Masri et al., "Aortic cross-sectional area/height ratio and outcomes in patients with bicuspid aortic valve and a dilated ascending aorta," *Circ. Cardiovasc Imaging,* vol. 2017, no. 10, p. e006249, 2017.

[10] T. Krüger et al., "Aortic elongation in aortic aneurysm and dissection: the Tübingen Aortic Pathoanatomy (TAIPAN) project," *Eur. J. Cardiothorac. Surg.,* vol. 54, no. 1, pp. 26-33, 2018.

[11] S. Heuts et al., "Aortic elongation part II: the risk of acute type A aortic dissection," *Heart,* vol. 104, no. 2018, pp. 1778-1782, 2018.

[12] J. Wu et al., "Ascending aortic length and risk of aortic adverse events: the neglected dimension," *J. Am. Coll. Cardiol.,* vol. 74, no. 15, p. 1883–1894, 2019.

[13] M. P. Poullis, R. Warwick, A. Oo and R. J. Poole, "Ascending aortic curvature as an independent risk factor for type A dissection, and ascending aortic aneurysm formation: a mathematical model," *Eur. J. Cardiothorac. Surg.,* vol. 33, no. 6, p. 995–1001, 2008.

[14] R. Franken et al., "Increased aortic tortuosity indicates a more severe aortic phenotype in adults with Marfan syndrome," *Int. J. Cardiol.,* vol. 194, no. 2015, pp. 7-12, 2015.

[15] E. M. J. van Disseldorp et al., "Quantification of aortic stiffness and wall stress in healthy volunteers and abdominal aortic aneurysm patients using time-resolved 3D ultrasound: a comparison study," *Eur. Heart J. Cardiovasc. Imaging,* vol. 20, no. 2, p. 185–191, 2019.

[16] S. Farzaneh, O. Trabelsi, B. Chavent and S. Avril, "Identifying Local Arterial Stiffness to Assess the Risk of Rupture of Ascending Thoracic Aortic Aneurysms," *Ann. Biomed. Eng.,* vol. 47, no. 4, p. 1038–1050, 2019.

[17] A. Gnasso et al., "In vivo association between low wall shear stress and plaque in subjects with asymmetrical carotid atherosclerosis," *Stroke,* vol. 28, no. 5, pp. 993-998, 1997.

[18] A. M. Malek, S. L. Alper and S. Izumo, "Hemodynamic shear stress and its role in atherosclerosis," *JAMA,* vol. 282, no. 21, p. 2035–2042, 1999.

[19] P. F. Davies, "Hemodynamic shear stress and the endothelium in cardiovascular pathophysiology," *NATURE CLINICAL PRACTICE CARDIOVASCULAR MEDICINE,* vol. 6, no. 1, pp. 16-26, 2009.

[20] Z. Wang et al, "Wall stress analyses in patients with ≥5 cm versus <5 cm ascending thoracic aortic aneurysm," *The Journal of Thoracic and Cardiovascular Surgery,* vol. 162, no. 9, pp. 1452-1459, 2021.

[21] S. Numata et al., "Blood flow analysis of the aortic arch using computational fluid dynamics," *Eur. J. Cardiothorac. Surg.,* vol. 49, no. 6, p. 1578–1585, 2016.

[22] T. A. Ramezan, R. Razaghi, A. Bahramifar, M. Morshedi, M. Mafi and A. Karimi, "Interaction of the Blood Components with Ascending Thoracic Aortic Aneurysm Wall: Biomechanical and Fluid Analyses," *Life (Basel),* vol. 12, no. 9, p. 1296, 2022.

[23] R. Campobasso, F. Condemi, M. Viallon, P. Croisille , S. Campisi and S. Avril, "Evaluation of Peak Wall Stress in an Ascending Thoracic Aortic Aneurysm Using FSI Simulations: Effects of Aortic Stiffness and Peripheral Resistance," *Cardiovasc. Eng. Technol.,* vol. 9, no. 4, p. 707–722, 2018.

[24] F. Condemi, S. Campisi, M. Viallon, P. Croisille and S. Avril, "Relationship Between Ascending Thoracic Aortic Aneurysms Hemodynamics and Biomechanical Properties," *IEEE Trans Biomed Eng,* vol. 67, no. 4, pp. 949-956, 2020.

[25] H. H. Yeh, S. W. Rabkin and D. Grecov, "Hemodynamic assessments of the ascending thoracic aortic aneurysm using fluid-structure interaction approach," *Med. Biol. Eng. Comput.,* vol. 56, no. 3, p. 435–451, 2018.

[26] G. C. Almeida et al., "Computational Fluid Dynamics to Assess the Future Risk of Ascending Aortic Aneurysms," *Arq. Bras. Cardiol.,* vol. 118, no. 2, pp. 448-460, 2022.

[27] A. D. Kaiser , R. Shad, N. Schiavone, W. Hiesinger and A. L. Marsden , "Controlled Comparison of Simulated Hemodynamics Across Tricuspid and Bicuspid Aortic Valves," *Ann Biomed Eng,* vol. 50, no. 9, pp. 1053-1072, 2022.

[28] M. D. Hope et al., "4D flow CMR in assessment of valve-related ascending aortic disease," *JACC Cardiovasc. Imaging.,* vol. 4, no. 7, pp. 781-787, 2011.

[29] A. J. Barker et al., "Bicuspid aortic valve is associated with altered wall shear stress in the ascending aorta," *Circ. Cardiovasc Imaging,* vol. 5, no. 4, p. 457–466, 2012.

[30] C. Meierhofer et al., "Wall shear stress and flow patterns in the ascending aorta in patients with bicuspid aortic valves differ significantly from tricuspid aortic valves: a prospective study," *Eur. Heart J. Cardiovasc. Imaging.,* vol. 14, no. 8, p. 797–804, 2013.

[31] A. Gomez et al., "Wall Stress Distribution in Bicuspid Aortic Valve-Associated Ascending Thoracic Aortic Aneurysms," *Ann. Thorac. Surg.,* vol. 110, no. 3, pp. 807-814, 2020.

[32] R. Jayendiran, S. Campisi , M. Viallon, P. Croisille and S. Avril , "Hemodynamics alteration in patient-specific dilated ascending thoracic aortas with tricuspid and bicuspid aortic valves," *J Biomech,* vol. 110, p. 109954, 2020.

[33] M. C. Arokiaraj, M. De Beule and G. De Santis, "A novel sax-stent method in treatment of ascending aorta and aortic arch aneurysms evaluated by finite element simulations," *J Med Vasc.,* vol. 42, no. 1, pp. 39-45, 2017.

[34] H. D. e. al., "Engineering analysis of aortic wall stress and root dilatation in the V-shape surgery for treatment of ascending aortic aneurysms," *Interact Cardiovasc Thorac Surg.,* vol. 34, no. 6, pp. 1124-1131, 2022.

[35] G. Nannini et al., "Aortic hemodynamics assessment prior and after valve sparing reconstruction: A patient-specific 4D flow-based FSI model," *Comput Biol Med.,* vol. 135, p. 104581, 2021.

[36] F. J. H. Nauta et al., "Computational Fluid Dynamics and Aortic Thrombus Formation Following Thoracic Endovascular Aortic Repair," *Ann Thorac Surg.,* vol. 103, no. 6, pp. 1914-1921, 2017.

[37] E. Vignali, E. Gasparotti, S. Celi and S. Avril, "Fully-Coupled FSI Computational Analyses in the Ascending Thoracic Aorta Using Patient-Specific Conditions and Anisotropic Material Properties," *Front. Physiol.,* vol. 12, p. 732561, 2021.

[38] A. Updegrove, N. M. Wilson, J. Merkow, H. Lan, A. L. Marsden and S. C. Shadden, "SimVascular: An Open Source Pipeline for Cardiovascular Simulation," *Annu. Rev. Biomed. Eng.,* vol. 45, no. 3, p. 525–541, 2016.

[39] H. Lan, A. Updegrove, N. M. Wilson, G. D. Maher, S. C. Shadden and A. L. Marsden, "A Re-Engineered Software Interface and Workflow for the Open-Source SimVascular Cardiovascular Modeling Package," *J. Biomech. Eng.,* vol. 140, no. 2, p. 024501, 2018.

[40] H. G. Sherifova S, "Biomechanics of aortic wall failure with a focus on dissection and aneurysm: A review," *Acta Biomater,* vol. 2019 Nov, no. 99, pp. 1-17, 2019.

[41] J. E. Wagenseil and R. P. Mecham, "Vascular Extracellular Matrix and Arterial Mechanics," *Physiol. Rev.,* vol. 89, no. 3, p. 957–989, 2009.

[42] S. Mochizuki, B. Brassart and A. Hinek, "Signaling pathways transduced through the elastin receptor facilitate proliferation of arterial smooth muscle cells," *J. Biol. Chem.,* vol. 277, no. 47, pp. 44854-44863, 2002.

[43] J. Z. Goldfinger, J. L. Halperin, M. L. Marin, A. S. Stewart, K. A. Eagle and V. Fuster, "Thoracic Aortic Aneurysm and Dissection," *J. Am. Coll. Cardiol.,* vol. 64, no. 16, pp. 1725-1739, 2014.

[44] J. A. Elefteriades and E. A. Farkas, "Thoracic aortic aneurysm clinically pertinent controversies and uncertainties," *J. Am. Coll. Cardiol.,* vol. 55, no. 9, pp. 841-857, 2010.

[45] E. M. Isselbacher, "Thoracic and Abdominal Aortic Aneurysms," *Circulation,* vol. 111, no. 6, p. 816–828, 2005.

[46] L. A. Pape et al., "Presentation, Diagnosis, and Outcomes of Acute Aortic Dissection: 17-Year Trends From the International Registry of Acute Aortic Dissection," *J. Am. Coll. Cardiol.,* vol. 66, no. 4, pp. 350-358, 2015.

[47] S. Jana, M. Hu, M. Shen and Z. Kassiri , "Extracellular matrix, regional heterogeneity of the aorta, and aortic aneurysm," *Exp. Mol. Med.,* vol. 51, no. 12, p. 160, 2019.

[48] M. Shen et al., "Divergent Roles of Matrix Metalloproteinase 2 in Pathogenesis of Thoracic Aortic Aneurysm," *Arterioscler. Thromb. Vasc. Biol.,* vol. 35, no. 4, p. 888–898, 2015.

[49] F. E. Thomas J.M.Schlatmann, "Histologic changes in the normal aging aorta: Implications for dissecting aortic aneurysm," *The American Journal of Cardiology,* vol. 39, no. 1, pp. 13-20, 1977.

[50] A. Tsamis, J. T. Krawiec and D. A. Vorp, "Elastin and collagen fibre microstructure of the human aorta in ageing and disease: a review," *J. R. Soc. Interface.,* vol. 10, no. 83, p. 20121004, 2013.

[51] D.-C. Guo, C. L. Papke, R. He and D. M. Milewicz, "Pathogenesis of Thoracic and Abdominal Aortic Aneurysms," *Ann. N. Y. Acad. Sci.,* vol. 1085, no. 1, pp. 339-352, 2006.

[52] P. C. Y. Tang et al., "Hyperplastic cellular remodeling of the media in ascending thoracic aortic aneurysms," *Circulation,* vol. 112, no. 8, p. 1098–1105, 2005.

[53] I. El-Hamamsy and M. H. Yacoub, "Cellular and molecular mechanisms of thoracic aortic aneurysms," *Nat. Rev. Cardiol.,* vol. 6, no. 12, p. 771–786, 2009.

[54] P. W. M. Fedak et al., "Vascular matrix remodeling in patients with bicuspid aortic valve malformations: implications for aortic dilatation," *J. Thorac. Cardiovasc. Surg.,* vol. 126, no. 3, pp. 797-806, 2003.

[55] P. C. Y. Tang et al. , "Transmural inflammation by interferon-gamma-producing T cells correlates with outward vascular remodeling and intimal expansion of ascending thoracic aortic aneurysms," *FASEB J.,* vol. 19, no. 11, pp. 1528-1530, 2005.

[56] R. He et al., "Characterization of the inflammatory and apoptotic cells in the aortas of patients with ascending thoracic aortic aneurysms and dissections," *J. Thorac. Cardiovasc. Surg.,* vol. 1311, no. 3, pp. 671-678.e2, 2006.

[57] S. W. Rabkin, "Chapter Seven - The Role Matrix Metalloproteinases in the Production of Aortic Aneurysm," in *Progress in Molecular Biology and Translational Science*, 2017, pp. 239-265.

[58] M. Nataatmadja at al., "Abnormal extracellular matrix protein transport associated with increased apoptosis of vascular smooth muscle cells in marfan syndrome and bicuspid aortic valve thoracic aortic aneurysm," *Circulation,* vol. 108, no. Suppl 1, p. II329–II334, 2003.

[59] P. Ren et al., "ADAMTS-1 and ADAMTS-4 levels are elevated in thoracic aortic aneurysms and dissections," *Ann. Thorac. Surg.,* vol. 95, no. 2, pp. 570-577, 2013.

[60] H. H. C. Yang, C. van Breemen and A. W. Y. Chung, "Vasomotor dysfunction in the thoracic aorta of Marfan syndrome is associated with accumulation of oxidative stress," *Vascul. Pharmacol.,* vol. 52, no. 1–2, pp. 37-45, 2010.

[61] H. Lu and M. Aikawa, "Many Faces of Matrix Metalloproteinases in Aortic Aneurysms," *Arteriosclerosis, Thrombosis, and Vascular Biology,* vol. 35, no. 4, p. 752–754, 2015.

[62] J. O. Deguchi et al., "Genetically engineered resistance for MMP collagenases promotes abdominal aortic aneurysm formation in mice infused with angiotensin II," *Lab Invest.,* vol. 89, no. 3, pp. 315-326, 2009.

[63] M. Carmo et al., "Alteration of elastin, collagen and their cross-links in abdominal aortic aneurysms," *Eur. J. Vasc. Endovasc. Surg.,* vol. 23, no. 6, pp. 543-549, 2002.

[64] Z. Tonar, P. Kochova, R. Cimrman, J. Perktold and K. Witter, "Segmental differences in the orientation of smooth muscle cells in the tunica media of porcine aortae," *Biomech. Model Mechanobiol.,* vol. 14, no. 2, p. 315–332, 2015.

[65] D. M. Milewicz et al., "Altered smooth muscle cell force generation as a driver of thoracic aortic aneurysms and dissections," *Arterioscler. Thromb. Vasc. Biol.,* vol. 37, no. 1, p. 26–34, 2017.

[66] C. Petit, S. J. Mousavi and S. Avril , "Chapter 6 - Review of the Essential Roles of SMCs in ATAA Biomechanics," in *Advances in Biomechanics and Tissue Regeneration*, Amsterdam, Academic Press, 2019, pp. 95-114.

[67] M. Bäck, T. C. Gasser, J.-B. Michel and G. Caligiuri, "Biomechanical factors in the biology of aortic wall and aortic valve diseases," *Cardiovasc. Res.,* vol. 99, no. 2, pp. 232-241, 2013.

[68] M. G. Keane and R. E. Pyeritz, "Medical Management of Marfan Syndrome," *Circulation,* vol. 117, no. 21, p. 2802–2813, 2018.

[69] M. A. Coady et al., "Familial patterns of thoracic aortic aneurysms," *Arch. Surg.,* vol. 134, no. 4, pp. 361-367, 1999.

[70] A. Karimi and D. M. Milewicz, "Structure of the Elastin-Contractile Units in the Thoracic Aorta and How Genes That Cause Thoracic Aortic Aneurysms and Dissections Disrupt This Structure," *Can J Cardiol,* vol. 32, no. 1, pp. 26-34, 2016.

[71] V. T. Nkomo et al., "Bicuspid aortic valve associated with aortic dilatation: a community-based study," *Arterioscler. Thromb. Vasc. Biol.,* vol. 23, no. 2, p. 351–356, 2003.

[72] D. Katritsis, L. Kaiktsis, A. Chaniotis, J. Pantos, E. P. Efstathopoulos and V. Marmarelis, "Wall Shear Stress: Theoretical Considerations and Methods of Measurement," *Prog. Cardiovasc. Dis.,* vol. 49, no. 5, pp. 307-329, 2007.

[73] X. Liu, A. Sun, Y. Fan and X. Deng, "Physiological Significance of Helical Flow in the Arterial System and its Potential Clinical Applications," *Ann. Biomed. Eng.,* vol. 43, no. 1, pp. 3-15, 2015.

[74] J. A. Elefteriades , A. Sang, G. Kuzmik and M. Hornick, "Guilt by association: paradigm for detecting a silent killer (thoracic aortic aneurysm)," *Open Heart,* vol. 2, no. 1, p. e000169, 2015.

[75] J. H. Chung, B. B. Ghoshhajra, C. A. Rojas, B. R. Dave and S. Abbara, "CT angiography of the thoracic aorta," *Radiol. Clin. North. Am.,* vol. 48, no. 2, pp. 249-264, 2010.

[76] E. D. Cesare et al., "CT and MR imaging of the thoracic aorta," *Open Med. (Wars.),* vol. 11, no. 1, pp. 143-151, 2016.

[77] K. G. Kallianos and N. s. Burris, "Imaging Thoracic Aortic Aneurysm," *Radiol. Clin. North. Am.,* vol. 58, no. 4, pp. 721-731, 2020.

[78] D. M. Dudzinski and E. M. Isselbacher, "Diagnosis and management of thoracic aortic disease," *Curr. Cardiol. Rep.,* vol. 17, no. 12, p. 106, 2015.

[79] D. A. Roberts, "Magnetic resonance imaging of thoracic aortic aneurysm and dissection," *Seminars in Roentgenology,* vol. 36, no. 4, pp. 295-308, 2001.

[80] M. Markl, A. Frydrychowicz, S. Kozerke, M. Hope and O. Wieben, "4D flow MRI," *J. Magn. Reson. Imaging.,* vol. 36, no. 5, pp. 1015-1036, 2012.

[81] T. Suzuki et al., "Biomarkers of aortic diseases," *Am. Heart. J.,* vol. 165, no. 1, pp. 15-25, 2013.

[82] J. S. Ikonomidis et al., "Plasma biomarkers for distinguishing etiologic subtypes of thoracic aortic aneurysm disease," *J. Thorac. Cardiovasc. Surg.,* vol. 145, no. 5, pp. 1326-1333, 2013.

[83] P. Nazerian et al., "Diagnostic Accuracy of the Aortic Dissection Detection Risk Score Plus D-Dimer for Acute Aortic Syndromes: The ADvISED Prospective Multicenter Study," *Circulation,* vol. 137, no. 3, p. 250–258, 2018.

[84] J. A. Elefteriades, "Natural history of thoracic aortic aneurysms: indications for surgery, and surgical versus nonsurgical risks," *The Annals of Thoracic Surgery,* vol. 74, no. 5, pp. S1877-S1880, 2002.

[85] M. A. Coady, J. A. Rizzo, G. L. Hammond, D. Mandapati, U. Darr, G. S. Kopf and J. A. Elefteriades, "What is the appropriate size criterion for resection of thoracic aortic aneurysms?," *The Journal of Thoracic and Cardiovascular Surgery,* vol. 113, no. 3, pp. 476-491, 1997.

[86] R. R. Davies, L. J. Goldstein, M. A. Coady, S. L. Tittle, J. A. Rizzo, G. S. Kopf and J. A. Elefteriades, "Yearly rupture or dissection rates for thoracic aortic aneurysms: simple prediction based on size," *Ann Thorac Surg,* vol. 73, no. 1, pp. 17-28, 2002.

[87] M. A. Coady, J. A. Rizzo, G. L. Hammond, G. S. Kopf and J. A. Elefteriades, "Surgical intervention criteria for thoracic aortic aneurysms: a study of growth rates and complicationsThe Annals of Thoracic Surgery," *Ann. Thorac. Surg.,* vol. 67, no. 6, pp. 1922-1926, 1999.

[88] B. Rylski et al., "How does the ascending aorta geometry change when it dissects?," *J. Am. Coll. Cardiol.,* vol. 63, no. 13, pp. 1311-1319, 2014.

[89] B. Rylski, E. Branchetti, J. E. Bavaria, P. Vallabhajosyula, W. Y. Szeto, R. K. Milewski and N. D. Desai, "Modeling of predissection aortic size in acute type A dissection: More than 90% fail to meet the guidelines for elective ascending replacement," *The Journal of Thoracic and Cardiovascular Surgery,* vol. 148, no. 3, pp. 944-948.e1, 2014.

[90] A. M. Mansour, S. Peterss, M. A. Zafar, J. A. Rizzo, H. Fang, P. Charilaou, B. A. Ziganshin, U. M. Darr and J. A. Elefteriades, "Prevention of Aortic Dissection Suggests a Diameter Shift to a Lower Aortic Size Threshold for Intervention. Cardiology," *Cardiology,* vol. 139, no. 3, pp. 139-146, 2018.

[91] A. M. Ganapathi et al., "Location of Aortic Enlargement and Risk of Type A Dissection at Smaller Diameters," *J. Am. Coll. Cardiol.,* vol. 79, no. 19, pp. 1890-1897, 2022.

[92] V. J. Sharma et al., "Can we better differentiate type A dissections: evaluating the role of aortic ratios," *Heart Lung Circ.,* vol. 31, no. 8, pp. 1126-1133, 2022.

[93] E. Bollache et al., "Aortic valve-mediated wall shear stress is heterogeneous and predicts regional aortic elastic fiber thinning in bicuspid aortic valve-associated aortopathy," *J. Thorac. Cardiovasc. Surg.,* vol. 156, no. 6, pp. 2112-2120.e2, 2018.

[94] K. Suwa et al., "Effect of Aortic Valve Disease on 3D Hemodynamics in Patients With Aortic Dilation and Trileaflet Aortic Valve Morphology," *J. Magn. Reson. Imaging,* vol. 51, no. 2, pp. 481-491, 2019.

[95] F.-K. Benra, H. J. Dohmen, J. Pei, S. Schuster and B. Wan, "A comparison of one-way and two-way coupling methods for numerical analysis of fluid-structure interactions," *J. Appl. Math.,* vol. 2011, p. 853560, 2011.

[96] M. Hirschhorn, V. Tchantchaleishvili, R. Stevens, J. Rossano and A. Throckmorton, "Fluid–structure interaction modeling in cardiovascular medicine – A systematic review 2017–2019," *Med. Eng. Phys.,* vol. 78, no. 2020, pp. 1-13, 2020.

[97] M. H. Friedman, G. M. Hutchins, C. B. Bargeron, O. J. Deters and F. F. Mark, "Correlation between intimal thickness and fluid shear in human arteries," *Atherosclerosis,* vol. 39, no. 3, pp. 425-436, 1981.

[98] C. K. Zarins, D. P. Giddens, B. K. Bharadvaj, V. S. Sottiurai, R. F. Mabon and S. Glagov, "Carotid bifurcation atherosclerosis. Quantitative correlation of plaque localization with flow velocity profiles and wall shear stress," *Circ. Res.,* vol. 53, no. 4, p. 502–514, 1983.

[99] S. Chien, S. Li and Y. J. Shyy, "Effects of mechanical forces on signal transduction and gene expression in endothelial cells," *Hypertension,* vol. 3, no. 1 Pt 2, pp. 162-169, 1998.

[100] M. M. Bissell et al., "Aortic dilation in bicuspid aortic valve disease: flow pattern is a major contributor and differs with valve fusion type," *Circ. Cardiovasc. Imaging,* vol. 6, no. 4, p. 499–507, 2013.

[101] S. K. Atkins, K. Cao, N. M. Rajamannan and P. Sucosky, "Bicuspid aortic valve hemodynamics induces abnormal medial remodeling in the convexity of porcine ascending aortas," *Biomech. Model Mechanobiol.,* vol. 13, p. 1209–1225, 2014.

[102] D. G. Guzzardi et al., "Valve-Related Hemodynamics Mediate Human Bicuspid Aortopathy: Insights From Wall Shear Stress Mapping," *J. Am. Coll. Cardiol.,* vol. 66, no. 8, pp. 892-900, 2015.

[103] S. Pasta et al., "Shear Stress and Aortic Strain Associations With Biomarkers of Ascending Thoracic Aortic Aneurysm," *Ann. Thorac. Surg.,* vol. 110, no. 5, pp. 1595-1604, 2020.

[104] X. He and D. N. Ku, "Pulsatile Flow in the Human Left Coronary Artery Bifurcation: Average Conditions," *J Biomech Eng,* vol. 118, no. 1, pp. 74-82, 1996.

[105] H. A. Himburg, D. M. Grzybowski, A. L. Hazel, J. A. LaMack, X. M. Li and M. H. Friedman, "Spatial comparison between wall shear stress measures and porcine arterial endothelial permeability," *Am. J. Physiol. Heart. Circ. Physiol.,* vol. 286, no. 5, pp. H1916-H1922, 2004.

[106] J.-J. Chiu and S. Chien, "Effects of Disturbed Flow on Vascular Endothelium: Pathophysiological Basis and Clinical Perspectives," *Physiological Reviews,* vol. 91, no. 1, pp. 327-387, 2011.

[107] J. Hwang et al., "Pulsatile versus oscillatory shear stress regulates NADPH oxidase subunit expression: implication for native LDL oxidation," *Circ. Res,* vol. 93, no. 12, pp. 1225-1232, 2003.

[108] Z. Chen et al., "Vascular Remodelling Relates to an Elevated Oscillatory Shear Index and Relative Residence Time in Spontaneously Hypertensive Rats," *Sci Rep.,* vol. 7, no. 1, p. 2007, 2017.

[109] R. Jayendiran, F. Condemi, S. Campisi, M. Viallon, P. Croisille and S. Avril, "Computational prediction of hemodynamical and biomechanical alterations induced by aneurysm dilatation in patient-specific ascending thoracic aortas," *Int. J. Numer. Method. Biomed. Eng.,* vol. 36, no. 6, p. e3326, 2020.

[110] M. Shojima et al,, "Magnitude and Role of Wall Shear Stress on Cerebral Aneurysm," *Stroke,* vol. 35, no. 11, p. 2500–2505, 2004.

[111] J. Xiang et al., "Hemodynamic-morphologic discriminants for intracranial aneurysm rupture," *Stroke,* vol. 42, no. 1, pp. 144-152, 2011.

[112] T. Plonek et al., "Wall stress correlates with intimal entry tear localization in Type A aortic dissection," *Interact. Cardiovasc. Thorac. Surg.,* vol. 27, no. 6, pp. 797-801, 2048.

[113] Ali N Azadani et al., "Biomechanical properties of human ascending thoracic aortic aneurysms," *Ann. Thorac. Surg.,* vol. 96, no. 1, pp. 50-58, 2013.

[114] V. DA, "Biomechanics of abdominal aortic aneurysm," *J Biomech,* vol. 40, no. 9, pp. 1887-1902, 2007.

[115] D. A. Vorp, B. J. Schiro, M. P. Ehrlich, T. S. Juvonen, M. Ergin and B. P. Griffith, "Effect of aneurysm on the tensile strength and biomechanical behavior of the ascending thoracic aorta," *Ann Thorac Surg,* vol. 75, no. 4, pp. 1210-1214, 2003.

[116] M. Nowak, "The protocol for using elastic wall model in modeling blood flow within human artery," *Eur. J. Mech. B/Fluids,* vol. 77, no. 11, pp. 273-280, 2019.

[117] Ansys inc., in *2022 R1 Ansys Fluent User's Guide*, Canonsburg, 2022.

[118] M. Lee, G. Park, C. Park and C. Kim, "Improvement of Grid Independence Test for Computational Fluid Dynamics Model of Building Based on Grid Resolution," *Adv. Civ. Eng.,* vol. 2020, no. 8827936, p. 11, 2020.

[119] H. L. Goldsmith and R. Skalak, "Hemodynamics," *Annual Review of Fluid Mechanics,* vol. 7, pp. 213-247, 1975.

[120] P. D. Morris et al., "Computational fluid dynamics modelling in cardiovascular medicine," *Heart,* vol. 102, no. 1, pp. 18-28, 2016.

[121] D. S. Long, M. L. Smith, A. R. Pries, K. Ley and E. R. Damiano, "Microviscometry reveals reduced blood viscosity and altered shear rate and shear stress profiles in microvessels after hemodilution," *Proc. Natl. Acad. Sci. U. S. A.,* vol. 101, no. 27, pp. 10060-10065, 2004.

[122] A. Arzani, "Accounting for residence-time in blood rheology models: do we really need non-Newtonian blood flow modelling in large arteries?," *J. R. Soc. Interface,* vol. 15, no. 146, p. 20180486, 2018.

[123] S.-W. Lee and D. A. Steinman, "On the Relative Importance of Rheology for Image-Based CFD Models of the Carotid Bifurcation," *J. Biomech. Eng.,* vol. 129, no. 2, p. 273–278, 2007.

[124] J. V. Soulis, O. P. Lampri, D. K. Fytanidis and G. D. Giannoglou, "Relative residence time and oscillatory shear index of non-Newtonian flow models in aorta," in *2011 10th International Workshop on Biomedical Engineering*, Kos, Greece, 2011.

[125] K. M. Tse, R. Chang, H. P. Lee, S. P. Lim, S. K. Venkatesh and P. Ho, "A computational fluid dynamics study on geometrical influence of the aorta on haemodynamics," *Eur. J. Cardiothorac. Surg.,* vol. 43, no. 4, pp. 829-38, 2013.

[126] B. M. Johnston, P. R. Johnston, S. Corney and D. Kilpatrick, "Non-Newtonian blood flow in human right coronary arteries: steady state simulations," *J. Biomech.,* vol. 37, no. 5, pp. 709-720, 2004.

[127] M. W. Siebert and P. S. Fodor, "Newtonian and Non-Newtonian Blood Flow over a BackwardFacing Step – A Case Study," *Proceedings of the COMSOL Conference, Boston,* vol. 27, 2009.

[128] Y. C. Fung, Biomechanics Circulation, New York: Springer, 1997.

[129] M. S. Olufsen, C. S. Peskin, W. Y. Kim, E. M. Pedersen, A. Nadim and J. Larsen, "Numerical Simulation and Experimental Validation of Blood Flow in Arteries with Structured-Tree Outflow Conditions," *Ann. Biomed. Eng.,* vol. 28, no. 11, p. 1281–1299, 2000.

[130] K. M. Tse, P. Chiu, H. P. Lee and P. Ho, "Investigation of hemodynamics in the development of dissecting aneurysm within patient-specific dissecting aneurismal aortas using computational fluid dynamics (CFD) simulations," *J. Biomech.,* vol. 44, no. 5, pp. 827-836, 2011.

[131] Ansys inc., in *2022 R1 Fluent Theory Guide*, Canonsburg, 2022.

[132] M. A. Zafar et al., "Height alone, rather than body surface area, suffices for risk estimation in ascending aortic aneurysm," *J. Thorac. Cardiovasc. Surg.,* vol. 115, no. 5, pp. 1938-1950, 2018.

[133] T. Krüger et al., "Ascending aortic elongation and the risk of dissection," *Eur. J. Cardiothorac. Surg.,* vol. 50, no. 2, pp. 241-247, 2016.

[134] T. Krüger et al., "Aortic elongation and the risk for dissection: the Tübingen Aortic Pathoanatomy (TAIPAN) project," *Eur. J. Cardiothorac. Surg.,* vol. 51, no. 6, pp. 1119-1126, 2017.

[135] S. Heuts et al., "Evaluating the diagnostic accuracy of maximal aortic diameter, length and volume for prediction of aortic dissection," *Heart,* vol. 106, no. 12, pp. 892-897, 2020.

[136] D. Eliathamby et al., "Ascending aortic length and its association with type A aortic dissection," *J. Am. Heart. Assoc.,* vol. 10, no. 13, p. e020140, 2021.

[137] D. N. Ku, D. P. Giddens, C. K. Zarins and S. Glagov, "Pulsatile flow and atherosclerosis in the human carotid bifurcation. Positive correlation between plaque location and low oscillating shear stress. Arteriosclerosis," *Arteriosclerosis,* vol. 5, no. 3, pp. 293-302, 1985.

[138] K. P. Papadopoulos, M. Gavaises, I. Pantos, D. G. Katritsis and N. Mitroglou, "Derivation of flow related risk indices for stenosed left anterior descending coronary arteries with the use of computer simulations,," *Medical Engineering & Physics,* vol. 38, no. 9, pp. 929-939, 2016.

[139] P. L. Walpola, A. I. Gotlieb and B. L. Langille, "Monocyte adhesion and changes in endothelial cell number, morphology, and F-actin distribution elicited by low shear stress in vivo," *Am. J. Pathol.,* vol. 142, no. 5, pp. 1392-1400, 1993.

[140] L. Boussel et al., "Aneurysm growth occurs at region of low wall shear stress: patient-specific correlation of hemodynamics and growth in a longitudinal study," *Stroke,* vol. 39, no. 11, pp. 2997-3002, 2008.

[141] M. Kiema et al., "Wall Shear Stress Predicts Media Degeneration and Biomechanical Changes in Thoracic Aorta," *Front Physiol.,* vol. 13, p. 934941, 2022.

[142] A. J. Boyd, D. C. S. Kuhn, R. J. Lozowy and G. P. Kulbisky, "Low wall shear stress predominates at sites of abdominal aortic aneurysm rupture," *J. Vasc. Surg.,* vol. 63, no. 6, pp. 1613-1619, 2016.

[143] R. Mahadevia et al., "Bicuspid aortic cusp fusion morphology alters aortic three-dimensional outflow patterns, wall shear stress, and expression of aortopathy," *Circulation,* vol. 129, no. 6, pp. 673-682, 2014.

[144] M. Y. Salmasi et al., "High Wall Shear Stress can Predict Wall Degradation in Ascending Aortic Aneurysms: An Integrated Biomechanics Study," *Front Bioeng. Biotechnol.,* vol. 9, p. 750656, 2021.

[145] H. Meng, V. M. Tutino, J. Xiang and A. Siddiqui, "High WSS or low WSS? Complex interactions of hemodynamics with intracranial aneurysm initiation, growth, and rupture: toward a unifying hypothesis," *AJNR Am. J. Neuroradiol.,* vol. 35, no. 7, pp. 1254-1262, 2014.

[146] R. D. Renapurkar, R. M. Setser, T. P. O'Donnell, J. Egger, M. L. Lieber, M. Y. Desai, A. E. Stillman, P. Schoenhagen and S. D. Flamm, "Aortic volume as an indicator of disease progression in patients with untreated infrarenal abdominal aneurysm," *European Journal of Radiology,* vol. 81, no. 2, pp. e87-e93, 2012.

[147] E. M. Guirguis and G. G. Barber, "The natural history of abdominal aortic aneurysms," *The American Journal of Surgery,* vol. 162, no. 5, pp. 481-483, 1991.

[148] S. C. Nicholls, J. B. Gardner, M. H. Meissner and K. H. Johansen, "Rupture in small abdominal aortic aneurysms," *Journal of vascular surgery,* vol. 28, no. 5, pp. 884-888, 1998.

[149] A. Kitagawa, T. M. Mastracci, R. von Allmen and J. T. Powell, "The role of diameter versus volume as the best prognostic measurement of abdominal aortic aneurysms," *Journal of Vascular Surgery,* vol. 58, no. 1, pp. 258-265, 2013.

[150] C. Kauffmann et al., "Measurements and detection of abdominal aortic aneurysm growth: Accuracy and reproducibility of a segmentation software," *Eur. J. Radiol.,* vol. 81, no. 8, pp. 1688-1694, 2012.

[151] A. Parr, C. Jayaratne, P. Buttner and J. Golledge, "Comparison of volume and diameter measurement in assessing small abdominal aortic aneurysm expansion examined using computed tomographic angiography," *European Journal of Radiology,* vol. 79, no. 1, pp. 42-47, 2011.

[152] A. W. den Hartog et al., "Aortic disease in patients with Marfan syndrome: aortic volume assessment for surveillance," *Radiology,* vol. 269, no. 2, p. 370–377, 2013.

[153] M. L. Liljeqvist, R. Hultgren, T. C. Gasser and J. Roy, "Volume growth of abdominal aortic aneurysms correlates with baseline volume and increasing finite element analysis-derived rupture risk,," *Journal of Vascular Surgery,* vol. 63, no. 6, pp. 1434-1442.e3, 2016.

[154] J. A. Elefteriades, S. K. Mukherjee and H. Mojibian, "Discrepancies in Measurement of the Thoracic Aorta: JACC Review Topic of the Week," *Journal of the American College of Cardiology,* vol. 76, no. 2, pp. 201-217, 2020.

[155] B. A. Ziganshin, M. A. Zafar and J. A. Elefteriades, "Descending threshold for ascending aortic aneurysmectomy: is it time for a “left-shift” in guidelines?," *J. Thorac. Cardiovasc. Surg.,* vol. 157, no. 1, p. 37–42, 2019.

[156] T. Matsumoto et al., "Biaxial tensile properties of thoracic aortic aneurysm tissues," *J. Biomech. Eng.,* vol. 4, no. 4, pp. 518-529, 2009.

[157] A. Duprey, K. Khanafer, M. Schlicht, S. Avril, D. Williams and R. Berguer, "In vitro characterisation of physiological and maximum elastic modulus of ascending thoracic aortic aneurysms using uniaxial tensile testing," *Eur. J. Vasc. Endovasc. Surg.,* vol. 39, no. 6, pp. 700-707, 2010.